TAMPEREEN TEKNILLINEN YLIOPISTO
TAMPERE UNIVERSITY OF TECHNOLOGY

Samu Järvinen

Single particle laser-induced breakdown spectroscopy for elemental analysis of water and bioaerosols

Julkaisu 1380 • Publication 1380

Tampere 2016

Tampereen teknillinen yliopisto. Julkaisu 1380
Tampere University of Technology. Publication 1380

Samu Järvinen

Single particle laser-induced breakdown spectroscopy for elemental analysis of water and bioaerosols

Thesis for the degree of Doctor of Science in Technology to be presented with due permission for public examination and criticism in Sähkötalo Building, Auditorium S4, at Tampere University of Technology, on the 22nd of April 2016, at 12 noon.

Tampereen teknillinen yliopisto - Tampere University of Technology
Tampere 2016

ISBN 978-952-15-3727-1 (printed)
ISBN 978-952-15-3731-8 (PDF)
ISSN 1459-2045

Abstract

Laser-induced breakdown spectroscopy (LIBS) is a selective and robust atomic emission spectroscopy method where a high intensity laser pulse thermally dissociates and excites a minute quantity of the sample material. In LIBS, all elements can be measured simultaneously which makes it useful in applications where fast multicomponent analysis is required. Trace element analysis technology based on LIBS was developed in this Thesis for monitoring of dissolved impurities in water. The concentrations of dissolved elements in industrial process water and effluent are measured for process steering and for emission management. At the moment, the chemical analysis of water is mainly done by manual sampling and laboratory analysis. Online measurement technology would contribute to the economical use of water, chemicals and energy in the process industry and further the safety of liquid emissions.

Two novel methods for improving the sensitivity of LIBS of dissolved elements were introduced in this Thesis. In the presented techniques, aerosol particles generated from the sample solution are analyzed individually with LIBS. The main benefits of single particle LIBS are the high preconcentration of the sample and the absence of the liquid matrix which suppresses the LIBS signal. In the first instrumentation, the particle travels along a narrow carrier gas flow and its presence in the small sampling volume is determined by an optical sensor. In the second presented technique, the generated droplet is trapped in three dimensions using electrodynamic balance (EDB) technology and the residual particle is analyzed after the complete drying of the droplet. A detailed characterization of LIBS of precisely trapped particles was also conducted in this Thesis. Clear improvement with respect to reproducibility and sensitivity was achieved in this work compared with the direct LIBS analysis of water. The limits of detection for the constructed EDB-LIBS system were at 50 μg/l level for several transition metals and are among the lowest values obtained with LIBS based trace element analysis. The flexible requirements for the LIBS laser pulse energy and the speed of operation improve the applicability of the aerosol based sample preparation to the monitoring of industrial and natural waters. Moreover, the concurrent detection of dissolved elements and microbiological contamination of water was demonstrated by the combination of laser-induced fluorescence and single particle LIBS.

Preface

The work of this Ph.D. thesis was carried out in the Optics Laboratory of Department of Physics of Tampere University of Technology during the years 2012–2015. I acknowledge the financial support from the Graduate School of Modern Optics and Photonics in Finland, Tekes, and all the participant companies in the Commonmine-NICK research project.

I acknowledge my supervisor Assoc. Prof. Juha Toivonen for the guidance and support during the research work, and for the opportunity to work with interesting topics in the field of optical measurement technology. I thank the pre-examiners Prof. Erkki Ikonen and Dr. Christophe Dutouquet for the important comments that helped me to improve this thesis. I also thank my co-authors Ph.D. Sampo Saari and Prof. Jorma Keskinen from the Aerosol Physics Laboratory for fruitful collaboration. I am grateful to my former colleagues Ph.D. Jaakko Saarela and Ph.D. Tapio Sorvajärvi for all the discussions and help with devices, writing, etc. especially at the time I was starting with my research. Thanks to Ph.D. Victor Contreras for the instructive discussions and for providing me with excellent LIBS signal processing software. Special thanks to Johan and Antti who have shared all the years of working in the Applied Optics research group with me. I would also like to address thanks to everyone in the Optics lab for the superb atmosphere.

Finally, I thank my amazing daughters Lilia and Selja for the everyday moments and my wife Julia for the immense support and understanding. Without you, this would not have been possible.

Tampere, March 2016

Samu Järvinen

Contents

List of publications

Paper 1 S. T. Järvinen, J. Saarela, and J. Toivonen, "Detection of zinc and lead in water using evaporative preconcentration and single-particle laser-induced breakdown spectroscopy," Spectrochimica Acta Part B: Atomic Spectroscopy **86**, 55 – 59 (2013).

Paper 2 S. T. Järvinen, S. Saari, J. Keskinen, and J. Toivonen, "Detection of Ni, Pb and Zn in water using electrodynamic single-particle levitation and laser-induced breakdown spectroscopy," Spectrochimica Acta Part B: Atomic Spectroscopy **99**, 9 – 14 (2014).

Paper 3 S. T. Järvinen and J. Toivonen, "Analysis of single mass-regulated particles in precisely controlled trap using laser-induced breakdown spectroscopy," Optics Express **24**(2), 1314 – 1323 (2016).

Paper 4 S. Saari, S. Järvinen, T. Reponen, J. Mensah-Attipoe, P. Pasanen, J. Toivonen, and J. Keskinen, "Identification of single microbial particles using electro-dynamic balance assisted laser-induced breakdown and fluorescence spectroscopy," Aerosol Science & Technology **50**(2), 126 – 132 (2016).

List of symbols

AAS	Atomic absorption spectroscopy
ADC	Analog-to-digital converter
ASD	Atomic spectra database
ASV	Anodic stripping voltammetry
CE	Capillary electrophoresis
CTE	Complete thermal equilibrium
CW	Continuous wave
EDB	Electrodynamic balance
FWHM	Full-width at half maximum
GF-AAS	Graphite furnace atomic absorption spectroscopy
IC	Ion chromatography
ICCD	Intensified charge-coupled device
ICP-AES	Inductively coupled plasma atomic emission spectrometry
ICP-MS	Inductively coupled plasma mass spectrometry
ICP-OES	Inductively coupled plasma optical emission spectrometry
ICT	Information and communications technology
IJAG	Ink jet aerosol generator
ISE	Ion-selective electrode

ISO	International Organization for Standardization
LIBS	Laser-induced breakdown spectroscopy
LIF	Laser-induced fluorescence
LOD	Limit of detection
LTE	Local thermal equilibrium
NIST	National Institute of Standards and Technology
PBR	Peak-to-background ratio
PE	Population equivalent
PMT	Photomultiplier tube
ppb	Parts per billion (10^{-9})
ppm	Parts per million (10^{-6})
RH	Relative humidity [%]
RLD	Reciprocal linear dispersion [nm/mm]
RSD	Relative standard deviation [%]
SFS	Finnish Standards Association
SNR	Signal-to-noise ratio
TOC	Total organic carbon
XRF	X-ray fluorescence
β	Field strength parameter
$\boldsymbol{\mu}$	Electric dipole moment operator
$\delta E_{ion,r}$	Suppression of ionization energy $E_{ion,r}$ [eV]
δ	Drag parameter
$\Delta\lambda_{Doppler}$	FWHM of Doppler broadened line [m]
$\Delta\lambda_{instr}$	FWHM of instrumental profile [m]
$\Delta\lambda_{Stark}$	FWHM of linearly Stark broadened line [m]
ϵ_{ki}	Volumetric line emission coefficient [$\mathrm{Wm^{-3}sr^{-1}}$]
η	Viscosity of air [$\mathrm{Pa \cdot s}$]
$\eta(\lambda)$	Quantum efficiency of detector including losses in optical components

$\hat{u}_{AC}$	Amplitude of AC voltage [V]
λ_{ki}	Wavelength of light taking part in transitions between states k and i [m]
$\mathbf{E_{AC}}$	Electric field due to AC voltage
$\mathbf{E_{DC}}$	Electric field due to DC voltage
$\mathbf{F_{DC}}$	Electrostatic force due to DC voltage
$\mathbf{F_{ext}}$	External resultant force
$\mathbf{r}$	Position vector
$\mathbf{R}^{ki}$	Transition moment vector
ν_{ki}	Frequency of light taking part in transitions between states k and i [Hz]
$\omega_{AC,i}$	Initial AC voltage angular frequency [rad/s]
ω_{AC}	AC voltage angular frequency [rad/s]
ψ_k	Wave function corresponding state k
ρ_s	Mean density of impurity salt [kg/m^3]
ρ_w	Density of the aqueous solution [kg/m^3]
θ_m	Diffraction angle [rad]
A_{ki}	Einstein coefficient of spontaneous emission [s^{-1}]
$C(n_e, T)$	Coefficient for determination of electron density from $\Delta\lambda_{Stark}$ [Å$^{-3/2}$cm^{-3}]
C_0	Geometrical constant
c_{tot}	Total mass concentration of impurities in water [ppm]
d_p	Droplet or dry particle size [m]
D_v	Diffusion coefficient of water vapor [m^2/s]
$d_{p,dry}$	Residual particle diameter [m]
d_{p0}	Initial droplet diameter [m]
d_{slit}	Slit width of spectrometer [m]
E_k	Energy of state k [eV]
$E_{ion,r}$	Ionization energy of r-times ionized atom [eV]
f	Spectrometer focal length [m]

f_{AC}	AC voltage frequency [Hz]
$F_{ext,z}$	External force in z-direction [N]
g	Gravitational acceleration [m/s^2]
g_k	Degeneracy of state k
I	Intensity of spectral line indicated by detector [a.u.]
M	Molar mass [g/mol]
m	Diffraction order
m_e	Electron rest mass [kg]
m_p	Mass of the particle [kg]
M_w	Molar mass of water [kg/mol]
n_e	Electron density [m^{-3}]
n_k	Number density of atoms in state k [m^{-3}]
n_r	Number density of ions in ionization stage r [m^{-3}]
p_d	Partial pressure of water vapor on droplet surface [Pa]
p_∞	Partial pressure of water vapor inside chamber [Pa]
q	Particle charge [C]
R	Molar gas constant [J mol^{-1}K^{-1}]
S	Saturation ratio
t_1	Droplet flight time from droplet generator to chamber center [s]
t_2	Time when AC frequency maximum is attained [s]
T_d	Droplet temperature [K]
T_e	Electron temperature [K]
T_i	Ionization temperature [K]
T_∞	Temperature inside chamber [K]
$t_{c.dry}$	Time for complete evaporation of droplet [s]
T_{exc}	Excitation temperature [K]
t_{trap}	Time when the droplet has settled at focal point [s]
$t_{trigger}$	LIBS pulse triggering time from droplet generation [s]

u_{AC}	AC voltage [V]
$U_{DC,0}$	Equilibrium DC voltage [V]
$U_{DC,f}$	Final DC voltage [V]
$U_{DC,i}$	Initial DC voltage [V]
U_{DC}	Potential difference between inner electrodes [V]
v_e	Electron velocity [m/s]
X	Chemical species in its ground state
X^*	Chemical species in excited state
X^+	Chemical species in its ionized state
z_0	Half of the distance between the inner electrodes [m]
$Z_r(T)$	Partition function of ion in ionization stage r

Chapter 1

Introduction

WATER resources have links to the state of the environment, the standard of living and political conflicts. Over the last decades, the global consumption of water has increased at the rate double of population growth. The climate change feeds the readily uneven distribution of fresh water on the planet. In 2012, 2.5 billion people were concerned by the shortage of clean water and over 1.2 billion people were living in the areas of physical water scarcity. [1]

While the obvious consequences of drought – difficulties in food production and limited access to safe drinking water, hygiene and sanitation services – are the most acute, the negative impacts on the economical growth sustain the regional water scarcity. Water is needed in almost every process industry including energy production, mining, metal and oil refining, paper and pulp industry. Water transports substances or kinetic energy within a process. It is used for cooling, as a raw material or as a solvent in industrial scale chemical reactions. In water treatment plants, pure water is the final product. In the traditional "take-make-consume and dispose" economy, water flows through the process and the portion that is not evaporated becomes waste water containing suspended matter, heavy metals, other chemicals or microbes. By adopting the principles of circular economy and sustainable development [2] in process industry and in the water resources engineering, the price of waste and pure water management could be brought down and the energy and raw material efficiency could be improved. [3]

In practical terms, these principles mean process optimization by solutions like recirculated process water cycles to cut down the water intake, optimizing the chemicals addition to the process and smart waste water treatment and monitoring systems.

Measurement of various element concentrations in water is one of the most common procedures for process steering. Concentration levels are used for ensuring the proper function of the process, for end-product quality control and for regulatory waste water monitoring. In the process optimization, measurement data should be generated and utilized in real-time. This is possible by implementing the modern ICT combined with water sensor technology in process automation systems. Although numerous online sensors are already on the market for many properties of water such as pH, turbidity or conductivity, a sensitive and cost-effective technology for the detection of wide range of dissolved elements is still missing. The current elemental analysis of water is most often performed manually in a laboratory by stoichiometric or spectroscopic analysis whereupon the time between the sample collection and the result-based action is too long for real-time process control or emission alert system.

Optical measurement technology is based on the interaction between light and matter. If an optical access to the object is provided, almost every physical property can be measured either directly or indirectly using light or a portion of the electromagnetic radiation that range from infrared through ultraviolet. Nowadays optical sensors are found everywhere in industry[4], transportation[5], defense[6], health care[7] and households[8]. Laser spectroscopy is a branch of modern optical measurement technology where the amount and frequency of the light emitted or absorbed by the sample is analyzed and the method involves one or several lasers. Typical measurement task for laser spectroscopy is to reveal the amount of certain substance in a sample material. In the chemical analysis of water, the benefits of *in situ* optical measurements in comparison with traditional laboratory methods are typically the absence of sampling, the measurement speed and frequency, sensitivity, selectivity, compact sensor size and chemical-free measurement.

1.1 Aim and Scope of This Work

The objective of this work was to develop laser spectroscopy -based technology for the detection of small metal concentrations in water. The technology was initially

purposed in mining sites to monitor the safety of the water released to the surrounding water systems and to detect metal concentrations, mainly nickel, in the recirculated process water streams. Part of the research was carried out in projects funded by Tekes – the Finnish Funding Agency for Innovation, mining companies and companies providing technology solutions for mines. The requirement for the lowest detectable concentrations was 0.1 mg/l or 0.1 ppm, and it was determined by the environmental permits conceded in Finland, the law of Finland[9,10], the European Union directives[11] and organizational recommendations[12].

The list of potential target applications was later expanded to cover other facilities where the measurement of dissolved elements due to process control, water safety and environmental monitoring is a mandatory practice. In many cases, moving on from conventional laboratory analysis towards online measurement would save resources and environment. Industrial waste waters commonly include trace amounts of heavy metals whose health hazards are well-known[13]. The source of metal discharges can be, for example, the cooling water or water from the enrichment and coating processes in metal production plants, the preparation of the crude oil in the oil refining or use of aluminum sulfate as retention aid in paper industry. In Finland, the facilities typically have their own water treatment plant that removes metals from the waste water to the level allowed in their environmental permit. Communal waste water treatment plants need to remove phosphorus from the received water. Removal is done by precipitating the phosphorus with soluble iron or aluminum salt. The dosing of the salt in the water under purification is controlled by measurements of the phosphorus levels. Secondly, waterworks treating waste waters from process industry require information about increased metal concentrations in the received water in order to prevent the metals from ending up in the sludge which is a by-product of the water treatment facilities[14]. Concentrations of oxygen, silicon and metals in the coolant circuit in thermal power plants can reveal early corrosion, the forming of depositions in the turbine or leaks in the heat exchanger between the primary circuit and a district heating network. Measurements are also required in closed system fish farming plants and many other branches of food industry as well as in the furthering of drinking water safety in the areas suffering water scarcity. The list of elements of interest in the above examples varies between applications and the required detection limits are between 0.1 μg/l and 10 mg/l.

Laser-induced breakdown spectroscopy (LIBS)[15] was studied as the analytical tech-

nique owing to its capability to measure the majority of elements rapidly with good selectivity. LIBS is a type of atomic emission spectroscopy which involves focusing a high intensity laser pulse on the surface or inside of the sample material. The leading edge of the pulse evaporates and ionizes a minute quantity of the sample. Optical power is converted to the kinetic energy of emerged electrons which leads to a rapid growth of free electron density at the laser focal point and further absorption of the pulse trailing edge. As the vapor heats up molecules will be dissociated and a significant portion of atoms and ions are thermally excited to upper energy states. After the laser pulse, ions and electrons recombine and the characteristic spectra of sample material atoms are observed due to radiative relaxation while the originated plasma cloud expands and cools down.

The major drawback of using LIBS is the insensitivity in direct measuring of liquid samples such as water streams due to numerous random processes that disrupt the signal formation. Thus, LIBS could not be used as a sole measurement technology. Combining optics and aerosol technology novel techniques were developed to circumvent the interfering processes and so to increase the sensitivity of LIBS analysis of water. This Thesis introduces two methods that perform a real-time sample preparation procedure by preconcentrating water droplets generated from the original sample and bringing the particles to the laser beam in a controlled way. The methodology led the research group to study the LIBS analysis of single particles which have links to other environmental research fields such as monitoring of atmospheric aerosols or industrial particle emissions. Besides elements, the developed technology enabled the detection of microbiological contamination in water which may increase the usability of the method in the online water quality control. This Thesis presents the novel measuring instruments and the main results of the research.

1.2 Structure of the Thesis

This Thesis consists of eight chapters that outline the background of the topic, the applied methods and obtained results. Chapter 2 describes the physical principles relevant in understanding how the signal from different elements forms in a LIBS measurement. Chapter 3 reviews the technologies currently utilized in the detection of elements in water and briefly describes their principle of measurement. Chapter 4

discusses the challenges of LIBS measurement of water and the approaches developed to enhance the LIBS sensitivity. The concept of single droplet sampling and preconcentration is introduced at the end of Chapter 4. The instrumentations built in this work for measuring elements in aqueous solutions using LIBS with aerosol-assisted preconcentration is presented in Chapter 5. Chapter 6 discusses the factors affecting the LIBS signal from a single precisely controlled aerosol particle and the optimization of the measurement parameters for water measurement. The applicability of the developed method to the qualitative trace element analysis of process and waste water samples is presented in Chapter 7. Detection of microbes in water by combining the information from LIBS and laser-induced fluorescence (LIF) measurement from the same micrometer scale particle is also described in Chapter 7. The work is summarized and the next development steps towards the online analysis applications are discussed in Chapter 8.

The research done within the framework of this Thesis is compiled in four peer-reviewed publications that are included in the appendices. Paper 1 concerns first of the two experimental instrumentations introduced in this work for LIBS analysis of water. Papers 2 and 3 covers the operation and characterization of the second measurement setup, respectively. Paper 4 deals with the addition of laser-induced fluorescence to the instrumentation presented in Paper 2 and application to microbe measurements. Short descriptions of the publication topics are described below.

Paper 1

An evaporative preconcentration method where trace metals are dopants on the surface of hollow 5 μm NaCl particles is introduced. The particles are concentrated and directed to a narrow sheath air flow. Individual particles trigger the LIBS analysis with the aid of a scattering detector. The use of sodium as an internal standard for improving the accuracy of the quantitative measurement is discussed and the detection limits for zinc and lead are provided. The measurement of LIBS signal as a function of pulse energy give a good reference for Paper 3 where the dependency is discussed in the case of precisely trapped particles.

Paper 2

LIBS of electrodynamically trapped NaCl particles is introduced and the appli-

cability of the scheme to the measurement of trace elements in water is demonstrated. As in Paper 1, the trace metals are present in the salt particles as additives. The operation of the experimental setup is described in detail. The excellent repeatability of the LIBS signal with low pulse energy is presented and the detection limits for nickel, lead and zinc are calculated.

Paper 3

The paper includes a description of the experiments done for studying of the factors affecting the elemental analysis of single precisely trapped droplets and dry particles using LIBS. Scattering-based feedback loop was build to control the trapping parameters in the scheme presented in Paper 2. The automatic adjustment of the parameters removes the requirement of adding salt in the analyzed water as done in the two previous papers and enables the three dimensional trapping of the droplet already in the drying phase. In Paper 3, LIBS signal dependency on the degree of evaporation of the droplet is presented and the influence of micrometer scale displacements in the position of the particle on the signal is quantified. Furthermore, the optimal applied laser fluence in the detection of elements in a finite sample mass is determined.

Paper 4

Identification of microbial particles in water based on their fluorescence properties and single-shot LIBS signal from potassium, sodium, calcium is introduced. LIF and single-shot LIBS spectra were recorded from single fungal spores and bacterial aggregates. The data analysis for detecting differences in the signals from different species is presented.

1.3 Author's Contribution

This Thesis summarizes the Author's research work during the years between 2012 and 2016. The Author's role in each of the four publications is presented in the following chapters. Group work and collaboration were naturally involved in all of the publications.

Paper 1

The Author modified the existing fluorescence measurement setup to be used in LIBS, planned and carried out all the measurements, designed the signal processing procedure and did the data analysis and most of the reporting.

Paper 2

The Author contributed considerably in the designing and building of the measurement system consisting of the measurement chamber and the optical setup around the chamber and designed and built the system automation. Also, the Author performed most of the measurements for the manuscript, processed the data, and wrote the manuscript.

Paper 3

The Author planned the measurements and did the required modifications to the instrumentation and to the automation program. The Author had the full responsibility for the measurements and data analysis and did most of the reporting.

Paper 4

The Author contributed equally to this work with the first author of the publication. The Author designed and modified the optical setup to include the LIF functionality and processed the raw measurement data. The Author also took part in the laboratory measurements and reporting.

Chapter 2

Laser-Induced Breakdown Spectroscopy

PRINCIPLES of laser-induced breakdown spectroscopy (LIBS) relevant in analysis of water and aerosols are presented in this Chapter. The discussion on plasma formation in air and measurement time scales in LIBS applies to the measurements with nanosecond-scale laser pulse durations. Also, the fundamentals of atomic energy structure and the origins of atomic spectra in a hot vapor are discussed in brief. Other measurement techniques for dissolved elements in water are presented in Chapter 3.

2.1 Atomic emission spectroscopy

The electrons in an atom have arranged into atom orbitals in a way that the lowest Coulombic potential energy is achieved and the rule of Pauli exclusion principle is not violated. The ground configuration of the lighter atoms can be deduced using the standard form of the periodic table of elements whereas more rigorous inspection is required for heavier elements. Each configuration describing the arrangement of the electrons in atom orbitals gives rise to one or more electronic energy states of an atom because of coupling between the total orbital angular momentum **L** and total

spin angular momentum **S** of the electrons. Figure 2.1 shows a Grotrian diagram of the ground state and the first excited states of Pb atom. The configuration of the electrons in unfilled orbitals is shown in the bottom row. The columns above represent the distribution of the energy levels arising from each configuration. They are labeled $^{2S+1}L_J$ where L = 0, 1, 2, 3, ... correspond to letters S, P, D, F, ... respectively. The negative values of the energy of each state in Figure 2.1 describe how firmly the outer electron is bound to the atom, and the first ionization energy $E_{ion,0}$ is the work required to remove an electron from an atom in its ground state. The energies in a Grotrian diagram are often expressed with relation to the ground state the energy of which is set as zero. [16]

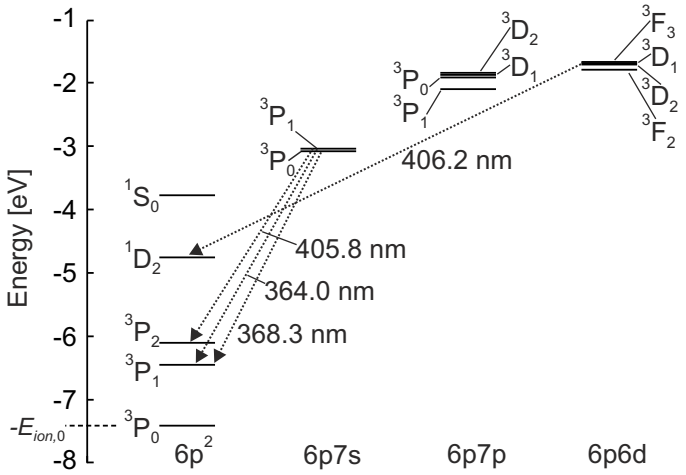

Figure 2.1 Levels of Pb atom and the transitions observed in this work.

The excited states of an atom or an ion in a high temperature vapor or plasma can be described as an atom or ion where one valence electron has been promoted to a higher atom orbital. The intensity of an observed optical spectral line corresponding the transition from state k to state i depends on the transition moment $\mathbf{R}^{ki}$, the amount of atoms in the state k, and the opacity of the hot vapor. The latter two parameters are discussed in the next section. A photon of emitted light has an energy that equals the energy difference of the states

$$E_k - E_i = h\nu_{ki} = \frac{hc}{\lambda_{ki}}, \tag{2.1}$$

where E_k and E_i are the energies of the upper and lower state, h is the Planck

constant and ν_{ki} and λ_{ki} are the frequency and the wavelength of the observed light, respectively. Atomic spectra databases[17,18] list the wavelengths of optical emission lines for most elements. Also, information about the spectral intensities is given to help in the recognition of unknown lines or in the modeling of the emission spectrum. Typically the reciprocal of the upper state lifetime i.e. the Einstein coefficient A_{ki} is given instead of $\mathbf{R}^{ki}$,

$$A_{ki} \propto |\mathbf{R}^{ki}|^2 = \left| \int \psi_k^* \boldsymbol{\mu} \psi_i d\tau \right|^2 . \tag{2.2}$$

In Equation 2.2, $\boldsymbol{\mu}$ is the electric dipole moment operator, τ is a volume element, and $|\mathbf{R}^{ki}|^2$ is called the transition probability. If $\mathbf{R}^{ki} = \mathbf{0}$, the transition is said to be forbidden and the quantum numbers characterizing the wave functions ψ_k and ψ_i do not fulfill the relations called the selection rules[16] which are not presented here. Even though a transition is forbidden as an electric dipole transition, it can be observed as a magnetic dipole or electric quadrupole radiation but these emission lines are typically weak. The arrows in Figure 2.1 show the Pb transitions measured in this work. The most persistent being the transition between states 6p7s $^3\mathrm{P}_1^o \rightarrow$ 6p^2 $^3\mathrm{P}_2$.[19]

2.2 Laser-induced plasma

In air, the laser irradiance about 100 GW/cm^2 obtained by focusing a pulsed laser beam will lead to a rapid growth of free electron density and significant absorption of the laser pulse. In the mechanism, called the breakdown of the material, the initial free electrons in the focal volume can be produced by multiphoton ionization or natural background radiation. The free electrons in the field of an atom or an ion gain kinetic energy from the laser via the process of inverse bremsstrahlung. Collision between a fast electron and an atom produces two electrons and the electron density n_e grows in a cascaded manner. Photoionization is an important process in the increase of the electron density at UV laser wavelengths. If the threshold of about $n_e > 10^{13}$ cm^{-3} is exceeded, the laser pulse absorption becomes strong enough for the formation of plasma which is characterized by electron densities above 10^{16} cm^{-3} and temperatures above 5000 K. The latter part of the laser pulse feeds energy to the plasma. Therefore, the plasma expansion is not homogeneous but fastest in the direction opposite to the propagation of the laser pulse, and after the pulse the plasma possesses elongated form.[20]

In an ideal plasma state of complete thermal equilibrium (CTE), the plasma is optically thick over a wide wavelength range, it is governed by a single temperature T, the thermal energy loss due to convection, conduction and diffusion is negligible, and the plasma is spatially homogeneous. Then the following conditions hold: 1) The plasma radiates as a blackbody the intensity of which follows the Planck radiation law. 2) All the species in the plasma have a Maxwellian velocity distribution. 3) Thermal energy or collisions are responsible for the excitation of the species. The number density n_k of each species in an excited state k follows the Boltzmann distribution

$$n_k = n_r \frac{g_k}{Z_r(T)} \exp\left(-\frac{E_k}{k_B T}\right), \tag{2.3}$$

where n_r is the total number density of the species, g_k is the degeneracy of the state k, $Z_r(T)$ is the partition function of the species and k_B is the Boltzmann constant. 4) Ionization is due to collisions and the number density ratio n_{r+1}/n_r, where r is the ionization stage ($r = 0$ for atoms), is described by the Saha equation

$$\frac{n_{r+1}}{n_r} = \frac{2Z_{r+1}(T)}{Z_r(T)} \frac{(2\pi m_e k_B T)^{3/2}}{n_e h^3} \exp\left(-\frac{E_{ion,r} - \delta E_{ion,r}}{k_B T}\right), \tag{2.4}$$

where m_e is the electron mass, $E_{ion,r}$ is the ionization energy of the species and $\delta E_{ion,r}$ its depression due to charged particles in the plasma.[21]

The plasma formed in a LIBS experiment is optically thin and gives out its energy by radiation. It also suffers from other energy losses. Therefore the continuum emission from the plasma is much weaker than the blackbody emission corresponding the plasma temperature. However, the conditions 2)-4) are valid in the regions where collisional processes govern the species ionization and excitation rather than radiative processes and where the temperature, electron density and heat conductivity gradients are sufficiently weak. This local thermal equilibrium (LTE) approximation holds typically in the center of the plasma where the electron density is the highest. In case of deviations from LTE, the above equations can still be used for describing how different components are distributed in the plasma if T is replaced by temperatures specific for each process. In the Boltzmann equation, T is replaced by the excitation temperature T_{exc} and in the Saha equation by the electron or ionization temperature T_e, T_i. Also, the species velocities can still have Maxwellian distribution but the kinetic temperatures vary for the species of different mass.[21,22]

2.3 Plasma radiation

The radiation from cooling plasma can be categorized into three classes depending on the formation mechanism. These mechanisms are illustrated in Figure 2.2. The free-bound and the free-free mechanisms contribute to the continuous background spectrum that extends from the deep-UV to the infrared whereas the bound-bound transitions produce the optical line spectrum.

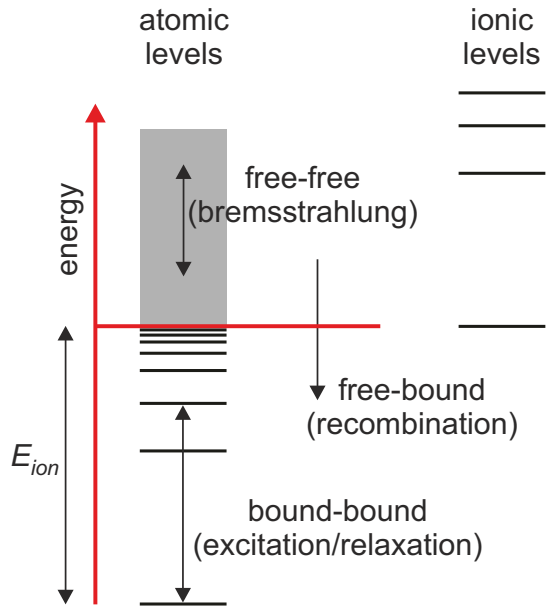

Figure 2.2 Free and bound electrons and classification of transitions.

The free-bound continuum is more prominent in the shorter wavelengths of the spectrum. In a radiative recombination between an electron e and the ion X^+, the resultant atom or ion remains in an excited state X^*

$$\begin{aligned} X^+ + e &\rightarrow X^* + h\nu \quad \text{and} \\ h\nu &= E_{ion} - \delta E_{ion} - E_k + \frac{1}{2} m_e v_e^2, \end{aligned} \tag{2.5}$$

where the last term is the kinetic energy of the electron. The recombination can also occur non-radiatively in the process of three-body recombination where a part of the neutralization energy is given to a third particle, usually to another electron. The

free-free radiation or bremsstrahlung arise when free electrons lose part of their kinetic energy in the interaction with positive ions and neutral atoms. The total background emission spectrum can be formed by summing up the contributions from the free-bound and the free-free radiation. At wavelengths shorter than about 500 nm, the resulting spectral volumetric emission coefficient for total continuous emission varies with the wavelength and has a sawtooth form due to the recombination. At longer wavelengths, the emission is practically independent of frequency until the plasma becomes optically thick at several micrometer wavelength and starts to radiate as a blackbody. The exact spectral shape of the background varies according to the concentration of each chemical species, the plasma temperature and electron density. [21]

Bound-bound transitions occur between discrete energy states. Electronic transitions in an atom or an ion are typically the most prominent in a LIBS spectrum but also molecular band systems are detected. The observed spectrum of lines at frequencies or wavelengths given by Equation 2.1 generate the desired LIBS signal. On the other hand, characteristic emission from the sample matrix or ambient air contribute to the background. For example, several nitrogen atomic lines as well as strong bands of N_2^+ and CN near 390 nm originate from standard air and distract the measurement of certain elements. In thermal equilibrium, the volumetric emission coefficient ϵ_{ki} corresponding atomic ($n_r = n_0$) line emission from state k to state i is given by

$$\epsilon_{ki} = \frac{1}{4\pi}\frac{hc}{\lambda}A_{ki}n_0\frac{g_k}{Z_0(T)}\exp\left(-\frac{E_k}{k_BT}\right). \tag{2.6}$$

Equation 2.6 can be used for determining the plasma temperature. One possibility is to measure intensity ratios between the atomic spectral lines of the same element and which are insensitive to self-absorption. The ratio is substituted into the rearranged form of Equation 2.6

$$\alpha := ln\left(\frac{\frac{I'}{\eta(\lambda')}A''_{ki}g''_k\lambda'}{\frac{I''}{\eta(\lambda'')}A'_{ki}g'_k\lambda''}\right) = \frac{1}{k_BT}\left(E''_k - E'_k\right), \tag{2.7}$$

where I is the intensity of a spectral line in detector specific units, $\eta(\lambda)$ is the quantum efficiency of the detection system at the spectral line wavelength, and the superscripts $'$ and $''$ refer to different transitions. In Figure 2.3, the left hand side of Equation 2.7 is plotted as a function of $(E''_k - E'_k)$ for four different lines measured in two separate measurements. The plasma temperature can be estimated from the slope $1/(k_BT)$ of the fitted line.

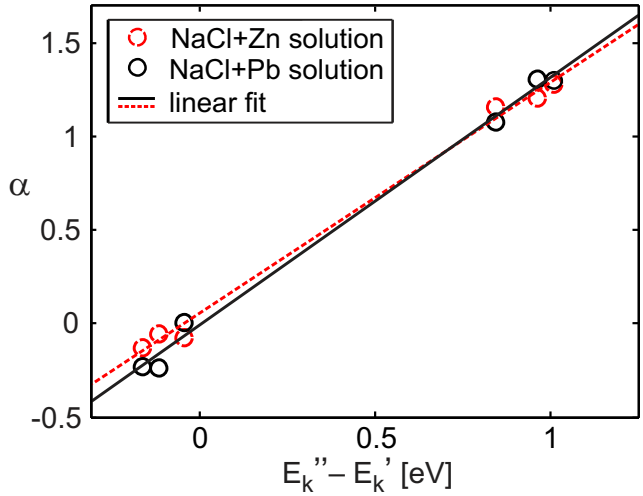

Figure 2.3 Boltzmann plots formed from measurement data of two separate measurements. The slopes indicate temperatures near 9000 K.

2.4 Line broadening

The dominant line broadening mechanisms in a LIBS spectrum are Stark, Doppler and instrumental broadening. At the early phase of plasma evolution, spectral lines are pressure broadened due to charged particles in a process of Stark broadening. Electric microfields generated by charged particles surrounding the atom produce a small shift in the position of atom's electron cloud with respect to the positive nucleus. The polarization causes splitting of the electronic levels and results in line broadening with a Lorentzian line profile. For hydrogenic atoms and ions, the splitting is symmetric with respect to unperturbed levels and the shift of one frequency component increases linearly with the external electric field. The theory of line broadening is the most accurate for hydrogen β line[23] and it is often used for estimating the electron density in the plasma. The relation can be written as

$$\Delta\lambda_{Stark} = \left[\frac{n_e}{C(n_e, T)}\right]^{2/3}. \tag{2.8}$$

In Equation 2.8, $\Delta\lambda_{Stark}$ is the full width at half maximum (FWHM) of the spectral line and C is a parameter tabulated in the literature[24]. Other atoms and ions undergo quadratic Stark effect which splits the energy levels asymmetrically. In the resulting

spectrum, the line center has been shifted towards longer wavelengths and the line profile has an asymmetric shape.

After a few microseconds from the laser pulse, the electron density has diminished and the spectral line profiles approach the Gaussian line shape caused by Doppler broadening. Due to Brownian motion, each radiating atom has a different velocity component along the line-of-sight of the observer which leads to a corresponding shift in the detected frequency described by the Doppler effect. The resulting FWHM linewidth is given by

$$\Delta\lambda_{Doppler} = 7.16 \times 10^{-7} \mathrm{g}^{1/2}\mathrm{K}^{-1/2}\mathrm{mol}^{-1/2}\sqrt{T/M}\lambda_{ki}, \tag{2.9}$$

where M is the molar mass of the atoms.

The degree and shape of instrumental broadening depend on the detection configuration and must be measured separately. When working far from the diffraction limited maximum resolution of a spectral apparatus, the instrumental broadening can be estimated from the bandpass

$$\Delta\lambda_{instr} = d_{slit} RLD = d_{slit} \frac{d\cos\theta_m}{fm}, \tag{2.10}$$

where RLD is the reciprocal linear dispersion of the grating, d is the grating constant, θ_m is the diffraction angle, f is the spectrometer focal length and m is the diffraction order. In spectrographs, d_{slit} is either the diameter of the entrance slit or two times the detector pixel size depending on which one is the largest. When two or more line broadening mechanisms have comparable effect the resulting line profile is a convolution of the lineshapes. In case of Lorentzian and Doppler profiles the overall function is then described by a Voigt function.

The assumption of optically thin plasma does not hold for spectral lines corresponding transitions from a low lying upper state to the ground state. With these wavelengths, plasma significantly absorbs its own emission and results further line broadening. In the early phase of plasma evolution, the temperature and the electron density are much lower near the boundaries of the plasma than in the center region. The broad line emission formed in the hotter regions therefore experiences self-absorption at wavelengths near the line center when it penetrates the colder boundary layer. The resulting line profile has a dip in the center as seen in Figure 2.4 and the phenomenon

is called self-reversal.

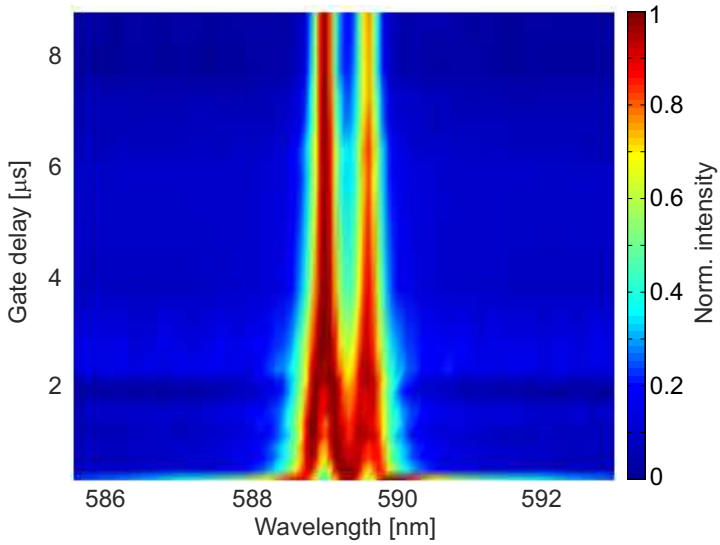

Figure 2.4 Time evolution of sodium D-lines at 589.0 nm and 589.6 nm wavelengths. Spectra measured from 5 μm NaCl particles in a sheath air flow using 400 ns ICCD gate width and variable gate delay. The self-reversal is clearly observed at short gate delay times of < 2 μs with respect to the initial laser pulse.

2.5 Signal retrieval and calibration

Because of non-selective excitation, LIBS is most often utilized in applications where several elements need to be measured at one step. The simultaneous detection of multiple elements is done using a spectrometer with a row or camera detector. The signal is retrieved from the recorded spectrum by calculating the peak height or area. In the case of interference by neighboring lines, signal calculations may involve the fitting of a modeled signal to the measured spectrum. A background removal algorithm is typically used prior to peak height evaluation. The algorithm fits a curve to the background and subtracts it from the recorded spectrum. In this work, noise is defined as three times the background standard deviation at the wavelength of the analyte spectral line. The signal or signal-to-noise ratio (SNR) response to analyte concentration can be linear within several orders of magnitude if a line not prone to self-absorption is selected as the analytic line. Figure 2.5 presents the determination

of the signal and the species concentration in the case of zinc in water solution. The limit of detection (LOD) presented in Figure 2.5 b) is one the most common figures-of-merit for LIBS analysis. LOD is the concentration when the signal equals the noise i.e. SNR is unity. Mainly due to deviations from the equilibrium conditions, the LIBS

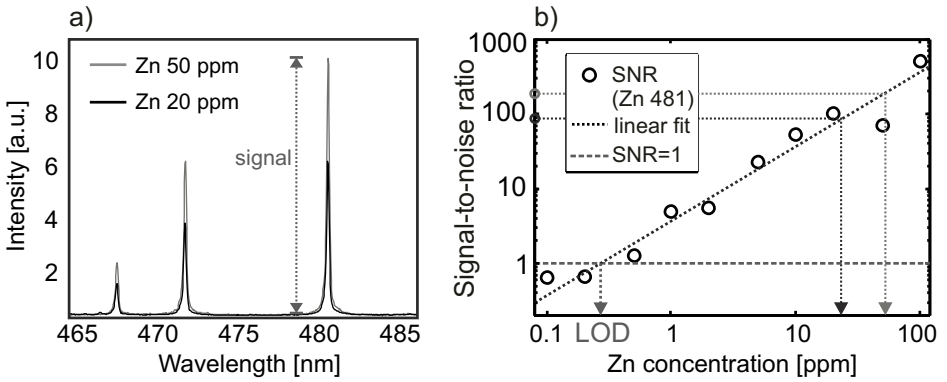

Figure 2.5 a) LIBS signal from zinc in aqueous solution using the instrumentation of **Paper 3**. b) Linear calibration curve of zinc and the retrieval of concentration. [Paper 1]

theory does not predict satisfactorily the observed signal and the quantitative analysis is best performed with calibration curves measured separately for each element. The calibration curves can be affected by sample composition because of matrix effects which mean variation of plasma electron density and temperature as a function of sample composition when analyte concentration is fixed. It also means variation in the analyte atom and ion number density due to the inhomogeneous vaporization of the sample. By sensitivity of the method it is usually meant the slope of a calibration line.

Randomness is always related to the LIBS signal formation leading to signal fluctuation between successive laser pulses.[25] Therefore, LIBS signal is typically an average value of several pulses and the relative standard deviation (RSD) or the ratio of standard deviation and the average signal, is used to describe the signal repeatability. The fluctuation can be diminished by the efforts of maintaining the excitation conditions unchanged or by signal processing techniques. Signal correction factors can be formed, for example, by measuring the laser pulse energy or plasma temperature from each pulse. Normalization can also be performed with the aid of internal standard which is an element whose concentration is known to remain constant in the sample. Figure 2.6 shows a calibration curve from the same data as in Figure 2.5 b) but the zinc signal

is divided by the signal from added sodium. After the normalization, the reliability of the measurement improved as indicated by the better correspondence between the linear fit and the data points.

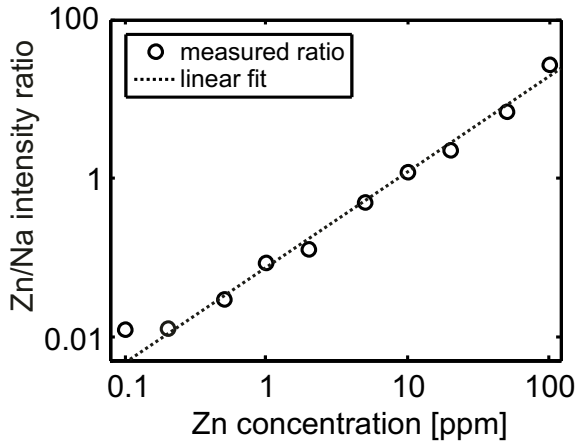

Figure 2.6 Zn/Na line intensity ratio calibration curve. Na 475.2 nm line was used for normalization. [Paper 1]

In this work, the plasma emission lifetime ranges from a few microseconds to tens of microseconds depending on the excitation pulse energy. At early times from the initial laser pulse, the LIBS spectrum is dominated by the intense background emission which decays faster than the line emission from the analyte atoms. The lines are also more easily resolved when the temperature and the electron density have lowered from their initial values as described in Section 2.4. The recording of LIBS spectrum is therefore often performed with a gateable detector to optimize the LIBS signal. The optimum delay with respect to the laser pulse and opening of the detector gate as well as the time the gate is kept open is transition specific. However, in a multicomponent analysis, single settings are typically used for all transitions, for simplicity.

Chapter 3

Measurement techniques for dissolved elements

THIS chapter lists instrumental techniques currently used in the quantitative analysis of dissolved elements. Most of the reviewed methods have been existing for decades and some are still under an active research. Methods can be divided into pure laboratory techniques and techniques possible to adapt for online measurements. Besides laser-induced breakdown spectroscopy (LIBS), other plasma spectroscopic methods, X-ray fluorescence, anodic stripping voltammetry, and ion chromatography are the only techniques that can measure a wide range of elements without an assembly of single parameter sensors or the need for element specific changes in the instrumentation. Application of LIBS to water samples is discussed in Chapter 4.

3.1 Current online analyzer technologies

Electroanalytical methods detect the trace elements by measuring the voltage or current in a sample cell. Two of the most common techniques are described here. An ion-selective electrode (ISE) contains a filling solution and a thin glass or crystalline membrane that allows the passage of specific ions. The potential of ISE depends

on the concentration difference of the specific ion between the solution where it has been dipped and the filling solution according to Nernst equation.[26] A concentration analyzer based on ISE has a separate electrode for each measured ion, a reference electrode of known potential and a potentiometer that measures the voltage between the ISEs and the reference electrode. A familiar example of such analyzer is the pH meter measuring the hydrogen ion concentration. Anodic stripping voltammetry (ASV)[27] is the most established method in the detection of metal ions in aqueous solutions. It involves a few minute preconcentration stage during which negative potential is applied to a working electrode to reduce the metal ionic species from the solution onto the electrode. At the second stage, the potential is raised continuously or stepwise and the current between the working electrode and an auxiliary electrode is monitored. Oxidation of the metal species back to the solution occurs selectively at different potential values which is observed as current peaks when the potential is scanned. The peak height is proportional to the concentration of the analyte in the original sample. The most common material for the working electrode is mercury although bismuth[28], carbon and gold[29,30] electrodes have shown to be a good low toxicity alternatives for some trace metals. Both ISE and ASV can detect ppb-level trace element concentrations and have a linear response to the analyte concentration when the concentration is very low. They are susceptible to interference due to the presence of other metals in the solution and to the changes of pH. In ASV, a buffer solution is used to ensure the proper oxidation state of the metals and to remove the potentially interfering compounds. The buffer solution also dilutes the sample in order to extend the dynamic range. The online measurement systems based on ASV are typically large fixed equipment. Electroanalytical devices require weekly maintenance due to analysis cell cleaning, calibration and replacing of the electrodes and used chemicals.

X-ray fluorescence (XRF)[31,32] is based on the removal of an inner electron from the K or L shell of an atom by primary X-ray radiation and a subsequent emission of secondary X-rays or fluorescence due to a relaxation where an outer electron is transferred to fill up the empty vacancy. In an energy dispersive analysis, the characteristic fluorescence spectrum of an analyte atom is recorded by a single photon detector. The charge produced by each X-ray photon in the semiconductor material of the detector is proportional to the photon energy, and the number of counts of the given energy photons is proportional to the concentration of the analyte in the sample. By averaging the signal over several minutes the current XRF analyzers can detect most elements in water at 1 ppm-10 ppb level[33,34] excluding the lighter atoms. The X-ray photons

emitted by elements lighter than silicon have low energy and the signal they produce is therefore typically too weak to be detected. The air between the sample and the detector also attenuates soft X-rays and, with light elements, the X-ray yield is low due to a competing nonradiative process of Auger electron ejection. The handling of XRF device requires precautions as it uses a source of penetrating ionizing radiation.

Biosensors cover many types of small size experimental analyzers where the interaction between the analyte and a bioreceptor element causes a physical signal, for example, optical, electrical or mechanical changes that can be detected by a secondary detector.[35] Currently, there is no established biosensor method for analyzing dissolved elements. The bioreceptor can be a cell antibody, nucleic acid[35], enzyme proteins[36] or an entire cell[37] and it is ion or molecule specific. In optical biosensors, the receptors are attached to the surface of a waveguide - typically a fiber core, planar waveguide or a prism. The optical field interacts with the receptors via evanescent field that propagates outside the waveguide. In the case where the surface plasmon resonance phenomenon is utilized[38,39] to concentrate the evanescent field on the space occupied by the receptors, they cover the surface of a thin metal, usually gold, nanostructure between the waveguide and the water. The typical attenuated total reflection setting is shown in Figure 3.1. The binding of a specific metal ion to the bioreceptor changes

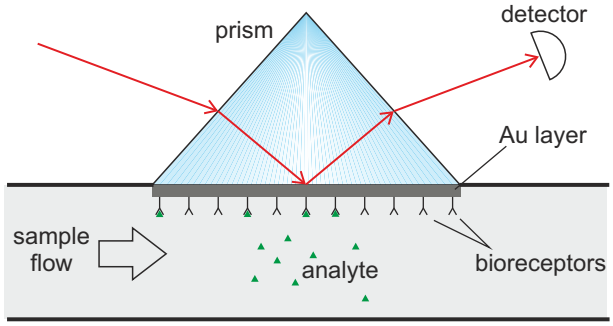

Figure 3.1 Typical attenuated total reflection configuration of plasmon enhanced biosensors. The gold and biosensor layers are not in scale.

its dipole moment and consequently the absorption, reflectivity, scattering or fluorescence properties of the receptors. The changes are observed by measuring the angle or the spectrum of the reflected light or spectrum of the light emitted or scattered by the bioreceptors. Optical biosensors have been reported being highly sensitive even down to ppt-level but have a very restricted dynamic range[38]. Other obstacles to their use in monitoring industrial waters are the interference due to multiple ions,

the pH-dependency[36] of the quantitative analysis and the need for chemicals to regenerate the biosensor surface. In electrical biosensors, the sensitivity and selectivity of the conventional electroanalytical methods have been improved by attaching the bioreceptors to the working electrode surface. Mechanical biosensors convert, for example, the intensity of acoustic waves or change in the receptor mass[40] into analyte concentration.

Spectrophotometry is a common technology in elemental analyzers that measure process and waste waters[39]. It measures absorption at certain wavelengths when light travels through a sample cell or cuvette. Bare atomic ions in a solution absorb light poorly in the visible or infrared regions and analysis in the UV region is unselective. Therefore a reagent is added in excess to the cuvette in order to form a colorful complex ion solution[41–43] and the method is alternatively called colorimetry. Also a buffer solution must be added to set the pH at the level where the complex formation is complete. A typical arrangement consists of a LED emitting at the wavelength specific to the complex ion under analysis and two detectors that measure the light intensity before and after the cuvette. The absorbance has a linear response to the analyte ion concentration according to Beer-Lambert law if interference due to other ions[43] is negligible. For each element, a separate cell, reagents and a light source are needed, and the technique is typically utilized in the analysis of a one specific ion. In spectrophotometric titration, the change in the absorption is monitored as the reagent is added to the water sample. The departure from the linear behavior indicates the equivalence point of the titration and the analyte concentration is calculated from the amount of added reagent.

Ion chromatography (IC) is an established method in water analysis[39]. It is used, inter alia, in the semiconductor industry to detect 0.1 ppb level impurity concentrations in deionized water. In addition to elemental ions, it can be used for the detection of charged organic and inorganic molecules. In IC, the sample is introduced into an ion separator column – a tube that has been filled with charged resin, for example modified polystyrene resin. The sample is transported through the column by a solvent or eluent such as hydrochloric acid. The drift velocity through the column is different for different ions in the sample and depends on ion charge and size as well as instrument specific factors like the eluent pH and flow rate. After the chromatography column, the eluent solution containing the separated ions is next conveyed to an eluent suppressor followed by a conductivity detector. The detector measures the solution conductivity

as a function of retention time in the ion separator column. The conductivity has a peak whenever specific ions from the original sample passes through the measurement point. Typical measurement lasts about 15 min. The purpose of the eluent suppressor is to replace the eluent with a solution such as water that has a low conductivity and thus to improve the SNR of the ionic peaks. The conversion is performed using ion exchange membranes.

In **capillary electrophoresis** (CE) the sample is introduced to a submillimeter capillaries filled with an electrolyte solution.[39] The source end of the capillary is submerged in a container containing an anode and the destination end has a cathode. The ions separate due to their different electrophoretic mobility in a static electric field. The detection of the separated ions can be performed electroanalytically or optically by colorimetric absorption measurement and, after chemically adding a fluorescence marker, with laser-induced fluorescence. Detection limits at 10 ppb level have been achieved for dissolved metals with experimental instrumentations.[44] In a laboratory, CE can be combined with mass spectrometry for achieving very low detection limits.

3.2 Laboratory atomic spectroscopy

In **inductively coupled plasma optical/atomic emission spectrometry** (ICP-OES/ICP-AES)[45] argon is injected through a coil. A radio frequency current flowing in the coil generates a time-varying magnetic field and a discharge arc typically from a Tesla coil is used to create the first charge carriers in the initially nonconducting argon. After the plasma ignition, the magnetic field induces current loops inside the conducting plasma medium and thus supplies power to the discharge. Stable plasma having the temperature near 9 000 K is sustained due to the collisions of charged particles and argon atoms. The aerosolized sample is injected directly to plasma whereupon the constituents are dissociated and the trace element atoms are repeatedly excited, relaxed, ionized and recombined. Light emission from the plasma is directed to a spectrometer in order to detect the trace element specific wavelengths. Multiple atomic emission spectroscopy methods similar to ICP-OES/ICP-AES exist and differ only in their way of producing the plasma.[21,46] These are, for example, capacitively coupled plasma, DC or AC current arcs, microwave discharges and heating vapors in a high temperature furnace. LIBS is also closely related to these technologies although,

in LIBS, the plasma is transient and lasts only a few microseconds. Besides observing the emission, plasma can be used only for atomization and the constituent atoms can be extracted into a mass spectrometry as in inductively coupled plasma mass spectrometry (ICP-MS). ICP techniques are highly sensitive and selective but, for the present, intended only for laboratory use due to the sample preparation procedure as well as size and price of the instrument.

Atomic absorption spectroscopy (AAS) involves atomizing the sample in the temperature between 1700-3300 K and a consequent absorption measurement.[39,45] Most common AAS technology is the flame AAS where the sample is nebulized into a flame. The light source is typically a hollow cathode lamp that emits a line spectrum of the atoms one aims to measure from the sample. Flame AAS requires constant calibration and the detection limits of metals lie in the ppm range. The sensitivity can be improved by using different atomizers, as in graphite furnace AAS (GF-AAS) at the expense of extra sample preparation and measurement time.

Chapter 4

Laser-Induced Breakdown Spectroscopy of dissolved trace elements

LASER-induced breakdown spectroscopy (LIBS) is an appealing technology for online and *in situ* monitoring of process and waste water streams and the state of the environment. It is selective for a wide range of elements and the straightforward analysis is free of chemicals. Unfortunately, LIBS is far from an ideal technique for the analysis of water and its use in these important applications has not become a common practice. This chapter reviews the challenges and the previous approaches of LIBS of aqueous samples and presents the advantages of performing the LIBS analysis from a dry particle generated from a droplet of the sample solution.

4.1 Elemental analysis of liquids using LIBS

The reported LIBS detection limits for dissolved transition metals have remained above ppm-level when the analysis has been performed directly from water without any sam-

ple preparation[47–49] and are thus worse than what is obtained using ICP or electroanalytical techniques. The mechanisms that disrupt the LIBS analysis of aqueous media are described in several studies concerning biotissue ablation, especially the eye surgery research[50–52] and in more recent laser-induced breakdown literature[53,54]. When plasma forms inside liquid, it cools down quickly compared with laser-induced plasma in air. The energy supplied by the laser pulse is consumed by the vaporization of the liquid, the conduction of heat to the liquid and mechanical work involved in formation of shockwaves and a cavitation bubble of water vapor about the plasma.[50] The high plasma pressure[50] inside the expanding bubble causes pressure and Stark broadening which, together with short-lived emission[55], weaken the amplitude and broaden the linewidth of analyte spectral lines. If the laser is focused on the liquid surface, plasma can be formed in air. However, the rippling of the liquid surface changes the mass vaporized from the sample and deteriorates the reproducibility. Plasma expansion also creates splashes and aerosols above the surface that scatter the light of the subsequent laser pulse and are likely to contaminate optical components. Collection of analyte emission is distracted in both methods due to bubbles and aerosols, and part of the emission is quenched by chemical reactions between water vapor and analyte atoms and ions. The following paragraphs list the various techniques and sample preparation procedures that have been used to circumvent some of the problems in LIBS of aqueous solutions.

Depositing the sample on solid surface or sample pelletizing transforms the measurement virtually to the analysis of solids. The sensitivity depends on the capability to accumulate the sample to the analyzed surface that can be a filter paper[56,57], a graphite disk[58], a wooden slice[59], an electrochemical electrode[60] or an ion exchange membrane[61]. The drawbacks are the compromise between the sensitivity and time required for the sample preparation and possible inhomogeneous distribution of trace elements on the surface. Compressing a dried sample into a pellet has also been reported[62] as well as the analysis of a frozen water sample[63].

Analysis of flowing liquid is a fast and low-cost sample preparation method for improving the liquid surface analysis. If the water layer is thin enough like in the cases of jets in air or thin planar streams on an inert surface, the vaporized sample amount is determined by the laser focus spot size and can be held constant. The reproducibility is further increased due to the absence of aerosols and splashes if the whole sampled material is vaporized. Reported detection limits for different elements

vary in the range of 0.1 ppm and 100 ppm for measurements in water[47,64,65] and in engine oils[66].

UV excitation wavelengths from an excimer laser such as ArF, XeCl or KrF lasers have been reported producing cooler plasma with similar electron density as longer, more traditional laser wavelengths. The UV photon energy is adequate for the photoionization of most elements and the two-photon photoionization of water which increase the electron density. On the other hand, plasma does not efficiently absorb UV wavelengths and does not get heated by the absorption of the trailing edge of the laser pulse. As a result, the LIBS spectrum shows the analyte emission lines over a weak continuum emission.[67,68] Obtained detection limits have been near 1 ppb for alkali and alkali earth metals and 300 ppb for Pb[65,69].

Generation of aerosols by nebulizer and focusing the LIBS laser to the liquid aerosol cloud is a robust technique for attaining detection limits on the order of 0.1 ppm for some trace metals in the original solution[70,71]. Although the sample preparation method reduces the analyte species concentration in the focal volume, the signal is more than compensated by allowing the plasma to form in gaseous medium. Analysis is performed using laser pulse energies greater than 100 mJ as a significant portion of the energy is consumed for vaporizing the droplets within the plasma.

Single droplet sampling is possible using a piezoelectric or thermal single droplet generator to inject one droplet on demand or a train of droplets towards the LIBS focal volume. Single droplet vaporizing can be based on statistical probability when the generator is producing droplets at certain frequency[72,73] or the droplet generation can be synchronized with the excitation laser[74]. Also, the approaching droplet may trigger the laser with the aid of a scattering based sensor[75]. The droplet diameters from the piezoelectric generators are typically between 40-100 μm and the sample consumption is naturally much less compared with analysis of nebulized liquid aerosol. The reported detection limits are similar to the analysis of droplet clouds.

Double pulse configuration has been used to lengthen the duration of line emission from the plasma in several studies. It can be applied to the surface, bulk, jet[76] or aerosol analysis configurations. With the second laser pulse, the liquid analysis can be transformed into an analysis of water vapor.[77] Significant enhancement factors compared with single pulse excitation have been presented for example in papers by Nakamura et al.[78], Cremers et al.[49] and Scaffidi et al.[79].

4.2 Preconcentration by droplet evaporation and sampling considerations

Laser-induced breakdown spectroscopy is applicable to dry aerosol analysis. Drying small droplets generated from trace metal solutions have been used for calibration and proof-of-concept demonstrations in several studies concerning monitoring of pollution particulates mainly from waste and coal combustion [80–86]. Similar rapid liquid-to-solid matrix conversion can also be utilized in the LIBS analysis of water. The benefits are:

1. Removal of water increases the mass concentration of the analyte atoms in the droplets by a factor of $10^6 \times c_{tot}^{-1}$ where c_{tot} is the total mass concentration of the impurities in water in the units of ppm.
2. Absence of all the water-related factors suppressing the LIBS signal.
3. Possibility to use laser pulse energies significantly lower than in the direct analysis of water or droplet clouds.

The third point enables recording the emission with a better signal-to-noise ratio and it is an important feature when the technology is transferred to industrial use.

In order to achieve sub-ppm detection limits for trace elements in the original solution with acceptable measurement time, the aerosol must be sampled efficiently and reproducibly. Even slight changes in the sampled aerosol mass affect the analyte emission in the plasma [87]. The number of particles sampled by a single laser pulse is determined by the number concentration of particles in the focal volume and the plasma volume. If high particle concentrations are used, the relative deviation in the amount of sampled particles is small and the plasma takes an ensemble average over the aerosol size distribution. On the other hand, concentrating particles inside a measurement chamber creates contamination related issues and slows down the measurement response time. Also, the high sample mass content in the plasma can lead to incomplete vaporization, matrix effects and overall plasma cooling. Another extreme to fix the sampled mass is to vaporize a single particle of a monodisperse aerosol with each laser pulse whereupon the vaporized analyte mass per each pulse is very small. For example, the detection of 10 ppb trace element concentration in water corresponds detection of only 5 fg in a 100 μm droplet. By increasing the initial droplet size, more analyte atoms

can be brought to LIBS focal volume but to maximize the method's capability for quantitative analysis, the dry particle size should remain below the threshold for the vaporization and atomization of the whole particle[82,88] with the laser pulse energy in use. In the study by Carranza and Hahn[89], the upper size limit was determined from the point where the silicon LIBS signal response to silica particle size deviates from the linear behavior.

The size of the residual dry particles formed from water droplets that contain dissolved salt as impurities can be estimated using the equation[90]

$$d_{p,dry} = \frac{d_{p0}}{100}\left[c_{tot}\frac{\rho_w}{\rho_s}\right]^{1/3}. \tag{4.1}$$

In Equation 4.1, $d_{p,dry}$ is the equivalent spherical diameter of the residual particle, d_{p0} is the initial droplet diameter and ρ_w and ρ_s are the density of the aqueous solution and the mean density of the ionic impurities, respectively. After drying, droplets of initial diameter in a range of 10–100 μm generated from water containing, for example, NaCl between 100–2000 ppm forms particles having diameter between 400 nm and 10 μm. Any soluble salt can be added in excess to the sample solution prior to dropletizing for the purpose of fixing the particle size, increasing the aerosol monodispersity or to be used as an internal standard in the signal processing. In this work, NaCl was used as an additive in **Papers 1** & **2** whereas no additive chemicals were required in the instrumentation of **Papers 3** & **4**.

In single particle measurements, a control or detection of the particle position is required as the hitting accuracy to a single particle or the sampling rate is less than 1%[91] by merely focusing the LIBS beam to an aerosol flow. Also, several single particle spectra would need to be recorded to average out the effects caused by fluctuation in the particle position[92] within the plasma. The number of averaged spectra can be reduced significantly if the particle location is precisely controlled i.e. the particle is trapped.

Chapter 5

Elemental analysis of single aerosol particles

REPEATABLE aerosol-based sampling and preconcentration of liquids for laser-induced breakdown spectroscopy (LIBS) starts from the generation of a monodisperse droplet or droplets which are representative samples of the water volume under analysis. The droplets are dried, and the solid residual particles containing the trace elements are introduced repeatably to LIBS focal volume. The latter part requires control of single particles that can be realized via external electric, magnetic[93,94] or optical fields[95–97]. The applied forces can also be mechanical such as acoustic[98,99] and aerodynamic forces. Analysis can be performed to moving particles which are known to pass a certain point at a certain moment of time, or a particle can be trapped in all three dimensions for a long period. This chapter describes the instrumentation for LIBS analysis of single-particles that were designed and used within this work. The discussion therefore concentrates on particle manipulation by electric fields and aerodynamic focusing by sheath air.

5.1 Sheath air focusing

Narrow particle streams with a small divergence angle can be obtained using a nozzle having two coaxial orifices as depicted in Figure 5.1. The particles travel along the sample flow from the inner orifice and are surrounded by a greater sheath air flow from the outer orifice. If there is no mixing between the slower sample flow and the faster sheath flow, the sample flow will be pressed towards the center axis of the nozzle and a narrow particle beam is formed in the downstream.[100–103] Using the sheath air focusing, the particle beam diameters of only tens of micrometers can be achieved for micrometer-size particles without the risk for orifice clogging. LIBS of aerodynamic focused particles has been previously reported in Refs. 104–106. In Ref. 104, Park et al. used also aerodynamic lenses which consist of consecutive flow contractions and enlargements to focus the particles[100,107].

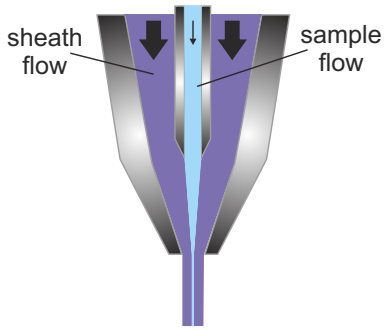

Figure 5.1 Principle of sheath air nozzle.

The experimental setup used in **Paper 1** is shown in Figure 5.2. It was modified from the bioaerosol fluorescence measurement system reported in Refs. 108–110. The initial 60 μm droplets are generated using an ink jet aerosol generator (IJAG) with an adjustable rate of approximately 3000 droplets/s. Before pouring the aqueous sample to IJAG cartridge, sodium chloride was added to the sample. The water is evaporated from the aerosol in a vertical tubular oven at 150 °C and a silica gel tube prevents the condensation of the water back on the particles. NaCl concentration of 600 ppm produces spherical and hollow dry particles of 5 μm in diameter with a monodisperse size distribution (Figure 5.3). The trace elements are present in the NaCl particles as impurities. After a balancing chamber, particles travel through a virtual impactor which concentrates the number density of the monodisperse particles by a factor of

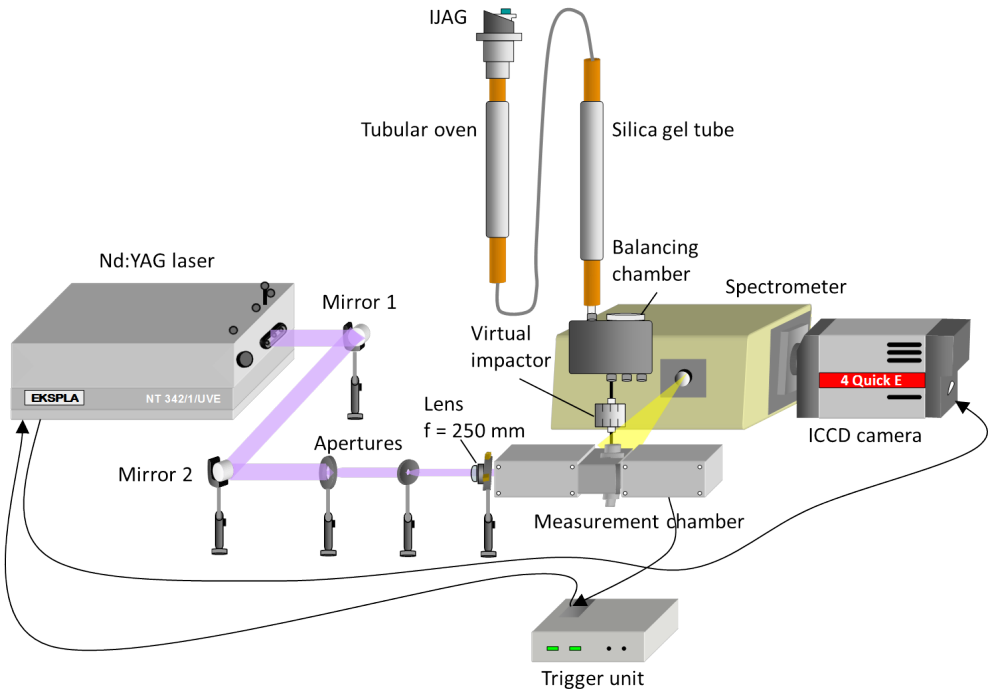

Figure 5.2 Single particle LIBS instrumentation of **Paper 1**.

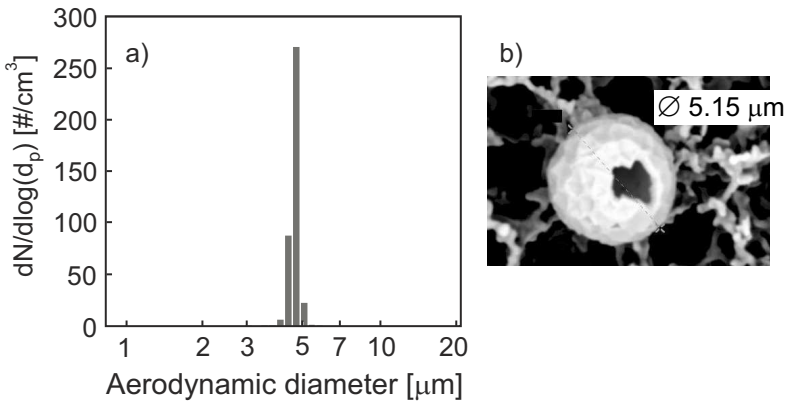

Figure 5.3 a) Size distribution of NaCl particles. b) Scanning electron microscope image of NaCl particle that has been adapted from publication by Putkiranta et al.[110]

10 to 100 particles/cm^3. The sample flow enters the measurement chamber from the sheath air nozzle having an outer diameter of 300 μm and passes through a beam

from a 650 nm continuous wave (CW) diode laser seen in Figure 5.4. The laser light scattered by a particle is detected by a photomultiplier tube (PMT) which sends a trigger signal to an actively Q-switched 10 Hz Nd:YAG laser. After a delay of 209 μs, the laser emits a 5 ns LIBS excitation pulse. During that time the same particle traveling at speed of 10 m/s has moved from the position of the CW beam to a focal point of a parabolic mirror. The excitation pulse hits the particle at this focal point and the plasma emission is collected using the parabolic mirror and focused into a spectrometer.

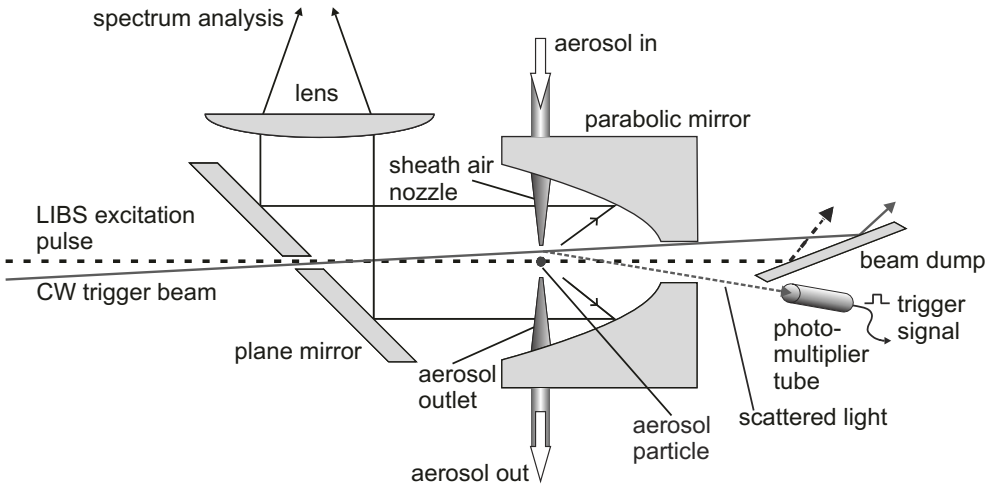

Figure 5.4 Schematic of measurement chamber. [Paper 1]

The diameter of the aerosol flow is approximately 100 μm which is about twice the size of the excitation laser focal spot. The particle concentration ensures the existence of a single particle in the vicinity of the focus within the majority of the laser duty cycles. Due to uncertainties in the sampling, especially in the precise horizontal and vertical position of the particle with respect to focal spot at the time of the plasma initiation, the LIBS signal fluctuates from pulse to pulse. Typically 400 single-shot spectra are collected and averaged per one LIBS measurement. About half of the recorded spectra are good enough to proceed to the averaging phase i.e. the sampling rate is 50%. Spectra corresponding insufficient hits are recognized and rejected by an algorithm that inspects the intensity of Na lines. Thus, the data acquisition lasts about 40 s and consumes about 14 μl of the sample solution whereas the response time of the system to the changes in the trace element concentration of the solution

in the IJAG cartridge is about 3 min. The signal processing program uses the stable sodium matrix also as an internal standard for correcting the fluctuating signal values and thus improving the quantitative analysis. In addition, Na lines are utilized in the wavelength calibration. The proportion of the successful spectra to the total number of recorded spectra could be improved from the 50% value by achieving even narrower aerosol flow after the sheath air nozzle. Another option is to increase the sensitivity of the triggering system towards particles traveling along the center axis of the flow for example by focusing the 650 nm CW laser beam. The first option, although technically more challenging, is preferred since it will also reduce the measurement time and the sample consumption.

A linear response between Zn concentration and LIBS signal was found up to 100 ppm level. The detection limits for Zn and Pb were estimated as 0.3 ppm and 0.1 ppm, respectively, using laser pulse energy of 14 mJ. At the detection limit, each particle contains 34 fg of zinc and 12 fg of lead. Due to constant sheath air flow through the chamber, no contamination was noticed on the optical components after the measurements.

5.2 Electrodynamic levitation

The electric trapping or levitation of particles have origins in Millikan's electrostatic balance and his experiment for measuring the charge of an electron in 1909[111]. While developing a new mass spectrometer in 1953, Paul and Steinwedel[112,113] found that ions could be stably trapped in a space surrounded by four hyperbolic electrodes which were connected to a sinusoidal AC voltage source. This quadrupole ion trap known as the first electrodynamic balance (EDB), did not enable an optical access to the trapped particle. In 1960, Müller found that only a single toroid with an AC potential can trap microparticles[114]. Since Müller, various electrode configurations[115] have been designed which possess the trade-off between the optical accessibility and stability of the particle in the trap. To date, the EDB has been a tool in many aerosol studies concerning the measurements of mass and charge, studies of chemical reactions, combustion research, Mie theory and many others.[115] EDB-assisted spectroscopic analyses of single particles have been performed by means of IR absorption[116], Raman[117,118], and fuorescence spectroscopies[119,120]. Study of plasma properties after a laser-induced

breakdown of a single LiH particle levitated in vacuum using the EDB configuration of Wuerker et al.[121] was reported by Haught and Polk in 1966[122]. In addition to **Papers 2-4**, LIBS experiment on electrodynamic levitating particle has been reported in a 2013 PhD thesis[123]. A LIBS analysis of an electrostatically levitated aerosol cloud has also been demonstrated by Dutouquet et al. by using an RF discharge cell[124].

A coaxial cylinder electrode geometry first presented in Ref. 118 provides a stable trap with good visibility to the particle and was therefore selected in the EDB-LIBS instrumentation. A drawing of the electrodes and the hexagonal measurement chamber built in this work are seen in Figure 5.5. The outer cylinders are grounded whereas

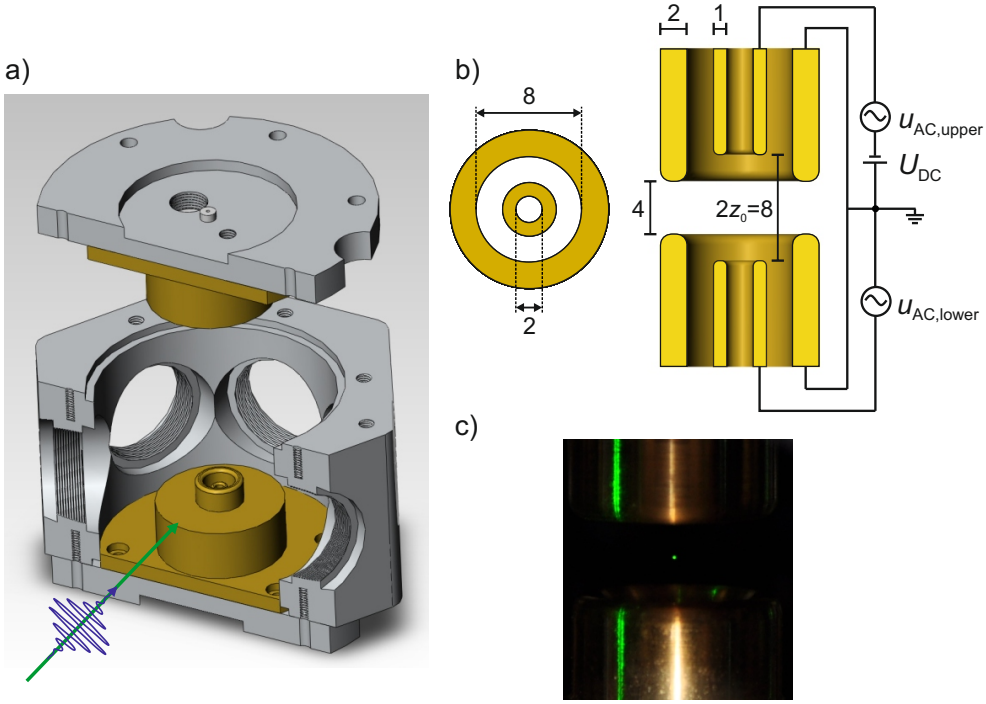

Figure 5.5 a) Cross-section view of the measurement chamber with top cover lifted upwards. The pulsed (violet arrow) and the CW (green arrow) laser beams enter the chamber horizontally through one of the chamber windows. The plasma emission is collected from another window at 60° angle from the laser beam axis. b) Electrode structure and connection diagram. c) Droplet levitating between the electrodes; ready to be analyzed [Paper 2].

a high-voltage AC potential is applied to the inner electrodes. Single droplets 74 μm in diameter are generated one at a time from a piezoelectric droplet generator that points perpendicularly to the center axis of the chamber. The droplet is charged by

an aperture disk in front of the generator orifice. The trajectory of the droplet is adjusted to reach the space between the inner cylinders by controlling the waveform that drives the piezo. Between the electrodes, the charged droplet starts to oscillate at the AC field frequency. The differential equation of motion is formed according to Newton's second law by summing up all the forces acting on the liquid particle. These are the frictional force due to ambient gas given by the Stokes law, electric force due to high voltage AC field and due to small DC voltage between the lower and the upper electrode, gravitation, and any external force such as laser radiation pressure.

$$-3\pi\eta d_p \frac{\mathrm{d}\mathbf{r}}{\mathrm{d}t} + q\mathbf{E_{AC}}(\mathbf{r},t) + q\mathbf{E_{DC}}(\mathbf{r}) + m_p\mathbf{g} + \mathbf{F_{ext}} = m\frac{\mathrm{d}^2\mathbf{r}}{\mathrm{d}t^2}, \tag{5.1}$$

where d_p and q are the size and the charge of the droplet or a dry particle and η is the gas viscosity. In the cylindrical EDB configuration, the forces in the horizontal directions are negligible. If the initial velocity of the droplet is correctly adjusted, the droplet gets quickly trapped in the xy-plane. It is therefore adequate to inspect the movement only in the vertical (z) direction and Equation 5.1 can be written in terms of dimensionless parameters $Z = z/z_0$ where $2z_0$ is the distance between the inner electrodes, and $\tau = \omega_{AC}t/2$[125],

$$\frac{\mathrm{d}^2 Z}{\mathrm{d}\tau^2} + \delta\frac{\mathrm{d}Z}{\mathrm{d}\tau} + 2\beta Z\cos(2\tau) = \sigma. \tag{5.2}$$

The control of the trapping is most conveniently done by the adjustment of the AC voltage angular frequency (ω_{AC}) and amplitude ($\hat{u}_{AC}$), and the DC voltage (U_{DC}). For the drag parameter δ, field strength parameter β and for the parameter σ which determines the amplitude and the midpoint of the oscillation, the following proportionalities hold

$$\delta \propto \frac{1}{d_p^2\omega_{AC}}, \quad \beta \propto \frac{\hat{u}_{AC}}{\omega_{AC}^2 U_{DC,0}}, \quad \text{and} \quad \sigma \propto \frac{{}^{U_{DC}}\!/_{U_{DC,0}} - 1}{\omega_{AC}^2}. \tag{5.3}$$

The equation has a stable solution, meaning the droplet does not escape, for certain (δ, β) points shown in Figure 5.6. The stable solution is an equilibrium point at the center point of the electrodes if $\sigma = 0$ which happens when the DC potential difference causes a force that compensates the gravitation and the external forces. Then $U_{DC} = U_{DC,0}$ where $U_{DC,0}$ satisfies the equation

$$qC_0\frac{U_{DC,0}}{2z_0} = m_p g - F_{ext,z}, \tag{5.4}$$

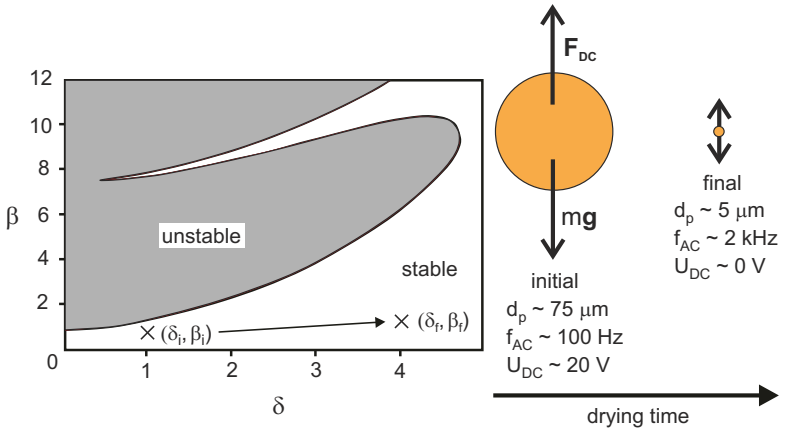

Figure 5.6 Part of the (δ, β) pairs[125] that result in successful trapping of the particle. The drying of the droplet is compensated by an increase in the AC frequency and decrease in the DC offset.

where C_0 is a geometrical constant. After the ejection from the generator, the mass of the droplet reduces by evaporation and the droplet diameter decreases towards the dry particle size. To prevent the increase in β to drive the solution of Equation 5.2 unstable, the EDB parameters must be adjusted during the drying process. In the instrumentation of this work, the effect caused by the reduction in the particle size is compensated by increasing the AC frequency $f_{AC} = \omega_{AC}/2\pi$ linearly from the initial value of 50-200 Hz to a final value of 1.6-1.9 kHz and by decreasing the DC voltage U_{DC} exponentially from 15-25 V to a value $|U_{DC}| < 1$ V. The amplitude of the AC potential $\hat{u}_{AC}$ is kept at 950 V. The rate which the AC frequency is raised depends on the relative humidity (RH) inside the chamber and weakly on the total impurity concentration in the analyzed water. The applied electrode potentials during the droplet trapping starting from the droplet generation at t=0 can be written as

$$\begin{aligned} u_{AC,upper} &= \hat{u}_{AC}\sin(\omega_{AC}t) - U_{DC}, \\ u_{AC,lower} &= \hat{u}_{AC}\sin(\omega_{AC}t), \end{aligned} \tag{5.5}$$

where

$$\omega_{AC} = \begin{cases} \omega_{AC,i}(d_{p0}) & 0 \le t < t_1 \\ S_\omega(\mathrm{RH}, c_{tot})(t - t_1) + \omega_{AC,i}(d_{p0}) & t_1 \le t < t_2 \end{cases}. \tag{5.6}$$

In Equation 5.6, t_1 is a short delay between the droplet generation and the start of the frequency increase and t_2 is the time which the frequency reaches the levitation

frequency maximum of the experimental setup, about 1.9 kHz. The LIBS excitation laser pulse is triggered after the desired droplet drying time set by the user $t_{trigger}$ has elapsed. After the laser pulse, the AC frequency is decreased gradually to the initial value. The time parameters of the setup and the control of the AC frequency are illustrated in Figure 5.7. t_{trap} shown in Figure 5.7 is the time the droplet settles at the trapping point. If the triggering time has been preset to be less than the settling time, the laser pulse is triggered right after the movement of the particle has stopped. Different time parameters in Figure 5.7 are summarized in Table 5.1.

In the instrumentation of **Paper 3**, t_1 and t_{trap} are determined automatically by inspecting the scattering signal from the drying droplet between the electrodes. The liquid particle scatter light from a CW laser and the scattered light is detected by a PMT or a low-cost photodiode which can be located behind a bandpass filter designed for the laser wavelength. Figure 5.7 a) shows the scattering signal using an inexpensive 3.5 mW 650 nm diode laser and a silicon photodiode. Furthermore, if the initial droplet does not get trapped or the droplet escapes the trap during the drying phase, it will be detected from the scattering signal and the program will iterate the slope S_ω and the initial frequency $\omega_{AC,i}$ until successful trapping is achieved.

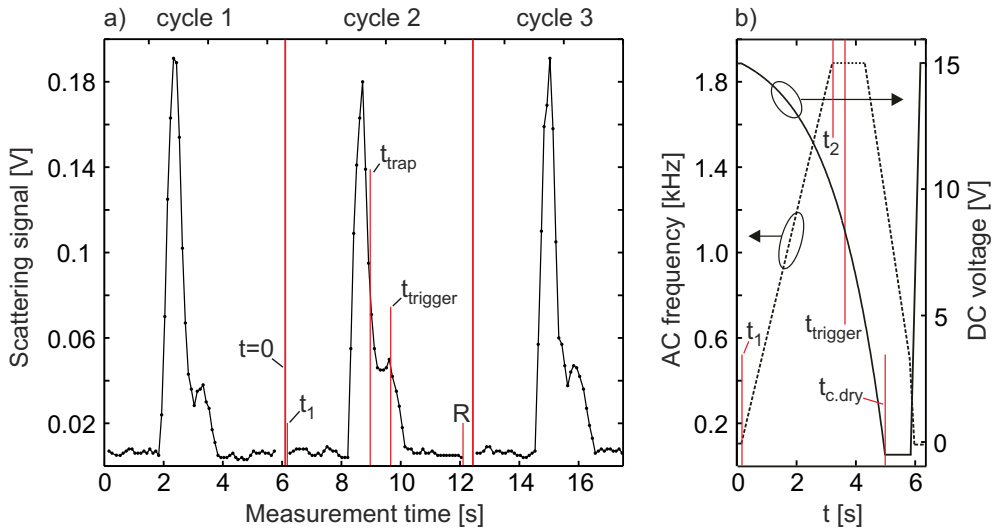

Figure 5.7 a) Example of scattering signal from the droplet and time parameters used for automatic operation of the system. Parameters are reset and a new droplet is generated by a subprogram starting at point R. b) Adjustment of AC frequency and DC voltage during one operational cycle corresponding the measurement in a).

Table 5.1. Summary of different time parameters. The chronological order of the times depend on the user defined settings and the ambient conditions and may be different than presented here.

Time parameter	Description
$t = 0$	Droplet is generated
t_1	Generated droplet first hits the illuminating laser beam and AC frequency starts to rise ($\approx$ flight time from droplet generator to electrodes)
t_2	Maximum AC frequency is reached
t_{trap}	Droplet settled at focal point
$t_{trigger}$	Trigger signal sent to laser
$t_{c.dry}$	Water in the droplet completely evaporated

If the relative variation in the water impurity concentration is small, for example due to additive salt, and the droplet is always completely dried, U_{DC} does not need to be adjusted at all during the drying. This was done in the experimental setup of **Paper 2**, where NaCl was used as the additive. In **Paper 3**, the LIBS analysis was performed to additive-free droplets at different evaporation stages using a DC voltage adjustment. The goal of the adjustment is to satisfy the condition $U_{DC} = U_{DC,0}$ throughout the process of drying to keep the droplet in focus. The DC voltage changes according to the function

$$U_{DC} = \begin{cases} U_{DC,i}(d_{p0}) & 0 \leq t < t_1 \\ U_{DC,i}(d_{p0}) - \exp\Big[\dfrac{t - t_1}{t_{c.dry}(RH, T_\infty, c_{tot}) - t_1} \\ \quad \ln\left(U_{DC,i}(d_{p0}) - U_{DC,f}(d_{p0}, c_{tot}) + 1\right)\Big] + 1 & t_1 \leq t \leq t_{c.dry} \end{cases}, \tag{5.7}$$

where the subindices i and f refer to the initial and final values. Due to a small external force that is lifting the dry particle, $U_{DC,i}$ has typically a different sign than $U_{DC,f}$ i.e. the force due to DC field points downwards after a complete drying. $t_{c.dry}$ is the time of the complete drying of the droplet. If the user defined drying time is longer than $t_{c.dry}$, the DC potential remains at $U_{DC,f}$ until $t_{trigger}$ has elapsed. In ambient temperature T_∞ and relative humidity $RH = S \cdot 100\%$, the complete drying time for micrometer sized droplets of pure water can be estimated using the relation [90]

$$t_{c.dry} = \frac{R\rho_w d_{p0}^2}{8 D_v M_w \left(\frac{p_d}{T_d} - \frac{p_\infty}{T_\infty}\right)}, \tag{5.8}$$

where the temperature of the droplet T_d and the partial pressures of water vapor on the surface of the droplet p_d and far away from the droplet p_∞ are

$$T_d = T_\infty + \frac{(6.65\text{K} + 0.345(T_\infty - 273.15\text{K}) + 0.0031\text{K}^{-1}(T_\infty - 273.15\text{K})^2)(S-1)}{1 + (0.082 + 0.00782\text{K}^{-1}(T_\infty - 273.15\text{K}))S}, \tag{5.9}$$

$$p_d = p_s(T_d), \quad p_\infty = Sp_s(T_\infty), \quad \text{and} \quad p_s(T) = \exp\left(16.7 - \frac{4060\text{K}}{T - 37\text{K}}\right)\text{kPa}. \tag{5.10}$$

In Equation 5.8, R, M_w and D_v are the molar gas constant, molar mass of water, and the diffusion coefficient of water vapor, respectively. Figure 5.8 represents how the relative humidity changes the theoretical evaporation curves of a 74 μm droplet at 20°C temperature. $U_{DC,i}$ and $U_{DC,f}$ are preset parameters. $U_{DC,i}$ affects the trapping

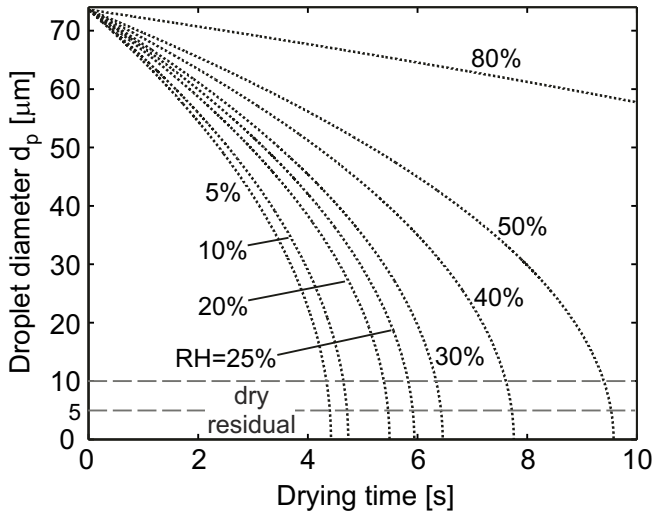

Figure 5.8 Theoretical droplet size as function of time spent in the trap for different RH values. The equivalent spherical diameter of the dry residual particle formed from a 74 μm droplet typically remains below 10 μm when $c_{tot} \leq 5$ g/l.

efficiency and the trapping time t_{trap} whereas $U_{DC,f}$ affects the exact trapping position after complete drying. Due to the $1/\omega_{AC}^2$ dependency of σ, the trapping point of the particle does not vary significantly as a function of droplet size when the AC frequency is high. A small offset from the condition of Equation 5.4 is therefore allowed and the system works without an active control of the $U_{DC,f}$. In the experimental setup of **Paper 3**, the long term standard deviation of the dry particle trapping points in the vertical direction was less than 4 μm.

In the EDB-LIBS measurements, the laser pulse is triggered only in the operational cycles where the particle trapping was successful and after successful trapping the laser will hit the particle every time. Hence, the particle sampling rate is 100%. Furthermore, the same amount of liquid is sampled by each pulse and all the recorded spectra are suitable for the final signal processing. The relative standard deviation of the emission line heights in single-shot spectra is about 15%. The signal can therefore be measured with less than 4% uncertainty after an averaging of only 20 single-shots. The combined data acquisition and processing time for 20 spectra in dry indoor conditions having RH about 25% lasts about 3 min and the total measurement time is similar to the sheath air focusing system. However, the sample consumption in the EDB-LIBS method is three orders of magnitude smaller. Also, the obtained limits of detection for Zn, Pb, and Ni in **Paper 2** were at 50 ppb level and are clearly better compared with the sheath air system which collects the plasma emission from over 35 times greater solid angle. 10-20 ppb level detection limits were further measured for Al, Mn, and Fe. Also, the persistent resonance lines of Na, K and Ca were estimated to yield significantly better limits of detection than what was achieved for transition metals. Increasing the amount of collected photons is considered the most convenient way to further improve the sensitivity of the current instrumentation. It can be realized by bringing a higher numerical aperture collection lens closer to the trapping point or guiding the emission to the spectrometer through several ports of the chamber. Because the position of the particle is precisely defined, the excitation laser pulse can be focused tightly on the particle. This gives an additional benefit of achieving a high laser fluence using compact size and cost-effective lasers which pulse energies are often limited to a value less than 10 mJ.

Chapter 6

Characterization of measurement parameters

CHARACTERIZATION of the key factors that influence the laser-induced breakdown spectroscopy (LIBS) signal from precisely controlled single droplets and dry particles was done in **Paper 3**. These are the degree of drying of the droplet, the displacement between the particle and the focal spot, the excitation pulse energy and the ICCD gate delay. The objective of the study was to further the sensitivity of the EDB-LIBS principle and account for the differences in performance and in used measurement parameters between this work and earlier LIBS literature. The main results reviewed in this Chapter can be applied to LIBS analysis of any precisely controlled micrometer sized aerosol particles regardless of trapping technique or aerosol origin.

6.1 Pulse energy in single particle measurements

Aerosols have been shown to act as seeds for the plasma formation in gas[20,126]. Thus, the LIBS analysis of a single particle can even be performed using laser irradiance that is below the threshold irradiance for the breakdown in the ambient gas. The recorded spectrum shows trace element emission from transitions associated with a

low upper state energy E_k and a high Einstein coefficient A_{ki} on top of a weak thermal background. Yet, using low laser pulse energies the particle can be incompletely vaporized which impairs the measurement reproducibility and detection of weaker transitions is prevented by the insufficient plasma temperature. Raising the pulse energy affects the LIBS signal through many processes:

Degree of sample atomization. The number of analyte atoms in the plasma can be increased up to the level where the whole particle, i.e. the maximum sample mass available, is vaporized. The laser pulse energy required for the complete vaporization depends on the particle size. This energy is 2–4 orders of magnitude greater than the energy needed to break the salt particle into its constituent atoms in consideration of the energies to accomplish the phase changes and to break down the ionic bonds.

Population of atoms in an excited state k grows first according to Equation 2.3 due to raise in the plasma temperature. The pulse energy where the occupation probability saturates depends on the magnitude of E_k of the specific transition and the temperature dependency of the atomic partition function $Z(T)$ of the element.

Ionization of the atoms reduces the analyte atom density in the plasma. The degree of ionization depends on the ionization energy of the atom and grows when the plasma temperature rises according to Equation 2.4.

Scattering of the emitting atoms. Typically, the whole plasma cannot be imaged with the spectrograph due to spectral resolution considerations. In **Paper 3**, the size of the vapor emitting the line emission of Pb was found to increase when the pulse energy was raised or when the gate delay was extended. Due to the expansion, a smaller portion of the emission can be collected with the narrow field-of-view of the spectrograph.

In **Paper 3**, the application of the moderate laser pulse energies of the order of 10 mJ in the single particle analysis was investigated. The laser beam was tightly focused on a 3 μm particle to improve the coupling of the optical energy to the particle dissociation. The LIBS SNR was found to be strongly dependent on the selection of the pulse energy and the gate delay. Pulse energy around 6 mJ with a gate delay of 1 μs was considered optimal in the detection of Pb at 405.8 nm wavelength in terms of SNR and pulse-to-pulse repeatability. At the optimum, the average irradiance was over 250 GW/cm^2. The result was also found to apply to other transitions having lower or comparable

upper state energy to that of Pb (E_k = 4.4 eV). On the other hand, the SNR of Zn 481.1 nm spectral line which has clearly higher E_k of 6.7 eV, was found to improve when the irradiance was raised to 450 GW/cm^2 using the fixed 1 μs delay. In this work, the LIBS signal saturated at significantly lower pulse energies than used in the single particle studies found in the literature[95,127] where pulse energies even above 250 mJ have been found to improve the signal. The differences are due to different focusing and plasma imaging optics, the used laser wavelength, particle size and the sampling stability of the particle.

Modeling can be used for selecting the optimal LIBS measurement parameters such as laser pulse energy for different analyte species. The dependencies of the processes

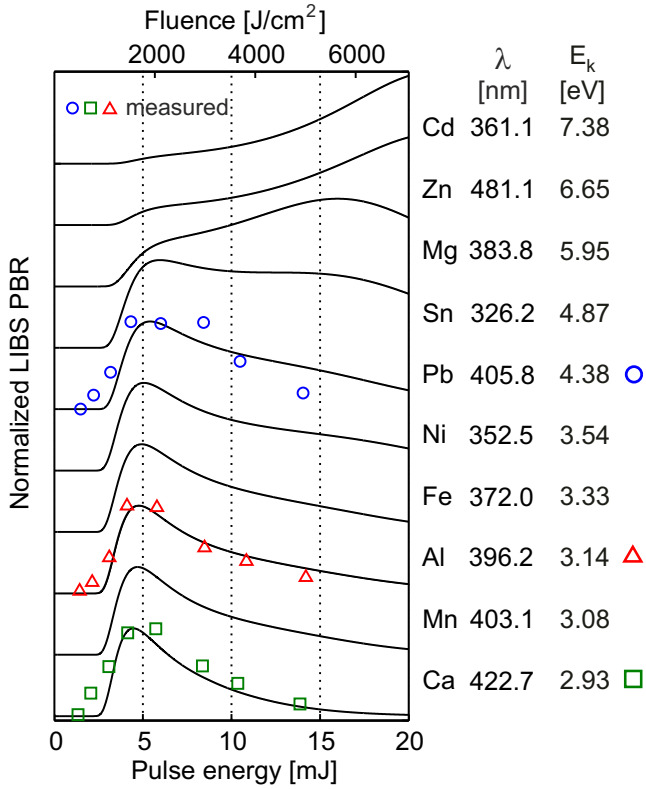

Figure 6.1 Estimated PBR versus laser pulse energy for strong emission lines of selected elements. The curves are arranged according to the corresponding transition upper state energies E_k which are listed in the rightmost column. The emission wavelength λ is shown in the middle column to identify the transition. The circles are measured values for Pb, Al and Ca.

listed above on pulse energy were evaluated computationally with the exception of the analyte vaporization degree which was treated as constant. Their combined effect on LIBS signal was estimated for several elements commonly monitored in process and waste water streams. Peak-to-background ratio (PBR) that behaves in the similar way as SNR, versus pulse energy is presented for ten elements in Figure 6.1. The curves have been normalized and shifted vertically for clarity and apply to the detection time window of 1 μs gate delay and 20 μs gate width. The selected transitions are considered the most persistent within the operating wavelength range of the spectrograph used in this work. Comparison between the measured and calculated values is shown for Pb, Al and Ca.

For calculating the curves in Figure 6.1 assumption of local thermal equilibrium (LTE) was made and the peak intensities were estimated using the equilibrium equations listed in Sections 2.2 and 2.3. The equations require information about the plasma temperature T and electron density n_e as a function of pulse energy. They were determined separately at pulse energies greater than about 4 mJ from the relative intensities of calcium ionic line at 393.4 nm and atomic line at 422.7 nm and the width of hydrogen β line at 486.1 nm using the Equation 2.8, respectively. The dependencies are shown in Figure 6.2. The total number density of the analyte species $\Sigma_r n_r$ was estimated by imaging the plasma size and by assuming a uniform distribution of the analyte species within the plasma. The plasma vertical diameter was found to increase linearly from 0.6 mm to 1.5 mm between the pulse energies of 4 mJ and 20 mJ. Nearly linear growth of the plasma diameter was also reported in Ref. 86. The number of spontaneous emission photons incident on the ICCD photocathode was calculated for each transition using the Equation 2.6, and taking into account the solid angle for light collection, the slit width and the efficiencies of the optical components between the particle trapping point and the ICCD. The conversion factors for photoelectrons per photocathode input photon and analog-to-digital converter (ADC) counts per photoelectron for different gain settings are given in the ICCD camera test data sheet provided by the manufacturer. In PBR estimations, the evolution of the background when the pulse energy is raised was measured for each wavelength due to its complex shape especially at near-UV wavelengths. After the signal conversions, both the spectral line and the measured background intensities have the units of ADC counts, and the peak-to-background ratio can be formed.

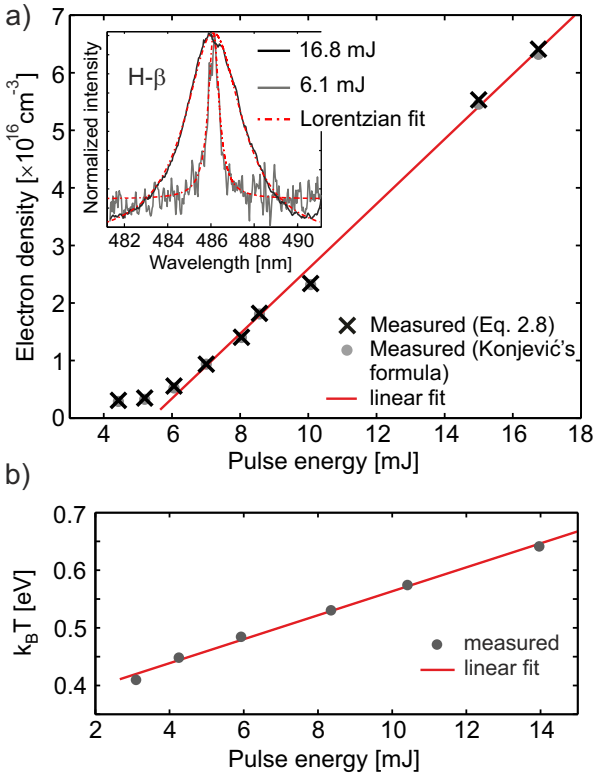

Figure 6.2 a) Plasma electron density as function of laser pulse energy. The electron density given by Equation 2.8 was used in the PBR calculations. The electron density given by Konjević's formula in Ref. 128 is shown for comparison. The inset shows the H-β line at 6.1 mJ and 16.8 mJ pulse energies. The H-β line was measured from laboratory air by averaging 300 spectra. b) Plasma k_BT in the units of eV versus laser pulse energy. Measured from the relative intensities of Ca lines.

6.2 Influence of preconcentration

The capability to highly preconcentrate the trace elements in the sampled water volume is the main idea behind the approach taken in the instruments of this work. In previous LIBS measurements of droplets[71,72], the signal has been found to enhance when smaller droplets are generated possibly due to more complete atomization of the sample. In the single droplet evaporation approach, the size of the initial droplet and the sampled analyte mass remain constant and only the amount of water is reduced. The experimental EDB-LIBS setup allows the investigation of the effect of the water content in the drying particle up to the formation of a dry residual particle

and thus the evaluation of the actual importance of the complete droplet drying. The measurement requires the DC voltage adjustment function to have carefully selected parameters in order to drive the droplet to the LIBS focal volume quickly after its ejection. The measurements were performed in the relative humidity of 25% where the time for complete evaporation for 74 μm water droplet is about 6 s. The benefit of preconcentration is obvious by looking at Figure 6.3 where the signal shows enhancement throughout the drying period. The signal remains constant at the saturation level even after significantly longer trapping times than presented in Figure 6.3.

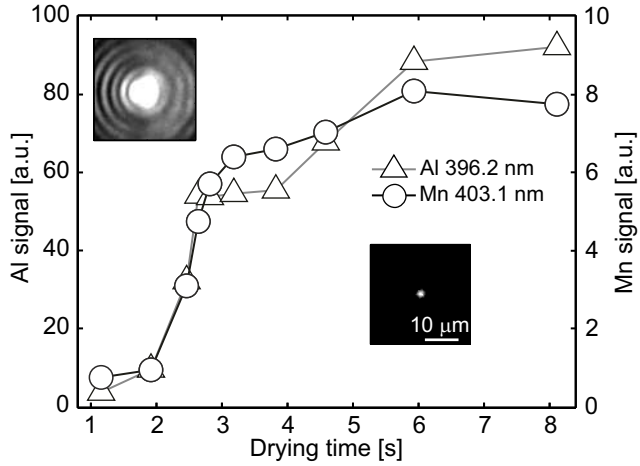

Figure 6.3 LIBS signal from 1 ppm Al and 1 ppm Mn as function of drying time. The insets show 30μm×30μm CMOS camera images of the particle at 1 s and 6 s after the droplet launch. [Paper 3]

6.3 Exact position of single particle

Several studies have reported major LIBS signal variation when the position of the particle shifts tens or hundreds of micrometers with respect to the focal point of the exciting laser[74,75,92,95,129,130]. Also, using similar particles, lower detection limits were found when the particle was precisely trapped in **Paper 2** instead of moving along about 100 μm wide air flow in **Paper 1**. For large displacements, the particle position is near the plasma boundary where the temperature is lower. As a result, the atomization is incomplete and the emission may remain localized during the detection

time window[131,132]. Localization fluctuates the signal because the detector field-of-view contains only a thin slice of the plasma volume instead of the whole plasma. The effect can be mitigated by using higher pulse energy and a longer gate delay time[133] so that the analyte atoms have enough time to diffuse to the overall plasma volume.

In **Paper 3**, the effect of particle position was studied in the low pulse energy regime, and the particle was shifted only a few micrometers by adjusting the DC voltage between the upper and the lower EDB electrode. The image of the particle was held in the middle of the spectrometer slit in order to have a constant light coupling efficiency at each position. The analyte line emission was found to remain stable when the position of the 5.5 μm particle was moved within the 19 μm focal spot diameter as shown in Figure 6.4. The fluctuation of the signal within the laser focal

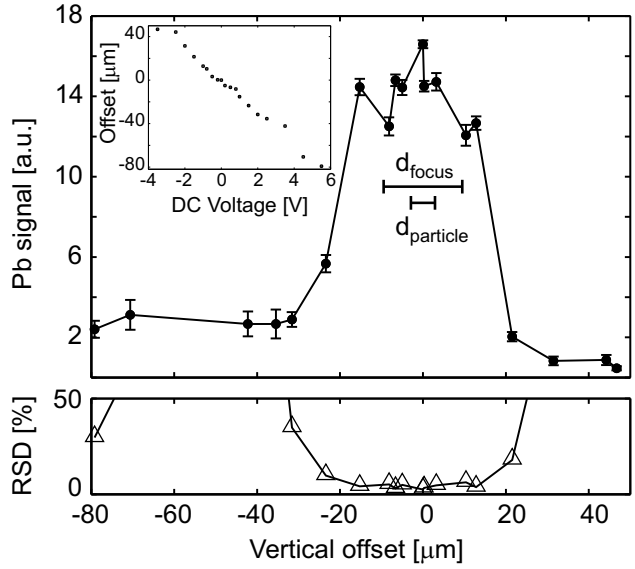

Figure 6.4 LIBS signal from Pb and signal RSD as function of particle position. Particle displacement versus bias voltage between upper and lower electrodes is shown in the inset. [Paper 3]

area is systematic and expected to arise from a non-Gaussian transverse intensity distribution containing local hot spots. When the particle lies about 20 μm outside the beam path, the emission intensity is at a significantly lower level and the shot-to-shot fluctuation is evidently higher. Having a particle in the beam path increases the absorption of the laser pulse by lowering the breakdown threshold of the ambient gas as discussed earlier. When using low laser pulse energies, the earlier breakdown may

have significant effect on the plasma temperature and electron density[134], and hence the degree of analyte atomization and excitation.

Chapter 7

Applications

The applicability of the LIBS methodologies introduced in this work to the trace element analysis of industrial waters was demonstrated by measuring water samples collected from different mining areas and a municipal wastewater treatment plant. The qualitative results obtained with EDB-LIBS system are discussed in the following section. The concentration of microbes also affects the water quality. The initial experiments of detecting microbial particles in water by combining laser-induced fluorescence (LIF) and LIBS are presented in detail in **Paper 4** and the principle is reviewed in this Chapter.

7.1 Multicomponent analysis

Water samples were collected from mines producing gold, nickel, zinc and copper ores and from a large municipal waste water treatment plant having the population equivalent (PE) number about 500 000. The samples were taken either from the middle of the water treatment process or from the stream of the treated effluent that is flowing to the nearby lake. Part of the samples were provided with a reference measurement data. The reference measurements were carried out according to standardized measurement procedures using ICP-OES (ISO 11885), ICP-MS (ISO 17294) and spectrophotometry

(Finnish Standards Association SFS 3026 and SFS 3028).

The LIBS spectra were recorded using fixed ICCD settings, a 1200 grooves/mm ruled grating, and by scanning the central wavelength over the spectral regions of interest. Figures 7.1 and 7.2 show three examples of the measured spectra and demonstrate the trace element detection procedure. Figure 7.1 a) presents a single-shot spectrum from a minewater sample around the center wavelength of 362 nm. The peak identification was done with the aid of LIBS spectrum modeling software[135] that uses the spectral data from NIST ASD database[17]. The computed LIBS spectra of the elements producing the strongest peaks in Figure 7.1 a) are superimposed in Figure 7.1 c). The modeled signal is a sum of the separate elemental spectra. The correspon-

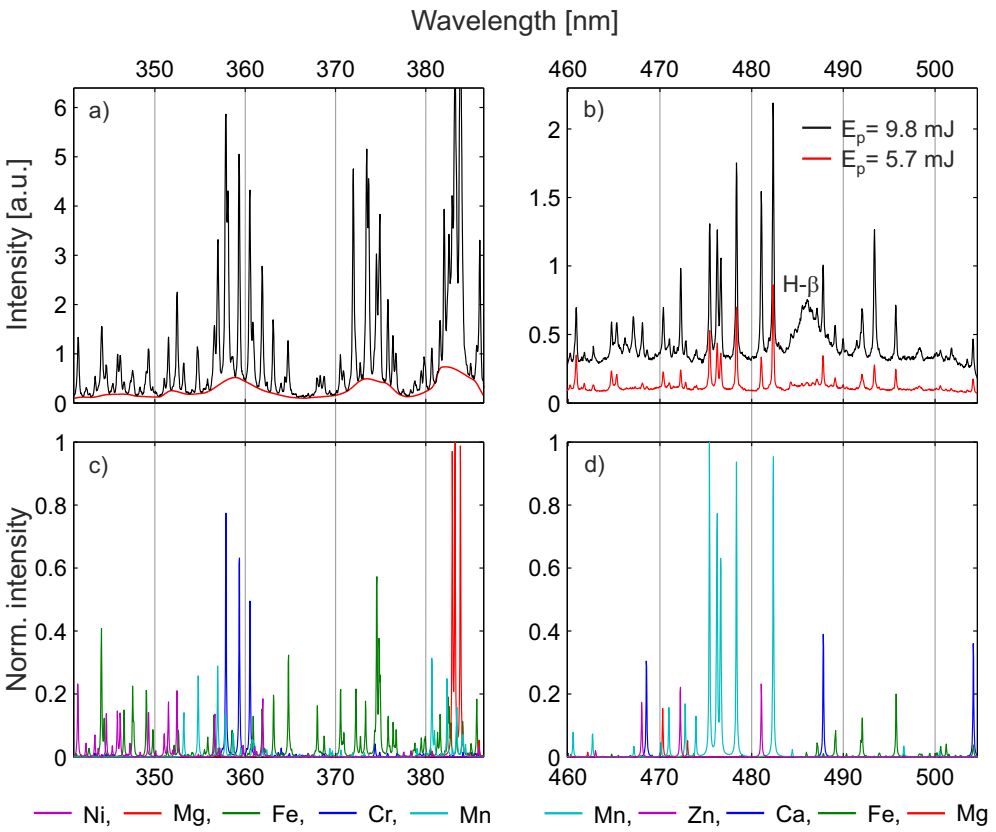

Figure 7.1 Qualitative analysis of minewater sample. a) Single-shot spectrum when the center wavelength is set at 362 nm and a corresponding background fit. b) Spectrum around 481 nm center wavelength using two different pulse energies. c),d) Modeled elemental spectra plotted on top of each other to help in the line recognition.

dence between the background subtracted spectrum and the modeled spectrum can be quantified by a correlation calculation. Laser pulse energy of 6 mJ was used in the measurements to optimize the SNR for lines of most metals. As expected of the results presented in Chapter 6, the SNR of zinc increased from 20 to 49 when the pulse energy was raised from 6 mJ to 10 mJ. The corresponding average spectra are shown in Figure 7.1 b). Figure 7.1 d) shows the computed spectra corresponding lines in b). The water sample taken downstream of the municipal treatment plant was reasonably free from trace elements apart from Ca, Na, Mg and K. Figure 7.2 shows the detection of copper the concentration of which in the purified water was only 20 ppb according to the reference measurement.

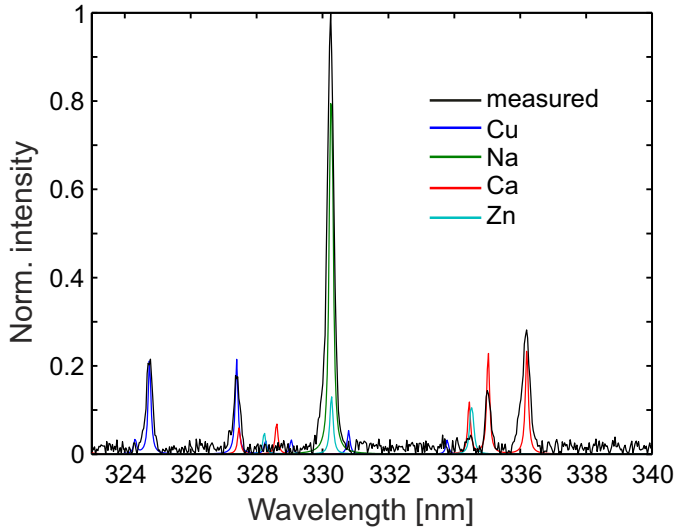

Figure 7.2 Determination of copper from municipal waste water treatment plant sample. The lines of Na and Ca interfere with the detection of Zn.

Table 7.1 shows the reference results of the two example samples and indicates if the particular element has been detected in the EDB-LIBS measurements. The parentheses denote that the identification has been based on one spectral line only and therefore has a higher uncertainty. The marking n.a. in the middle column signifies that the element has not been analyzed in the reference measurement but its spectral lines were clearly detected from the EDB-LIBS spectra. The persistent lines of As and P fall outside the operating wavelength range, 320 nm – 850 nm, of the spectrograph used throughout this work. The amount of solid matter that is sampled in the EDB-LIBS and in the reference analyses may differ and hence affect the comparability of

Table 7.1. Reference results and detectability in the EDB-LIBS. n.a.=not analyzed.

Element	Concentration [mg/l]	Detected
Minewater sample		
Al	12	X
As	0.0048	-
Ca	28	X
Cd	0.030	(X)
Co	0.17	(X)
Cr	n.a.	X
Fe	7.6	X
Mg	35	X
Mn	18	X
Na	1.8	X
Ni	5.0	X
U	0.036	-
Zn	13.4	X
Municipal water treatment plant sample		
Al	0.13	X
C	n.a.	X
Ca	110	X
Cd	<0.0003	-
Co	<0.005	-
Cr	<0.005	-
Cu	0.020	X
Fe	0.1	X
K	n.a.	X
Mg	n.a.	X
Mn	0.039	-
Na	n.a.	X
Ni	0.013	-
P	0.03	-
Pb	0.00053	-
Si	4.0	X
Zn	0.038	-

the results. In the EDB-LIBS instrumentation, a solid matter removing filter before the droplet generator removes particulates bigger than 10 μm in diameter. In the case of municipal water treatment plant, the reference measurement sample was taken from the same location but on a different day.

7.2 Detection of microbiological contamination

Besides the concentration of trace elements, the amount and species of microbes in purified water indicate the waste water treatment plant efficiency or safety of drinking water. Microbial content is commonly analyzed in a laboratory although biological pollutants can be partially monitored by many indirect online methods such as turbidity, total organic carbon (TOC) or UV-absorbance analyzers. LIBS, as such, is not suitable for the detection of molecules of biological origin due to its destructive nature. **Paper 4** demonstrates the first measurements where microbial particles, bacteria and fungal spores, inside the sampled water droplet are detected by a hyphenated technique that performs a laser-induced fluorescence (LIF) analysis to the particle before the LIBS analysis. Information from the LIF and LIBS signals is possible to utilize in the observation of the microbiological contamination of water.

The fundamental difference between LIBS and LIF is the pumping process to the upper energy state. While LIBS is based on thermal excitation, in LIF the molecules are excited optically. Microbial particles contain a large number of organic compounds such as amino acids, flavins and cofactors [109,110] that, due to their fused ring structures, strongly absorb light in the UV and visible wavelength regions. In the absorption of a photon, the molecule excites to a vibrational level of an upper electronic state. Owing to the molecular complexity and the solid sample matrix, the vibrational states of the biomolecules form a quasicontinuum as illustrated with the gray area in Figure 7.3. Because there are no restrictions in the change of vibrational quantum number, the upper electronic states are possible to excite with a broad wavelength range. After 10^{-10}–10^{-7} s from the absorption, part of the molecules relax back to their ground electronic level S_0 by spontaneous emission or fluorescence. The transition occurs from the lowest vibrational level of the electronic state S_1 to the vibrational levels of the ground state. Because the excitation occurs from the ground vibrational level of S_0, the energy of the fluorescence photons cannot be higher than the excitation

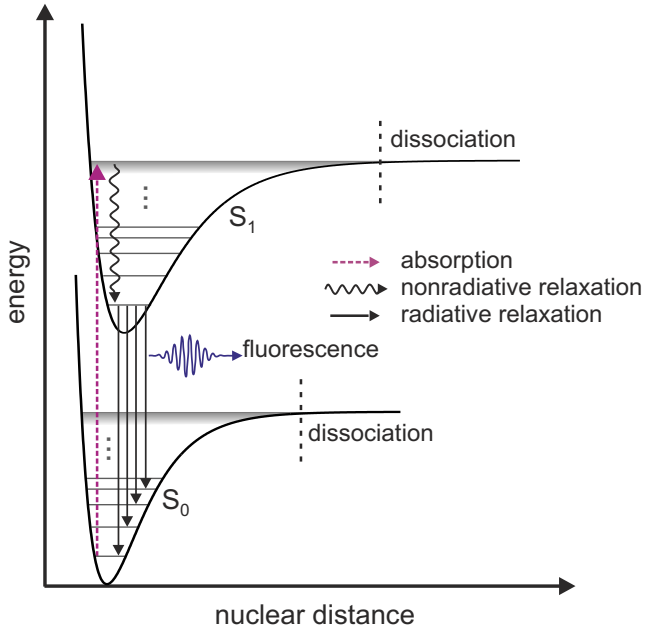

Figure 7.3 Potential energy curves for ground and excited electronic states of diatomic molecule and generation of fluorescence. The horizontal lines and shaded areas correspond the vibrational states. The relaxation to the lowest vibrational state of S_1 is very fast and occurs in 10^{-12}–10^{-10} s after absorption. The potential energy of the states of complex biomolecules is a multidimensional hypersurface.

photon energy. Due to the limited resolution of the imaging system, the fluorescence spectrum is similarly broad and its intensity distribution is proportional to the Franck-Condon factors[16] between the lowest vibrational state of S_1 and the vibrational states of S_0. In common biological fluorophores, 10%–30%[136,137] of the absorbed photons will result in an emission of a fluorescence photon and the rest of the molecules undergo a nonradiative relaxation to their ground electronic state.

The microbial particle or particles are trapped when water suspension containing the spores of bacteria or fungus is injected to the EDB-LIBS system. In the instrumentation of **Paper 4**, a 450 nJ LIF excitation laser pulse is produced from the same 355 nm laser as the LIBS pulse by two window reflections as depicted in Figure 7.4. A single-shot LIF spectrum is adequate for the detection of fluorescence from a single fungal spore or a few bacteria in the droplet residual but several spectra can be averaged to improve the resolution of spectral details. Figure 7.5 shows the average LIF spectra of three species and a single-shot spectrum from a single P.b. spore. Most inorganic

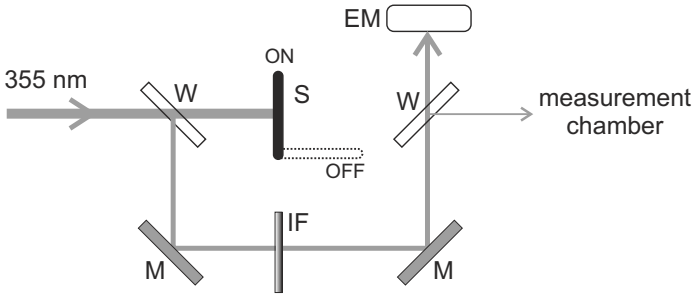

Figure 7.4 Switching between LIBS and LIF excitation pulses. The arrow thickness describes the pulse energy (not in scale). In LIBS, the shutter (S) is in the OFF position. The 355 nm bandpass interference filter (IF) is used for removing 532 nm radiation from the laser pulse. EM measures the reference pulse energy of both LIF and LIBS pulses. W=Window, M=Mirror.

impurities in water are not fluorescent when exposed to 355 nm laser light which is essential for the discrimination between microbiological and other type of contamination of water by LIF. In other words, the emission of light of longer wavelengths

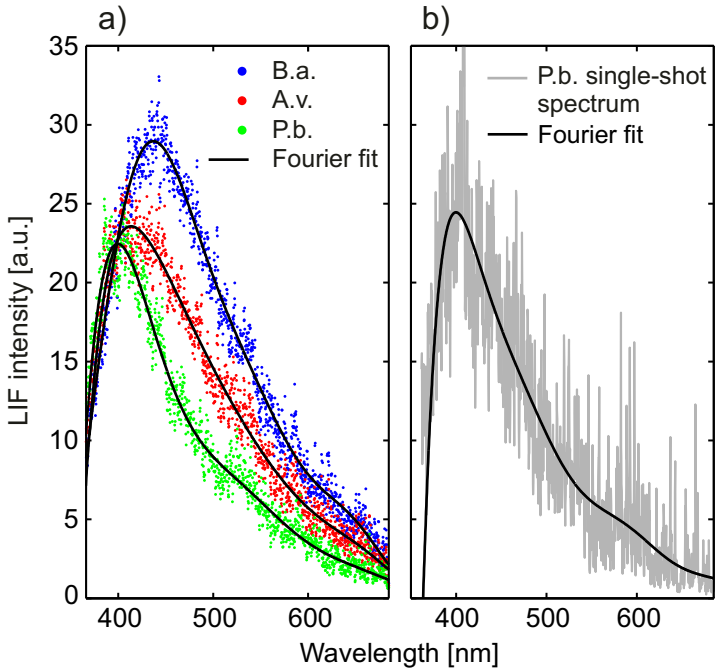

Figure 7.5 Fluorescence signal from bacterial and fungal spores. a) Average spectrum of 20 pulses. b) Single shot spectrum from P.b. spore. [Paper 4]

was detected only when at least one microbial particle was trapped in the EDB. The LIF pulse can be applied 10-20 times onto the same microbial particle before the fluorescence signal starts to attenuate. The shape of the recorded fluorescence spectrum is corrected by extracting the effect of the imaging optics. The fluorescence spectra are cut from the short wavelength side due to a long-pass filter used for blocking the scattering of the excitation laser pulse. The LIBS elemental analysis is performed for the same particle that was analyzed with LIF in the previous step. After the LIF analysis, the shutter in Figure 7.4 is opened and the spectrograph settings are adjusted to increase the resolution of the following LIBS analysis and to decrease the thermal background. The particle is waiting in the trap while the settings are changed.

In **Paper 4**, differences in the single-shot LIBS spectra between the spores of different species were found when they were suspended in pure water. LIBS signals from two fungal spore species (*Aspergillus versicolor*, A.v. and *Penicillium brevicompactum*, P.b.) and from one bacteria species (*Bacillus aureus*, B.a.) were recorded. The investigated elements were Na, Ca and K which have strong LIBS signals and are, together with O, C, H, N, P, and S, the most common elements in microbes. Furthermore, they are not present in standard air where the plasma forms in the experiment. Figure 7.6 shows four examples of single-shot LIBS spectra from trapped microbes. Clearly stronger Na emission was observed from P.b. fungal spores than from the A.v. spores as shown in Figure 7.6 a). According to a calibration measurement, the mass of calcium in the aggregate of about 20 bacterial spores was about 2 pg whereas almost no

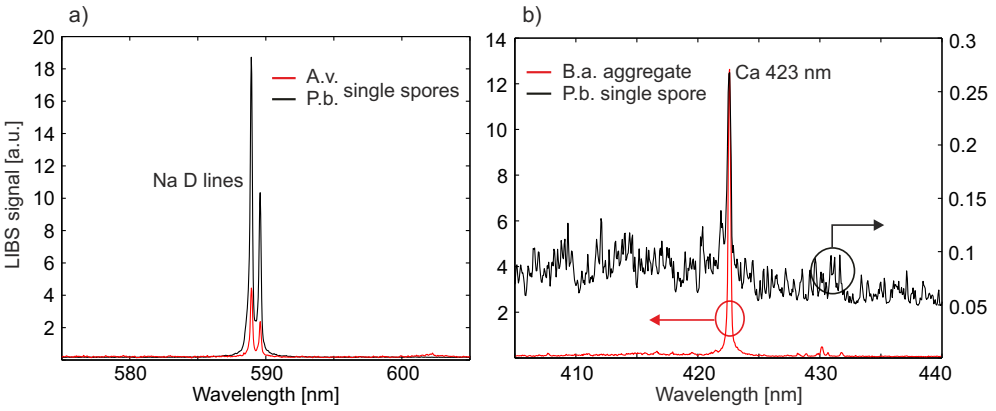

Figure 7.6 Single shot LIBS spectra from single fungal spores and bacterial aggregate. a) Difference in sodium signal between A.v. and P.b. fungal spores. b) Bacteria emit strong calcium lines whereas the calcium content of fungal spores is near the system detection limit.

calcium was found in the fungal spores (Figure 7.6 b). Based on the differences in Na, Ca and K signals, the three species can be discriminated in pure water. However, impurities in the authentic waste and drinking water set a major challenge in the identification of microbes as the droplet samples both the microbe and the dissolved elements. The preconcentration is important also in LIF measurements because higher fluorescence cross sections have been reported for bacteria in dry aerosol particles in comparison with bacteria in suspension [109]. In monitoring of industrial and municipal water, the sensitive online LIF measurement could act as an initial trigger for a more specific and slower laboratory measurement and would be more selective than the current UV-absorbance meters. The degree of microbiological contamination could also be determined via the amount of sampled droplets that contain a fluorescent particle within a fixed time frame. On the other hand, the LIF-LIBS based identification of the microbial particles could be utilized in other fields besides water quality measurements. Indeed, the presented methodology can have applications in the monitoring of indoor and outdoor aerosols when particles can be collected from the ambient air and injected to the EDB chamber.

Chapter 8

Summary

Laser-induced breakdown spectroscopy (LIBS) for the elemental analysis of water was studied in this Thesis. LIBS is a fast and selective technique that can detect practically all elements from a sample. The obstacle to its use in online water monitoring is the poor sensitivity when LIBS is applied directly to aqueous samples. As discussed at the beginning of the Thesis, real-time monitoring of dissolved metals and other elements could be used in process diagnostics in several areas of industry. Environmental monitoring and furthering the safety of the domestic water are naturally important applications. This research was initiated by the measurement needs of mining industry where the general requirement for the limit of detection is 0.1 mg/l for many elements.

An overview of the physical principles responsible for signal formation in a LIBS experiment was presented in Chapter 2 and the most common instrumental methods for the chemical analysis of water were reviewed in Chapter 3. The problems encountered in the LIBS analysis of liquid samples and the previous approaches to avoid these effects were discussed in Chapter 4. Two new techniques for more sensitive LIBS based elemental analysis were introduced in this work. In the techniques, fast liquid-to-solid matrix conversion is carried out by drying the droplets of the sample solution as presented at the end of Chapter 4. The formed aerosol particles that consist of the trace elements in water, are individually analyzed with LIBS. How to introduce the parti-

cles in a reproducible manner to the LIBS focal volume, is described in Chapter 5. The instrumentation where the particles travel along a narrow sheath air flow and the moment they arrive at the laser beam focal point is determined by a scattering sensor, is discussed in more detail in **Paper 1**. **Paper 2** presents the EDB-LIBS method that was developed within the framework of this thesis. In the EDB-LIBS, the particle is precisely trapped in all dimensions by an electric field before the hit of the vaporizing laser pulse. The characteristics of LIBS analysis of precisely trapped particles were further studied in **Paper 3**. The results validated the importance of the exact position of the particle and the sufficient drying of the original droplet. Optimal laser pulse energy with respect to LIBS signal-to-noise ratio was also found for each detection time windows. Additional modeling results were presented in Chapter 6 which estimated the value of optimal pulse energy for the selected transitions of different elements.

In the analysis of laboratory-made trace metal solutions, the fast sample preparation methods introduced in this work were found to enhance the sensitivity of the laser-induced breakdown spectroscopy (LIBS) measurement of trace elements compared with the direct analysis of water. Comparison between the limits of detection obtained in this work with the values found in various LIBS studies is presented in Table 8.1. The achieved detection limits are among the best that have been obtained for the listed metals in Table 8.1 with other LIBS sample preparation methods. The laser pulse energies required in the approach presented in this work are relatively low compared with previous LIBS studies of dissolved elements and may further its transfer to commercial applications. The performance of the EDB-LIBS technique was also demonstrated by the qualitative measurements of industrial water samples where several elements were detected simultaneously. Due to the stable signal between excitation pulses, a spectrum from a single laser pulse was typically adequate for the recognition of a specific peak. According to reference results shown in Chapter 7, the lowest detected concentrations were at the level of 20 μg/l. The detection limits are already sufficient for most process and waste water monitoring applications, albeit the limits could be improved by generating and trapping larger droplets and by increasing the solid angle for plasma emission collection. The benefits of the technique with relation to existing trace element analyzer technologies are the applicability to a wide range of elements, the speed of detection and the chemical free analysis.

Calibration measurements in order to produce quantitative results as well as the construction of an online analyzer are the obvious next developments in this research.

Table 8.1. Comparison of limits of detection (LOD) of this work with other results

Element	LOD, this work [ppm]	LOD, other LIBS studies [ppm] (Approach)
Al	0.01	33 (single droplets, double pulse[73])
		18 (water surface[47])
		5.2 (single droplets[72])
		0.01 (water evaporated on graphite[58])
Mn	0.02	10 (water surface[47])
		7.2 (single droplets[72])
		0.08 (double pulse, inside liquid[138])
Ni	0.06	18 (water surface[139])
		0.31 (preconcentration into polymer membrane[61])
		0.01 (water evaporated on graphite[58])
Pb	0.06	20 (sample pelletizing[62])
		12.5 (plasma formation inside liquid[140])
		2 (water evaporated on graphite[58])
		1.1 (preconcentration into polymer membrane[61])
		0.3 (vertical jet, excimer laser[69])
		0.075 (water evaporated on filter paper[141])
		0.06 (vertical jet, 200 mJ pulse energy[142])
Zn	0.05	21 (sample pelletizing[62])
		1 (water evaporated on graphite[58])
		0.85 (preconcentration into polymer membrane[61])

Compact spectrographs and pulsed laser sources currently available enable the measurement technology to be encapsulated in an easily movable casing. Although the performance of a miniaturized EDB-LIBS prototype remains to be shown, the technology has aroused curiosity in process industry and above all, in the fields of water treatment and metal refining.

The measurement scheme where laser-induced fluorescence (LIF) measurement is combined with LIBS to detect the microbiological contamination of water was discussed in **Paper 4** and in Chapter 7. The EDB instrumentation also enables studies with other optical measurement technologies such as Raman spectroscopy. Hyphenated methods can be especially useful in the research of atmospheric or room air aerosols where, for example, the online recognition of pathogenic microbes may be possible. The transformation of the EDB-LIBS water measurement instrumentation to an aerosol

analyzer can be realized by replacing the droplet generator with a technical solution that collects the particles from air and, after charging, guides them between the EDB electrodes.

References

[1] WWAP (United Nations World Water Assessment Programme), "The united nations world water development report 2015: Water for a sustainable world," (2015).

[2] S. Sauvé, S. Bernard, and P. Sloan, "Environmental sciences, sustainable development and circular economy: Alternative concepts for trans-disciplinary research," Environmental Development (2015).

[3] W.-W. Li, H.-Q. Yu, and B. E. Rittmann, "Reuse water pollutants," Nature **528**, 29–31 (2015).

[4] R. Noll, C. Fricke-Begemann, M. Brunk, S. Connemann, C. Meinhardt, M. Scharun, V. Sturm, J. Makowe, and C. Gehlen, "Laser-induced breakdown spectroscopy expands into industrial applications," Spectrochimica Acta Part B: Atomic Spectroscopy **93**, 41 – 51 (2014).

[5] M. Kumar, M. N. Islam, F. L. Terry, M. J. Freeman, A. Chan, M. Neelakandan, and T. Manzur, "Stand-off detection of solid targets with diffuse reflection spectroscopy using a high-power mid-infrared supercontinuum source," Applied Optics **51**, 2794–2807 (2012).

[6] C. Lopez-Moreno, S. Palanco, J. J. Laserna, F. DeLucia Jr, A. W. Miziolek, J. Rose, R. A. Walters, and A. I. Whitehouse, "Test of a stand-off laser-induced breakdown spectroscopy sensor for the detection of explosive residues on solid surfaces," Journal of Analytical Atomic Spectrometry **21**, 55–60 (2006).

[7] S. Hanf, T. Bögözi, R. Keiner, T. Frosch, and J. Popp, "Fast and highly sensitive fiber-enhanced raman spectroscopic monitoring of molecular H_2 and CH_4 for point-of-care diagnosis of malabsorption disorders in exhaled human breath," Analytical Chemistry **87**, 982–988 (2015).

[8] A. Hangauer, J. Chen, R. Strzoda, M. Fleischer, and M.-C. Amann, "Performance of a fire detector based on a compact laser spectroscopic carbon monoxide sensor," Optics Express **22**, 13680–13690 (2014).

[9] "Government decree on substances dangerous and harmful to the

aquatic environment 1022/2006," (last accessed: 27-Oct-2015). http://www.finlex.fi/en/laki/kaannokset/2006/en20061022.pdf .

[10] "Government decree on urban waste water treatment 888/2006," (last accessed: 27-Oct-2015). http://www.finlex.fi/en/laki/kaannokset/2006/en20060888.pdf .

[11] "Directive 2008/105/ec of the European Parliament and of the Council," (last accessed: 27-Oct-2015). http://eur-lex.europa.eu/LexUriServ/LexUriServ.do?uri=OJ:L:2008:348:0084:0097:en:PDF.

[12] Helsinki Comission (HELCOM), Baltic Marine Environment Protection Commission, "Recommendation 23/11: requirements for discharging of waste water from the chemical industry," (last accessed: 27-Oct-2015). http://helcom.fi/recommendations/rec%2023-11.pdf .

[13] J. O. Nriagu and J. M. Pacyna, "Quantitative assessment of worldwide contamination of air, water and soils by trace metals," Nature **333**, 134–139 (1988).

[14] G. Carletti, F. Fatone, D. Bolzonella, and F. Cecchi, "Occurrence and fate of heavy metals in large wastewater treatment plants treating municipal and industrial wastewaters," Water Science and Technology **57** (2008).

[15] T. Loree and L. Radziemski, "Laser-induced breakdown spectroscopy: Time-integrated applications," Plasma Chemistry and Plasma Processing **1**, 271–279 (1981).

[16] J. M. Hollas, *Modern Spectroscopy* (John Wiley & Sons, 2004), 4th ed.

[17] A. Kramida, Y. Ralchenko, J. Reader, and NIST ASD Team (2014), "Nist atomic spectra database (version 5.2))," (last accessed: 26-Oct-2015). http://www.nist.gov/pml/data/asd.cfm .

[18] P. L. Smith, C. Heise, J. R. Esmond, and R. L. Kurucz, "Atomic spectral line database," (last accessed: 26-Oct-2015). http://www.pmp.uni-hannover.de/cgi-bin/ssi/test/kurucz/sekur.html .

[19] D. R. Wood and K. L. Andrew, "Arc spectrum of lead," Journal of the Optical Society of America **58**, 818–828 (1968).

[20] D. W. Hahn and U. Panne, "LIBS for aerosol analysis," in "Laser-Induced Breakdown Spectroscopy," , J. Singh and S. Thakur, eds. (Elsevier, 2007), pp. 381–417.

[21] M. I. Boulos, P. Fauchais, and E. Pfender, *Thermal Plasmas, Fundamentals and Applications, Volume 1* (Plenum Press, 1994).

[22] G. Cristoforetti, E. Tognoni, and L. Gizzi, "Thermodynamic equilibrium states in laser-induced plasmas: From the general case to laser-induced breakdown spectroscopy plasmas," Spectrochimica Acta Part B: Atomic Spectroscopy **90**, 1 – 22 (2013).

[23] J. Cooper, "Plasma spectroscopy," Reports on Progress in Physics **29**, 35 (1966).

[24] H. R. Griem, *Plasma Spectroscopy* (McGraw-Hill, 1964).

[25] E. Tognoni and G. Cristoforetti, "Signal and noise in laser induced breakdown spectroscopy: An introductory review," Optics & Laser Technology **79**, 164 – 172 (2016).

[26] S. S. Zumdahl, *Chemical Principles* (Houghton Mifflin, 2003), 5th ed. Chap. 11.

[27] J. Herovsky, *Practical Polarography; an Introduction for Chemistry Students* (Academic Press, 1968).

[28] J. Wang, J. Lu, S. B. Hocevar, P. A. M. Farias, and B. Ogorevc, "Bismuth-coated carbon electrodes for anodic stripping voltammetry," Analytical Chemistry **72**, 3218–3222 (2000).

[29] J. Wang, N. Foster, S. Armalis, D. Larson, A. Zirino, and K. Olsen, "Remote stripping electrode for in situ monitoring of labile copper in the marine environment," Analytica Chimica Acta **310**, 223 – 231 (1995).

[30] J. Wang and B. Tian, "Mercury-free disposable lead sensors based on potentiometric stripping analysis of gold-coated screen-printed electrodes," Analytical Chemistry **65**, 1529–1532 (1993).

[31] X. Hou and B. T. Jones, "Field instrumentation in atomic spectroscopy," Microchemical Journal **66**, 115 – 145 (2000).

[32] F. Melquiades and C. Appoloni, "Application of XRF and field portable XRF for environmental analysis," Journal of Radioanalytical and Nuclear Chemistry **262**, 533–541 (2004).

[33] Hobré Instruments, "The metorex C100 technology," (last accessed: 3-Nov-2015). http://hobre.com/products/metorex-c100-on-line-elemental-analysis .

[34] American Micro Detection System, "Rex dissolved metals analysis instrument," (last accessed: 3-Nov-2015). http://amdsinc.com .

[35] M. Marazuela and M. Moreno-Bondi, "Fiber-optic biosensors - an overview," Analytical and Bioanalytical Chemistry **372**, 664–682 (2002).

[36] S. Haron and A. K. Ray, "Optical biodetection of cadmium and lead ions in water," Medical Engineering & Physics **28**, 978–981 (2006).

[37] I. Karube and K. Nakanishi, "Immobilized cells used for detection and analysis," Current Opinion in Biotechnology **5**, 54–59 (1994).

[38] C. V. Hoang, M. Oyama, O. Saito, M. Aono, and T. Nagao, "Monitoring the presence of ionic mercury in environmental water by plasmon-enhanced infrared spectroscopy," Scientific Reports **3**, 1–6 (2013).

[39] D. Harris, *Quantitative Chemical Analysis* (Freeman, New York, 2010), 8th ed.

[40] J. L. Arlett, E. B. Myers, and M. L. Roukes, "Comparative advantages of mechanical biosensors," Nature Nanotechnology **6**, 203–215 (2011).

[41] L. L. Stookey, "Ferrozine—a new spectrophotometric reagent for iron," Analytical Chemistry **42**, 779–781 (1970).

[42] W. Morrison, "A fast, simple and reliable method for the microdetermination of phosphorus in biological materials," Analytical Biochemistry **7**, 218 – 224 (1964).

[43] J. Murphy and J. Riley, "A modified single solution method for the determination of

phosphate in natural waters," Analytica Chimica Acta **27**, 31 – 36 (1962).

[44] M. Macka and P. R. Haddad, "Determination of metal ions by capillary electrophoresis," Electrophoresis **18**, 2482–2501 (1997).

[45] H. H. Willard, L. L. Merrit, J. A. Dean, and F. A. Settle, *Instrumental Methods of Analysis* (Wadsworth, Inc., 1988), 7th ed.

[46] A. Montaser and D. W. Golightly, eds., *Inductively Coupled Plasmas in Analytical Atomic Spectrometry* (VCH Publishers, Inc., 1987).

[47] O. Samek, D. C. S. Beddows, J. Kaiser, S. V. Kukhlevsky, M. Lika, H. H. Telle, and J. Young, "Application of laser-induced breakdown spectroscopy to in situ analysis of liquid samples," Optical Engineering **39**, 2248 (2000).

[48] P. Fichet, P. Mauchien, J.-F. Wagner, and C. Moulin, "Quantitative elemental determination in water and oil by laser induced breakdown spectroscopy," Analytica Chimica Acta **429**, 269 – 278 (2001).

[49] D. A. Cremers, L. J. Radziemski, and T. R. Loree, "Spectrochemical analysis of liquids using the laser spark," Applied Spectroscopy **38**, 721–729 (1984).

[50] P. K. Kennedy, D. X. Hammer, and B. A. Rockwell, "Laser-induced breakdown in aqueous media," Progress in Quantum Electronics **21**, 155–248 (1997).

[51] V. Golovlyov and V. Letokhov, "Laser ablation of absorbing liquids," Applied Physics B: Lasers and Optics **57**, 417–423 (1993).

[52] R. Esenaliev, A. Karabutov, N. Podymova, and V. Letokhov, "Laser ablation of aqueous solutions with spatially homogeneous and heterogeneous absorption," Applied Physics B: Lasers and Optics **59**, 73–81 (1994).

[53] V. Lazic and S. Jovićević, "Laser induced breakdown spectroscopy inside liquids: Processes and analytical aspects," Spectrochimica Acta Part B: Atomic Spectroscopy **101**, 288 – 311 (2014).

[54] A. D. Giacomo, A. D. Bonis, M. Dell'Aglio, O. D. Pascale, R. Gaudiuso, S. Orlando, A. Santagata, G. S. Senesi, F. Taccogna, and R. Teghil, "Laser ablation of graphite in water in a range of pressure from 1 to 146 atm using single and double pulse techniques for the production of carbon nanostructures," The Journal of Physical Chemistry C **115**, 5123–5130 (2011).

[55] C. Haisch, J. Liermann, U. Panne, and R. Niessner, "Characterization of colloidal particles by laser-induced plasma spectroscopy (LIPS)," Analytica Chimica Acta **346**, 23 – 35 (1997).

[56] M. Gondal and T. Hussain, "Determination of poisonous metals in wastewater collected from paint manufacturing plant using laser-induced breakdown spectroscopy," Talanta **71**, 73–80 (2007).

[57] A. Sarkar, D. Alamelu, and S. K. Aggarwal, "Determination of thorium and uranium in solution by laser-induced breakdown spectrometry," Applied Optics **47**, G58–G64 (2008).

[58] R. L. Vander Wal, T. M. Ticich, J. R. West, and P. A. Householder, "Trace metal detection by laser-induced breakdown spectroscopy," Applied Spectroscopy **53**, 1226–1236 (1999).

[59] Z. Chen, H. Li, M. Liu, and R. Li, "Fast and sensitive trace metal analysis in aqueous solutions by laser-induced breakdown spectroscopy using wood slice substrates," Spectrochimica Acta Part B: Atomic Spectroscopy **63**, 64 – 68 (2008).

[60] M. Pardede, H. Kurniawan, M. O. Tjia, K. Ikezawa, T. Maruyama, and K. Kagawa, "Spectrochemical analysis of metal elements electrodeposited from water samples by laser-induced shock wave plasma spectroscopy," Applied Spectroscopy **55**, 1229–1236 (2001).

[61] N. E. Schmidt and S. R. Goode, "Analysis of aqueous solutions by laser-induced breakdown spectroscopy of ion exchange membranes," Applied Spectroscopy **56**, 370–374 (2002).

[62] D. Díaz Pace, C. D'Angelo, D. Bertuccelli, and G. Bertuccelli, "Analysis of heavy metals in liquids using laser induced breakdown spectroscopy by liquid-to-solid matrix conversion," Spectrochimica Acta Part B: Atomic Spectroscopy **61**, 929–933 (2006).

[63] J. Cáceres, J. T. López, H. Telle, and A. G. Ureña, "Quantitative analysis of trace metal ions in ice using laser-induced breakdown spectroscopy," Spectrochimica Acta Part B: Atomic Spectroscopy **56**, 831 – 838 (2001).

[64] Y. Ito, O. Ueki, and S. Nakamura, "Determination of colloidal iron in water by laser-induced breakdown spectroscopy," Analytica Chimica Acta **299**, 401–405 (1995).

[65] W. F. Ho, C. W. Ng, and N. H. Cheung, "Spectrochemical analysis of liquids using laser-induced plasma emissions: Effects of laser wavelength," Applied Spectroscopy **51**, 87–91 (1997).

[66] P. Yaroshchyk, R. J. Morrison, D. Body, and B. L. Chadwick, "Quantitative determination of wear metals in engine oils using laser-induced breakdown spectroscopy: A comparison between liquid jets and static liquids," Spectrochimica Acta Part B: Atomic Spectroscopy **60**, 986 – 992 (2005).

[67] C. W. Ng, W. F. Ho, and N. H. Cheung, "Spectrochemical analysis of liquids using laser-induced plasma emissions: Effects of laser wavelength on plasma properties," Applied Spectroscopy **51**, 976–983 (1997).

[68] R. Nyga and W. Neu, "Double-pulse technique for optical emission spectroscopy of ablation plasmas of samples in liquids," Optics Letters **18**, 747–749 (1993).

[69] K. M. Lo and N. H. Cheung, "ArF laser-induced plasma spectroscopy for part-per-billion analysis of metal ions in aqueous solutions," Applied Spectroscopy **56**, 682–688 (2002).

[70] M. Essien, L. J. Radziemski, and J. Sneddon, "Detection of cadmium, lead and zinc in aerosols by laser-induced breakdown spectrometry," Journal of Analytical Atomic Spectrometry **3**, 985–988 (1988).

[71] A. Kumar, F. Y. Yueh, T. Miller, and J. P. Singh, "Detection of trace elements in

liquids by laser-induced breakdown spectroscopy with a meinhard nebulizer," Applied Optics **42**, 6040–6046 (2003).

[72] H. A. Archontaki and S. R. Crouch, "Evaluation of an isolated droplet sample introduction system for laser-induced breakdown spectroscopy," Applied Spectroscopy **42**, 741–746 (1988).

[73] E. M. Cahoon and J. R. Almirall, "Quantitative analysis of liquids from aerosols and microdrops using laser induced breakdown spectroscopy," Analytical Chemistry **84**, 2239–2244 (2012).

[74] S. Groh, P. K. Diwakar, C. C. Garcia, A. Murtazin, D. W. Hahn, and K. Niemax, "100% efficient sub-nanoliter sample introduction in laser-induced breakdown spectroscopy and inductively coupled plasma spectrometry: Implications for ultralow sample volumes," Analytical Chemistry **82**, 2568–2573 (2010).

[75] C. Janzen, R. Fleige, R. Noll, H. Schwenke, W. Lahmann, J. Knoth, P. Beaven, E. Jantzen, A. Oest, and P. Koke, "Analysis of small droplets with a new detector for liquid chromatography based on laser-induced breakdown spectroscopy," Spectrochimica Acta Part B: Atomic Spectroscopy **60**, 993–1001 (2005).

[76] A. Kumar, F. Y. Yueh, and J. P. Singh, "Double-pulse laser-induced breakdown spectroscopy with liquid jets of different thicknesses," Applied Optics **42**, 6047–6051 (2003).

[77] A. Casavola, A. D. Giacomo, M. Dell'Aglio, F. Taccogna, G. Colonna, O. D. Pascale, and S. Longo, "Experimental investigation and modelling of double pulse laser induced plasma spectroscopy under water," Spectrochimica Acta Part B: Atomic Spectroscopy **60**, 975 – 985 (2005).

[78] S. Nakamura, Y. Ito, K. Sone, H. Hiraga, and K.-i. Kaneko, "Determination of an iron suspension in water by laser-induced breakdown spectroscopy with two sequential laser pulses," Analytical Chemistry **68**, 2981–2986 (1996).

[79] J. Scaffidi, J. Pender, W. Pearman, S. R. Goode, B. W. Colston, J. C. Carter, and S. M. Angel, "Dual-pulse laser-induced breakdown spectroscopy with combinations of femtosecond and nanosecond laser pulses," Applied Optics **42**, 6099–6106 (2003).

[80] D. W. Hahn, W. L. Flower, and K. R. Hencken, "Discrete particle detection and metal emissions monitoring using laser-induced breakdown spectroscopy," Applied Spectroscopy **51**, 1836–1844 (1997).

[81] G. Gallou, J. B. Sirven, C. Dutouquet, O. L. Bihan, and E. Frejafon, "Aerosols analysis by LIBS for monitoring of air pollution by industrial sources," Aerosol Science and Technology **45**, 918–926 (2011).

[82] D. K. Ottesen, J. C. F. Wang, and L. J. Radziemski, "Real-time laser spark spectroscopy of particulates in combustion environments," Applied Spectroscopy **43**, 967–976 (1989).

[83] D. K. Ottesen, L. L. Baxter, L. J. Radziemski, and J. F. Burrows, "Laser spark emission spectroscopy for in-situ, real-time monitoring of pulverized coal particle composition," Energy & Fuels **5**, 304–312 (1991).

[84] D. W. Hahn, J. E. Carranza, G. R. Arsenault, H. A. Johnsen, and K. R. Hencken,

"Aerosol generation system for development and calibration of laser-induced breakdown spectroscopy instrumentation," Review of Scientific Instruments **72**, 3706–3713 (2001).

[85] G. Lithgow, A. Robinson, and S. Buckley, "Ambient measurements of metal-containing PM2.5 in an urban environment using laser-induced breakdown spectroscopy," Atmospheric Environment **38**, 3319 – 3328 (2004).

[86] L. J. Radziemski, T. R. Loree, D. A. Cremers, and N. M. Hoffman, "Time-resolved laser-induced breakdown spectrometry of aerosols," Analytical Chemistry **55**, 1246–1252 (1983).

[87] S. Groh, C. C. Garcia, A. Murtazin, V. Horvatic, and K. Niemax, "Local effects of atomizing analyte droplets on the plasma parameters of the inductively coupled plasma," Spectrochimica Acta Part B: Atomic Spectroscopy **64**, 247–254 (2009).

[88] R. Neuhauser, U. Panne, R. Niessner, G. Petrucci, P. Cavalli, and N. Omenetto, "On-line and in-situ detection of lead aerosols by plasma-spectroscopy and laser-excited atomic fluorescence spectroscopy," Analytica Chimica Acta **346**, 37 – 48 (1997).

[89] J. E. Carranza and D. W. Hahn, "Assessment of the upper particle size limit for quantitative analysis of aerosols using laser-induced breakdown spectroscopy," Analytical Chemistry **74**, 5450–5454 (2002).

[90] W. C. Hinds, *Aerosol Technology* (John Wiley & Sons, 1999), 2nd ed.

[91] D. W. Hahn, "Laser-induced breakdown spectroscopy for sizing and elemental analysis of discrete aerosol particles," Applied Physics Letters **72**, 2960–2962 (1998).

[92] G. Lithgow and S. Buckley, "Influence of particle location within plasma and focal volume on precision of single-particle laser-induced breakdown spectroscopy measurements," Spectrochimica Acta Part B: Atomic Spectroscopy **60**, 1060 – 1069 (2005).

[93] J. W. Beams, "Magnetic suspension for small rotors," Review of Scientific Instruments **21**, 182–184 (1950).

[94] H. Lee, A. M. Purdon, and R. M. Westervelt, "Manipulation of biological cells using a microelectromagnet matrix," Applied Physics Letters **85**, 1063–1065 (2004).

[95] F. J. Fortes, A. Fernández-Bravo, and J. J. Laserna, "Chemical characterization of single micro- and nano-particles by optical catapulting-optical trapping-laser-induced breakdown spectroscopy," Spectrochimica Acta Part B: Atomic Spectroscopy **100**, 78 – 85 (2014).

[96] A. Ashkin, "Acceleration and trapping of particles by radiation pressure," Physical Review Letters **24**, 156–159 (1970).

[97] A. Ashkin, J. M. Dziedzic, J. E. Bjorkholm, and S. Chu, "Observation of a single-beam gradient force optical trap for dielectric particles," Optics Letters **11**, 288–290 (1986).

[98] L. V. King, "On the acoustic radiation pressure on spheres," Proceedings of the Royal Society of London A: Mathematical, Physical and Engineering Sciences **147**, 212–240 (1934).

[99] N. A. Fuchs, *The Mechanics of Aerosols* (Pergamon, Oxford, 1964).

[100] P. Liu, P. J. Ziemann, D. B. Kittelson, and P. H. McMurry, "Generating particle beams of controlled dimensions and divergence: I. theory of particle motion in aerodynamic lenses and nozzle expansions," Aerosol Science and Technology **22**, 293–313 (1995).

[101] B. Dahneke and H. Flachsbart, "An aerosol beam spectrometer," Journal of Aerosol Science **3**, 345 – 349 (1972).

[102] A. Karimi, S. Yazdi, and A. M. Ardekani, "Hydrodynamic mechanisms of cell and particle trapping in microfluidics," Biomicrofluidics **7**, 021501 (2013).

[103] O. Kievit, J. Marijnissen, P. Verheijen, and B. Scarlett, "Some improvements on the particle beam generator," Journal of Aerosol Science **21, Supplement 1**, S685 – S688 (1990).

[104] K. Park, G. Cho, and J.-h. Kwak, "Development of an aerosol focusing-laser induced breakdown spectroscopy (aerosol focusing-LIBS) for determination of fine and ultrafine metal aerosols," Aerosol Science and Technology **43**, 375–386 (2009).

[105] D. Mukherjee, A. Rai, and M. Zachariah, "Quantitative laser-induced breakdown spectroscopy for aerosols via internal calibration: Application to the oxidative coating of aluminum nanoparticles," Journal of Aerosol Science **37**, 677 – 695 (2006).

[106] T. Tjärnhage, P.-A. Gradmark, A. Larsson, A. Mohammed, L. Landström, E. Sagerfors, P. Jonsson, F. Kullander, and M. Andersson, "Development of a laser-induced breakdown spectroscopy instrument for detection and classification of single-particle aerosols in real-time," Optics Communications **296**, 106 – 108 (2013).

[107] X. Wang, F. E. Kruis, and P. H. McMurry, "Aerodynamic focusing of nanoparticles: I. guidelines for designing aerodynamic lenses for nanoparticles," Aerosol Science and Technology **39**, 611–623 (2005).

[108] A. Manninen, M. Putkiranta, A. Rostedt, J. Saarela, T. Laurila, M. Marjamäki, J. Keskinen, and R. Hernberg, "Instrumentation for measuring fluorescence cross sections from airborne microsized particles," Applied Optics **47**, 110–115 (2008).

[109] A. Manninen, M. Putkiranta, J. Saarela, A. Rostedt, T. Sorvajärvi, J. Toivonen, M. Marjamäki, J. Keskinen, and R. Hernberg, "Fluorescence cross sections of bioaerosols and suspended biological agents," Applied Optics **48**, 4320–4328 (2009).

[110] M. Putkiranta, A. Manninen, A. Rostedt, J. Saarela, T. Sorvajärvi, M. Marjamäki, R. Hernberg, and J. Keskinen, "Fluorescence properties of biochemicals in dry NaCl composite aerosol particles and in solutions," Applied Physics B: Lasers and Optics **99**, 841–851 (2010).

[111] R. A. Millikan, "A new modification of the cloud method of determining the elementary electrical charge and the most probable value of that charge," Philosophical Magazine **19**, 209–228 (1910).

[112] W. Paul and H. Steinwedel, "Notizen: Ein neues massenspektrometer ohne magnetfeld," Zeitschrift für Naturforschung A **8**, 448–450 (1953).

[113] W. Paul and H. Steinwedel, "Verfahren zur trennung bzw. zum getrennten nachweis von ionen verschiedener spezifischer ladung," German Patent DE944900 (1956).

[114] A. Müller, "Theoretische untersuchungen über das verhalten geladener teilchen in sattelpunkten elektrischer wechselfelder," Annalen der Physik **461**, 206–220 (1960).

[115] E. J. Davis, "A history of single aerosol particle levitation," Aerosol Science and Technology **26**, 212–254 (1997).

[116] G. S. Grader, S. Arnold, R. C. Flagan, and J. H. Seinfeld, "Fourier transform infrared spectroscopy of a single aerosol particle," The Journal of Chemical Physics **86**, 5897–5903 (1987).

[117] K. Fung and I. Tang, "Raman spectra of singly suspended supersaturated ammonium bisulfate droplets," Chemical Physics Letters **147**, 509 – 513 (1988).

[118] C. Heinisch, J. B. Wills, J. P. Reid, T. Tschudi, and C. Tropea, "Temperature measurement of single evaporating water droplets in a nitrogen flow using spontaneous raman scattering," Physical Chemistry Chemical Physics **11**, 9720–9728 (2009).

[119] S. Arnold and L. M. Folan, "Fluorescence spectrometer for a single electrodynamically levitated microparticle," Review of Scientific Instruments **57**, 2250–2253 (1986).

[120] T. L. Ward, S. Zhang, T. Allen, and E. J. Davis, "Photochemical polymerization of acrylamide aerosol particles," Journal of Colloid and Interface Science **118**, 343 – 355 (1987).

[121] R. Wuerker, H. Goldenberg, and R. Langmuir, "Electrodynamic containment of charged particles by three phase voltages," Journal of Applied Physics **30** (1959).

[122] A. F. Haught and D. H. Polk, "High-temperature plasmas produced by laser beam irradiation of single solid particles," Physics of Fluids (1958-1988) **9**, 2047–2056 (1966).

[123] R. Warren, "Laser induced breakdown spectroscopy on suspended particulate matter in an electrodynamic balance: Interaction processes and analytical considerations," Ph.D. thesis, University of Florida (2013).

[124] C. Dutouquet, G. Wattieaux, L. Meyer, E. Frejafon, and L. Boufendi, "Determination of the elemental composition of micrometric and submicrometric particles levitating in a low pressure radio-frequency plasma discharge using laser-induced breakdown spectroscopy," Spectrochimica Acta Part B: Atomic Spectroscopy **83-84**, 14–20 (2013).

[125] E. J. Davis, "Electrodynamic levitation of particles," in "Aerosol Measurement - Principles, Techniques, and Applications," , P. A. Baron and K. Willeke, eds. (John Wiley & Sons, 2001), pp. 603–625, 2nd ed.

[126] D. E. Lencioni, "Laser-induced air breakdown for 1.06-μm radiation," Applied Physics Letters **25**, 15–17 (1974).

[127] J. Carranza and D. Hahn, "Sampling statistics and considerations for single-shot analysis using laser-induced breakdown spectroscopy," Spectrochimica Acta Part B: Atomic Spectroscopy **57**, 779 – 790 (2002).

[128] N. Konjević, M. Ivković, and N. Sakan, "Hydrogen balmer lines for low electron number density plasma diagnostics," Spectrochimica Acta Part B: Atomic Spectroscopy **76**, 16 – 26 (2012).

[129] G. A. Lithgow and S. G. Buckley, "Effects of focal volume and spatial inhomogeneity on uncertainty in single-aerosol laser-induced breakdown spectroscopy measurements," Applied Physics Letters **87**, – (2005).

[130] E. S. Simpson, G. A. Lithgow, and S. G. Buckley, "Three-dimensional distribution of signal from single monodisperse aerosol particles in a laser induced plasma: Initial measurements," Spectrochimica Acta Part B: Atomic Spectroscopy **62**, 1460 – 1465 (2007).

[131] P. K. Diwakar, S. Groh, K. Niemax, and D. W. Hahn, "Study of analyte dissociation and diffusion in laser-induced plasmas: implications for laser-induced breakdown spectroscopy," Journal of Analytical Atomic Spectrometry **25**, 1921–1930 (2010).

[132] P. Diwakar, P. Jackson, and D. Hahn, "The effect of multi-component aerosol particles on quantitative laser-induced breakdown spectroscopy: Consideration of localized matrix effects," Spectrochimica Acta Part B: Atomic Spectroscopy **62**, 1466–1474 (2007).

[133] V. Hohreiter and D. W. Hahn, "Plasma-particle interactions in a laser-induced plasma: Implications for laser-induced breakdown spectroscopy," Analytical Chemistry **78**, 1509–1514 (2006).

[134] C. Favre, V. Boutou, S. C. Hill, W. Zimmer, M. Krenz, H. Lambrecht, J. Yu, R. K. Chang, L. Woeste, and J.-P. Wolf, "White-light nanosource with directional emission," Physical Review Letters **89**, 035002 (2002).

[135] V. Contreras, "Double-pulse and calibration-free laser-induced breakdown spectroscopy (LIBS) on quantitative analysis," Ph.D. thesis, Centro de Investigaciones en Óptica A.C. (2013).

[136] H. J. Lee, A. Laskin, J. Laskin, and S. A. Nizkorodov, "Excitation-emission spectra and fluorescence quantum yields for fresh and aged biogenic secondary organic aerosols," Environmental Science & Technology **47**, 5763–5770 (2013).

[137] S. C. Hill, R. G. Pinnick, S. Niles, N. F. Fell, Y.-L. Pan, J. Bottiger, B. V. Bronk, S. Holler, and R. K. Chang, "Fluorescence from airborne microparticles: dependence on size, concentration of fluorophores, and illumination intensity," Applied Optics **40**, 3005–3013 (2001).

[138] S. Koch, R. Court, W. Garen, W. Neu, and R. Reuter, "Detection of manganese in solution in cavitation bubbles using laser induced breakdown spectroscopy," Spectrochimica Acta Part B: Atomic Spectroscopy **60**, 1230 – 1235 (2005).

[139] L. M. Berman and P. J. Wolf, "Laser-induced breakdown spectroscopy of liquids: Aqueous solutions of nickel and chlorinated hydrocarbons," Applied Spectroscopy **52**, 438–443 (1998).

[140] R. Knopp, F. Scherbaum, and J. Kim, "Laser induced breakdown spectroscopy (LIBS) as an analytical tool for the detection of metal ions in aqueous solutions," Fresenius' Journal of Analytical Chemistry **355**, 16–20 (1996).

[141] Y. Lee, S.-W. Oh, and S.-H. Han, "Laser-induced breakdown spectroscopy (LIBS) of heavy metal ions at the sub-parts per million level in water," Applied Spectroscopy **66**, 1385–1396 (2012).

[142] Y. Feng, J. Yang, J. Fan, G. Yao, X. Ji, X. Zhang, X. Zheng, and Z. Cui, "Investigation of laser-induced breakdown spectroscopy of a liquid jet," Applied Optics **49**, C70–C74 (2010).

Appendices

Paper 1

Samu T. Järvinen, Jaakko Saarela and Juha Toivonen

Detection of zinc and lead in water using evaporative preconcentration and single-particle laser-induced breakdown spectroscopy.

Spectrochimica Acta Part B: Atomic Spectroscopy **86**, 55 – 59 (2013).

doi: 10.1016/j.sab.2013.04.010

Spectrochimica Acta Part B 86 (2013) 55–59

Contents lists available at ScienceDirect

Spectrochimica Acta Part B

journal homepage: www.elsevier.com/locate/sab

Detection of zinc and lead in water using evaporative preconcentration and single-particle laser-induced breakdown spectroscopy

Samu T. Järvinen *, Jaakko Saarela, Juha Toivonen

Tampere University of Technology, Department of Physics, Optics laboratory P.O. Box 692, FI-33101 Tampere, Finland

ARTICLE INFO

Article history:
Received 21 November 2012
Accepted 23 April 2013
Available online 6 June 2013

Keywords:
Laser-induced breakdown spectroscopy
LIBS
Aerosol
Zinc
Lead

ABSTRACT

A novel laser-induced breakdown spectroscopy (LIBS)-based measurement method for metals in water is demonstrated. In the presented technology a small amount of sodium chloride is dissolved in the sample solution before spraying the sample into a tubular oven. After water removal monodisperse dry NaCl aerosol particles are formed where trace metals are present as additives. A single-particle LIBS analysis is then triggered with a scattering based particle detection system. Benefits are the highly increased metal concentration in the LIBS focal volume and the static NaCl-matrix which can be exploited in the signal processing procedure. Emitted light from the emerged plasma plume is collected with wide angle optics and dispersed with a grating spectrometer. In an aqueous solution, the respective limits of detection for zinc and lead were 0.3 ppm and 0.1 ppm using a relatively low 14 mJ laser pulse energy. Zn/Na peak intensity ratio calibration curve for zinc concentration was also determined and LIBS signal dependence on laser pulse energy was investigated.

1. Introduction

Ecotoxic metals, often referred as heavy metals, are harmful to living organisms. Such metals as arsenic, lead, antimony, zinc and cadmium can pollute underground waters if dumped onto the soil. Industrial process and waste waters commonly include trace amounts of heavy metals. Current monitoring of the industrial waters is based on sampling and subsequent laboratory analysis. While being very sensitive such process has a long delay between successive measurements as well as between the sampling and completion of analytic results [1]. Therefore they are not ideal for active monitoring and cannot, for example, give early warnings of heavy metal leakages that can lead to process disruptions and environmental accidents. In order to obtain online information about metal concentrations in industrial processes and sudden fault situations novel measurement approaches are needed. For such real-time monitoring system of major metal concentrations, the limit of detection (LOD) in the order of 0.1 mg/l or 0.1 ppm is often required [2].

Laser-induced breakdown spectroscopy (LIBS) is able to perform a simultaneous analysis of several elements with good selectivity. It involves focusing a high intensity laser pulse or a pulse train on the surface or inside of the sample material. The leading edge of the pulse evaporates and ionizes a minute quantity of the sample. Optical power is converted to the kinetic energy of emerged electrons which leads to a rapid growth of free electron density at the focal point and further absorption of the pulse trailing edge. The vapor heats up and expands and more sample material is ablated. After the laser pulse, ions and electrons recombine and the characteristic spectra of sample material atoms are observed due to radiative relaxation while the originated plasma cloud cools down [3].

LIBS has been applied to liquid samples in order to detect metals in several applications. Analysis of water solutions suffers from a poor sensitivity and a high limit of detection due to short emission lifetime and LIBS shock wave induced splashes when plasma forms in the bulk liquid and on the surface, respectively [4,5]. In many cases, the reproducibility of LIBS signal between successive pulses has been improved by a double pulse configuration [6,7], sample preparation such as collecting the sample to a filter paper which is analyzed after drying [8] or by focusing a laser pulse on flowing liquid [9]. Some studies [10–12] describe LIBS measurement of aerosols generated from a sample solution via nebulizer and possible subsequent water removal. Compared with focusing a laser beam on the center of a polydisperse aerosol cloud, a single particle LIBS analysis of monodisperse aerosols has the advantage of maintaining the mass and the elemental composition of the substance in the focal volume uniform from pulse to pulse.

In this paper, we introduce a novel measurement scheme where trace metals in the sample solution are rapidly preconcentrated inside salt water droplets. When droplets dry off, metals remain in the shells of the formed hollow NaCl aerosol particles and their mass concentration increases several orders of magnitude. The LIBS analysis is performed from a single aerosol particle using moderate laser pulse energy. Obtained LIBS spectrum shows emission lines of the metals

* Corresponding author. Tel.: +358 503237520.
E-mail address: samu.jarvinen@tut.fi (S.T. Järvinen).

0584-8547/$ – see front matter © 2013 Elsevier B.V. All rights reserved.
http://dx.doi.org/10.1016/j.sab.2013.04.010

superimposed over the sodium spectrum. The spectral lines of sodium can be used for wavelength and intensity calibration. We demonstrate the performance of the technique in the detection of zinc and lead which both are metals of interest in monitoring the industrial waste and process waters. They are also among the difficult metals to detect on a ppm level using LIBS.

2. Experimental

Experiments were carried out using a setup which was based on the LIF instrumentation used in references [13–15]. A water sample with diluted sodium chloride is placed in an ink jet aerosol generator (IJAG) and sprayed into a tubular oven. As the water from the droplets evaporates off, spherical, hollow and monodisperse dry NaCl aerosol particles are formed [15] where trace metals are present as dopants. At the same time, metal concentration in the particle increases a thousand fold as the water evaporates. The aerosol stream is directed to a measurement chamber where a single aerosol particle is detected by a scattering based sensor as shown in Fig. 1. The sensor sends a trigger signal to a Nd:YAG laser (NT 342/1/UVE, Ekspla Ltd.). The laser has 10 Hz repetition rate with 10 ms activation window of the flashlamp pumping the laser gain material. The trigger signal must arrive within the activation window to cause the emission of a frequency-tripled 355 nm laser pulse towards the detected particle. The light emitted by the formed plasma cloud is collected using a 2π solid angle and dispersed with a Czerny–Turner spectrometer with 150 μm slit width. All the numerical results presented in this article were obtained using a 1200 g/mm grating whereas the shown broadband LIBS example spectra were recorded using a 300 g/mm grating. Both gratings are blazed at 500 nm.

The water samples were prepared by diluting a solution of known metal concentration in volumetric flasks. The chloride salts of zinc and lead, $ZnCl_2$ and $PbCl_2$, were used as sources of metals. Sodium chloride was added to the solution before inserting it into the IJAG. The IJAG produces initial droplets of 60 μm in diameter into a vertical tubular oven. After the oven and the following virtual impactor the size of dry and monodisperse particles depends on the amount of added NaCl [15]. The scattering signal intensity at the photomultiplier tube and an effort to maintain the vaporized mass small determine the suitable particle diameter. The used NaCl concentration of about 0.6 g/l in the sample solution produces particles 5 μm in diameter with a size distribution having geometric standard deviation less than 1.10 [15]. Small, less than 10% changes in NaCl concentration don't affect the size distribution. The sample flow through the measurement chamber was 60 cm^3/min and the particle concentration inside the chamber was adjusted by the IJAG drive electronics. The droplet generation frequency of approximately 3000 droplets/s resulted in a particle concentration of about 100 particles/cm^3 which ensured a trigger signal and thus a recorded LIBS spectrum within the majority of the activation windows of the UV laser pulse. On the other hand, the concentration of aerosol particles in the carrier gas flow was sufficiently low in order to have a small probability of having extra particles in the focal volume. A vertical gas jet from a 300 μm inlet nozzle carries the aerosols in the center axis of the jet with the velocity of about 10 m/s. The jet passes through a focal point of an Al-coated parabolic mirror. The LIBS excitation UV laser pulse hits a targeted single particle at this focal point. The beam of the UV laser pulses was 3 mm in diameter before a focusing lens (LA4158, Thorlabs Inc.) placed in front of the measurement chamber entry. The focal length of the lens was 250 mm and the consequent beam diameter at the focus was about 40 μm. The pulse energy was varied in the range of 3–35 mJ. The temporal FWHM width of the laser pulse was 5 ns and the resulting irradiance at the focal point was 50–600 GW/cm^2. Filtered air having RH of approximately 20% is used as a carrier gas through the equipment. It also acts as sheath air preventing the deposition of metals or particle fragments onto the surface of the measurement chamber. After tens of hours of LIBS experiments no significant contamination in the measurement chamber optics was noticed.

The plasma emission spectrum is recorded with an ICCD camera (4 Quik E, Stanford Computer Optics Inc.). LIBS signal-to-noise ratio (SNR) was investigated with different delay and exposure times of the ICCD. The optimal detection time window producing the highest SNR for certain pulse energy was found to be, not only element specific, but also emission line and sample composition specific. While a time-resolved measurement improves the sensitivity of the LIBS measurement, the experimental device of this study uses a fixed detection time window that was chosen in a way the device would be suitable for diverse sample solutions. The fixed time window has an exposure time of 400 ns and a 400 ns delay time between the plasma initiation and emission detection.

The outcome of a single pulse from the ICCD camera is a TIFF image file having 573 × 733 pixels. For a single LIBS measurement, 200 successful images were collected. Due to a small fluctuation in the horizontal location of the particles in the aerosol jet, about 50% of all the recorded images didn't proceed to the signal processing. Thus, the data acquisition lasted about 40 s during which 4000 aerosol particles had passed the focal point and single-shot spectra of about 400 particles had recorded. For producing 4000 dry particles in the measurement chamber flow the IJAG had generated about 120,000 droplets corresponding a consumed sample solution volume of 14 μl. Images where the pulse had gone past the aerosol particle or the hit had been inadequate for forming hot plasma were detected and omitted by observing the intensity of atomic Na lines. Images with a successful single particle hit were converted into numerical

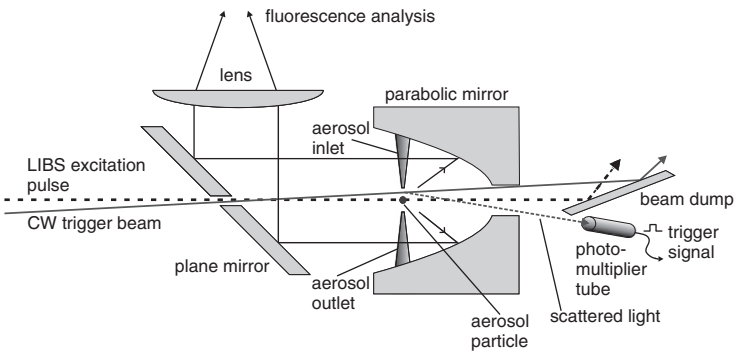

Fig. 1. Schematic of measurement chamber. Scattered light from a particle triggers an UV laser pulse that hits the particle at the focal point of a parabolic mirror.

data pixel matrices and averaged. A dark background was subtracted from the averaged pixel matrix and the final LIBS spectrum was formed by summing up the rows of the averaged pixel matrix. The LIBS spectrum was obtained within 3 min after pouring the sample solution to the IJAG.

A LIBS spectrum is composed of several spectral components. In our measurements, the strongest components were the sodium spectrum and the spectra of induced Zn and Pb. The strong emission lines of chlorine lie outside the operating wavelength range of the spectrograph. The spectral lines of atomic sodium with their spectroscopic parameters are well listed in NIST Atomic Spectra Database [16]. Signal processing program uses their location for calibrating the wavelength axis of the LIBS spectrum. Spectral lines of the metal atoms are then recognized using NIST database. The electron temperature T_e of laser-induced plasma was estimated from emission line intensity ratios using the Boltzmann plot method [3] with the assumed existence of local thermodynamic equilibrium (LTE) in the plasma. By using Zn emission lines at 335 nm, 472 nm and 481 nm, the calculated electron temperature in our single-particle measurements using 14 mJ pulse energy was about 5000 K on average.

3. Results and discussion

Superimposed LIBS spectra between 400 nm and 490 nm from zinc and lead measurements using 300 g/mm grating and 14 mJ pulse energy are shown in Fig. 2. Strong calcium spectral line at 423 nm is due to water hardness. The typical calcium concentration of tap water in Finnish city area is about 20 mg/l.

The effect of LIBS excitation pulse energy on the intensity of the 481 nm Zn spectral line, corresponding a transition $4s5s\ ^3S_1 \rightarrow 4s4p\ ^3P_2^0$ [17], was studied and the dependency is presented in Fig. 3. Maximum error in the obtained signal due to instability in the laser pulse energy measurement is indicated with vertical error bars on top of each measurement point. The noise floor is the standard deviation of the background signal multiplied by the factor of three. After the threshold energy of about 7 mJ the background subtracted Zn peak intensity increases linearly. The LIBS signal, however, was found to plummet with pulse energies larger than approximately 32 mJ as the difference between the emission peak intensity and the thermal continuum background decreases in the used detection time window.

The LIBS signal calibration curve for zinc was determined using 14 mJ excitation laser pulses to point out the technique's capability to perform LIBS analysis with low pulse energies. The 14 mJ pulse energy was chosen on a basis of being roughly twice the threshold value. Fig. 4a shows the linear behavior of the Zn 481 nm spectral line signal-to-noise ratio as a function of Zn concentration. The limit

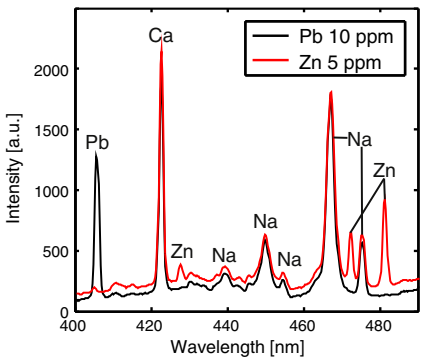

Fig. 2. LIBS spectra of zinc and lead with the same pulse energy, grating, spectrometer slit width and detection time window.

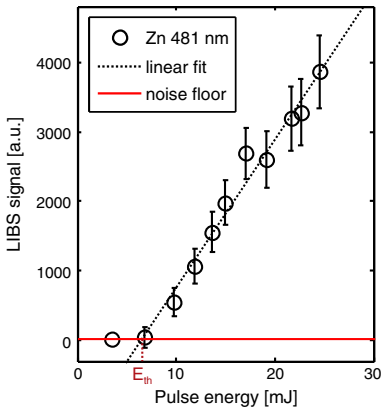

Fig. 3. Zn 481 nm background subtracted emission line intensity dependence on LIBS excitation pulse energy. E_{th} is the threshold energy of Zn LIBS signal. Noise floor is three times the standard deviation of the background.

of detection for zinc, 0.3 ppm obtained from the calibration curve, is at the level required in the industrial online measurement of water.

Assuming that the sample itself doesn't contain considerable amount of sodium, its concentration in the focal volume remains constant in our technique. Thus, it can be used as an internal standard [3]. The Zn and Na line intensity ratio in Fig. 4b has a linear dependency on metal concentration like the zinc emission line SNR but it is less affected to the fluctuation in excitation conditions. This can be seen as better correspondence between the linear fit and measured data points in Fig. 4b than in a. A smaller error in quantitative measurement is therefore achieved by using the defined Zn/Na-ratio calibration curve. The intensity ratio calibration curve was derived using the Zn line at 481 nm and Na line at 475 nm.

The strongest lead emission line in the spectrograph operating wavelength region is 406 nm peak arising from a transition $6p7s\ ^3P_1^0 \rightarrow 6p^2\ ^3P_2$ [18]. Its signal-to-noise ratio using 1200 g/mm grating is 88 when the lead concentration in the original solution is 10 ppm. Assuming that the SNR has a linear dependency on lead concentration, as in the case of zinc, the limit of detection can be calculated from these two parameters. Eq. (1) [19] defines the $3\sigma_b$ detection limit as

$$LOD = \frac{3\sigma_b}{\Delta S} c = \frac{c}{SNR}, \tag{1}$$

where σ_b is the standard deviation of the background, ΔS is the intensity difference between emission peak and background level intensities and c is the concentration of the measured sample. It yields an estimated LOD of 0.1 ppm for Pb using 14 mJ pulse energy.

When comparing our results with those studies that have reported the limit of detection for Zn and Pb in terms of mass in aqueous solution, our limits of detection appear to be of the same order or smaller using significantly lower laser pulse energy. For example, Schmidt and Goode [20] reported 0.85 ppm LOD for zinc and 1.1 ppm LOD for lead using an ion exchange membrane for collecting the trace metal ions and 80 mJ pulse energy. In another study reported by Díaz Pace et al. [21] the liquid sample was dried and compressed into CaO pellets. The obtained detection limits were 21 ppm and 20 ppm for zinc and lead respectively with 160 mJ pulse energy. Lo and Cheung [22] were able to achieve 0.3 ppm detection limit for lead without a liquid-to-solid matrix conversion by focusing a 193 nm 14.4 mJ ArF laser pulse on a vertical flow of aqueous solution containing 0.8 M HCl. It is also appropriate to compare our results with those aerosol studies which have determined the LIBS limit of detection in terms of the smallest detected

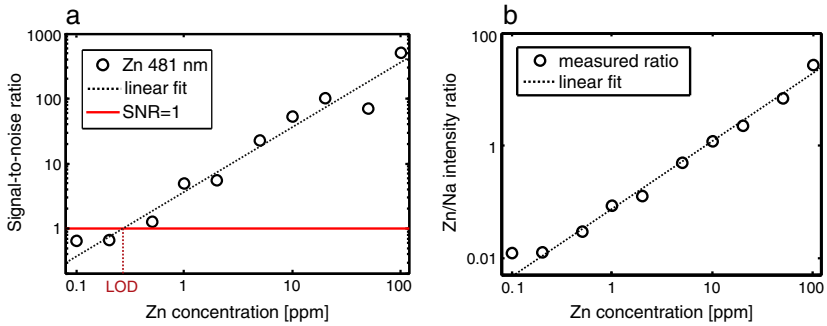

Fig. 4. a) LIBS signal calibration curve and detection limit (LOD) for Zn using emission line at 481 nm ($R^2 = 0.934$). b) Zn/Na line intensity ratio calibration curve for better quantitative determination of Zn concentration ($R^2 = 0.995$).

trace metal mass in each particle. Expressed in this way, the obtained limits of detection for Zn and Pb are 500 μg/g and 180 μg/g respectively or equivalently each aerosol particle contains 34 fg of zinc and 12 fg of lead at the limit of detection. Hahn and Lunden [23] demonstrated the detection of Ca and Mg down to the mass of 3 fg in single aerosol particles using 400 mJ pulse energy. Yet, the comparison of these results is not straightforward due to the different spectral properties of the alkali earth metals and Zn and Pb. Most papers concerning LIBS analysis of aerosol particles express their limit of detection in terms of aerosol mass concentration. These include studies by Fisher et al. [24] and Neuhauser et al. [25] who measured lead in aerosols down to the mass concentration of 190 μg/m^3 and 155 μg/m^3 respectively. The limits of detection for zinc and lead in our monodisperse NaCl aerosols with the used particle concentration are 3.4 μg/m^3 and 1.2 μg/m^3. However, in our measurement scheme, particle concentration is an adjustable parameter and decreasing it only extends the duration of the measurement.

Important factors for good LIBS limits of detection for Zn and Pb in water using only 14 mJ pulse energy are the high degree preconcentration and the scheme where a small amount of sample material can be reproducibly brought to focal volume. Increasing the laser pulse energy, LIBS signal from a single hit can be further improved as presented in Fig. 3. Alternatively, the irradiance at the focal point could be increased by focusing the beam using a large numerical aperture lens. Due to the dimensions of our measurement chamber, the beam diameter at the focus is currently much larger than the NaCl aerosols and most of the laser power goes past the particle without contributing to the particle breakdown. On the other hand, a small diameter focus might lengthen the duration of collecting successful spectra if the beam diameter is about the same size as the horizontal fluctuation of the aerosol particles within the carrier gas jet.

In conclusion, we presented a novel LIBS-based instrumentation for determining trace metals in water and applied it to the detection of zinc and lead. Both are among the most common heavy metals monitored in industrial facilities. Naturally, the technique is applicable to the detection of other metals as well. Our device introduces metals in the sample solution as dopants of dry and monodisperse NaCl aerosol particles to focal volume. Calibrated LIBS spectrum is obtained in 3 min after pouring the solution under examination in the sample holder. Linear dependence was found between the LIBS signal and exciting laser pulse energy. Using low pulse energy of 14 mJ and generalized delay and exposure time parameters we achieved 0.3 ppm detection limit for zinc and 0.1 ppm detection limit for lead. We also demonstrated the use of sodium as an internal standard in quantitative zinc measurement. The Zn/Na line calibration curve can be used if the intrinsic sodium concentration of the sample is low. The presented methodology allows the development of a sensitive monitoring device for heavy metals in industrial waters.

This research is financially supported by the Finnish Funding Agency for Technology and Innovation (TEKES), Outotec Oyj, Agnico-Eagle Finland Ab, Pyhäsalmi Mine Oy, Labtium Oy, and EHP Tekniikka Oy. The authors also like to acknowledge Aerosol Physics Laboratory at TUT for assistance in particle generation.

References

[1] D. Harris, Quantitative Chemical Analysis, Fifth edn Freeman, New York, 1999.
[2] Helsinki Comission (HELCOM), Baltic Marine Environment Protection Commission, Recommendation 23/11: requirements for discharging of waste water from the chemical industry. URL http://www.helcom.fi/Recommendations/en_GB/rec23_11, (last accessed: 27-Feb-2013).
[3] R.S. Adrain, J. Watson, Laser microspectral analysis: a review of principles and applications, J. Phys. D: Appl. Phys. 17 (1984) 1915–1940.
[4] O. Samek, D.C.S. Beddows, J. Kaiser, S.V. Kukhlevsky, M. Liška, H.H. Telle, J. Young, Application of laser-induced breakdown spectroscopy to in situ analysis of liquid samples, Opt. Eng. 39 (2000) 2248–2262.
[5] B. Charfi, M. Harith, Panoramic laser-induced breakdown spectrometry of water, Spectrochim. Acta Part B 57 (2002) 1141–1153.
[6] A. De Giacomo, M. Dell'Aglio, F. Colao, R. Fantoni, Double pulse laser produced plasma on metallic target in seawater: basic aspects and analytical approach, Spectrochim. Acta Part B 59 (2004) 1431–1438.
[7] S. Nakamura, Y. Ito, K. Sone, H. Hiraga, K.-i. Kaneko, Determination of an iron suspension in water by laser-induced breakdown spectroscopy with two sequential laser pulses, Anal. Chem. 68 (1996) 2981–2986.
[8] M. Gondal, T. Hussain, Determination of poisonous metals in wastewater collected from paint manufacturing plant using laser-induced breakdown spectroscopy, Talanta 71 (2007) 73–80.
[9] Y. Ito, O. Ueki, S. Nakamura, Determination of colloidal iron in water by laser-induced breakdown spectroscopy, Anal. Chim. Acta 299 (1995) 401–405.
[10] H.A. Archontaki, S.R. Crouch, Evaluation of an isolated droplet sample introduction system for laser-induced breakdown spectroscopy, Appl. Spectrosc. 42 (1988) 741–746.
[11] M. Essien, L.J. Radziemski, J. Sneddon, Detection of cadmium, lead and zinc in aerosols by laser-induced breakdown spectrometry, J. Anal. At. Spectrom. 3 (1988) 985–988.
[12] A. Kumar, F.Y. Yueh, T. Miller, J.P. Singh, Detection of trace elements in liquids by laser-induced breakdown spectroscopy with a Meinhard nebulizer, Appl. Opt. 42 (2003) 6040–6046.
[13] A. Manninen, M. Putkiranta, A. Rostedt, J. Saarela, T. Laurila, M. Marjamäki, J. Keskinen, R. Hernberg, Instrumentation for measuring fluorescence cross sections from airborne microsized particles, Appl. Opt. 47 (2008) 110–115.
[14] A. Manninen, M. Putkiranta, J. Saarela, A. Rostedt, T. Sorvajärvi, J. Toivonen, M. Marjamäki, J. Keskinen, R. Hernberg, Fluorescence cross sections of bioaerosols and suspended biological agents, Appl. Opt. 48 (2009) 4320–4328.
[15] M. Putkiranta, A. Manninen, A. Rostedt, J. Saarela, T. Sorvajrvi, M. Marjamki, R. Hernberg, J. Keskinen, Fluorescence properties of biochemicals in dry NaCl composite aerosol particles and in solutions, Appl. Phys. B Lasers Opt. 99 (2010) 841–851.
[16] Y. Ralchenko, A. Kramida, J. Reader, NIST ASD Team, NIST Atomic Spectra Database (Version 4.1), 2011 , (last accessed: 24-May-2012).
[17] D. Gullberg, U. Litzén, Accurately measured wavelengths of Zn I and Zn II lines of astrophysical interest, Phys. Scr. 61 (2000) 652–656.
[18] D.R. Wood, K.L. Andrew, Arc spectrum of lead, J. Opt. Soc. Am. 58 (1968) 818–828.

[19] Analytical chemistry division (IUPAC), Nomenclature, symbols, units and their usage in spectrochemical analysis-II. Data interpretation, Spectrochim. Acta Part B 33 (1978) 241–245.
[20] N.E. Schmidt, S.R. Goode, Analysis of aqueous solutions by laser-induced breakdown spectroscopy of ion exchange membranes, Appl. Spectrosc. 56 (2002) 370–374.
[21] D. Díaz Pace, C. D'Angelo, D. Bertuccelli, G. Bertuccelli, Analysis of heavy metals in liquids using laser induced breakdown spectroscopy by liquid-to-solid matrix conversion, Spectrochim. Acta Part B 61 (2006) 929–933.
[22] K.M. Lo, N.H. Cheung, ArF laser-induced plasma spectroscopy for part-per-billion analysis of metal ions in aqueous solutions, Appl. Spectrosc. 56 (2002) 682–688.
[23] D.W. Hahn, M.M. Lunden, Detection and analysis of aerosol particles by laser-induced breakdown spectroscopy, Aerosol Sci. Tech. 33 (2000) 30–48.
[24] B.T. Fisher, H.A. Johnsen, S.G. Buckley, D.W. Hahn, Temporal gating for the optimization of laser-induced breakdown spectroscopy detection and analysis of toxic metals, Appl. Spectrosc. 55 (2001) 1312–1319.
[25] R. Neuhauser, U. Panne, R. Niessner, G. Petrucci, P. Cavalli, N. Omenetto, On-line and in-situ detection of lead aerosols by plasma-spectroscopy and laser-excited atomic fluorescence spectroscopy, Anal. Chim. Acta 346 (1997) 37–48.

Paper 2

Samu T. Järvinen, Sampo Saari, Jorma Keskinen and Juha Toivonen

Detection of Ni, Pb and Zn in water using electrodynamic single-particle levitation and laser-induced breakdown spectroscopy.

Spectrochimica Acta Part B: Atomic Spectroscopy **99**, 9 – 14 (2014).

doi: 10.1016/j.sab.2014.06.007

Spectrochimica Acta Part B 99 (2014) 9–14

Contents lists available at ScienceDirect

Spectrochimica Acta Part B

journal homepage: www.elsevier.com/locate/sab

Detection of Ni, Pb and Zn in water using electrodynamic single-particle levitation and laser-induced breakdown spectroscopy☆

Samu T. Järvinen *, Sampo Saari, Jorma Keskinen, Juha Toivonen

Tampere University of Technology (TUT), Department of Physics, P.O. Box 692, FI-33101 Tampere, Finland

ARTICLE INFO

Article history:
Received 29 November 2013
Accepted 12 June 2014
Available online 24 June 2014

Keywords:
Laser-induced breakdown spectroscopy
LIBS
Heavy metal
Single-particle
Electrodynamic balance

ABSTRACT

We report the development of a unique laser-induced breakdown spectroscopy (LIBS) based method for the trace metal analysis of water. The method is further applied to the analysis of aqueous samples containing known concentrations of nickel, lead and zinc. Effects that reduce the sensitivity of the LIBS analysis of aqueous samples were avoided in the presented technology by performing the LIBS analysis from a single dried salt particle which was levitated in an electric field. The salt is added to the water sample prior to analysis. A single-droplet generator injects a droplet of the solution to the measurement chamber. The droplet is trapped using electrodynamic balance technology and metals are highly concentrated as the water from the droplet rapidly evaporates without a need for additional heating. The resultant solid 7 μm particle is levitated with a high spatial stability in the LIBS focal volume. The constant mass and position of the particle enable the high reproducibility of the LIBS signal. The limits of detection in the original solution were recorded low 60 ppb, 60 ppb, and 50 ppb for nickel, lead, and zinc, respectively using low, 14 mJ excitation pulse energy. The methodology is applicable to the online monitoring of industrial waters due to the achieved sensitivity and robust instrumentation.

1. Introduction

In the mining industry, a great amount of water is needed in many stages of ore preparation. Part of this water is evaporated in the process, part is recycled to the process and part is disposed to the surrounding water system after purification. Malfunction in the ore preparation or in the purification processes results in changes in the metal concentrations of the process water and in the surroundings of the mine. By the online measurements of the metal concentrations, these processes could be controlled and the purification could be monitored in a short time-scale. Despite the benefits, real-time analysis of heavy metal content in water at concentrations below 100 ppb remains a seldom used technology in minimizing environmental risks and optimizing enrichment processes. Typical requirements for the online detector of dissolved metals are applicability to a wide range of different metals with good selectivity, a data acquisition period limited to the maximum of a few minutes, and a low risk of sample contamination. The detector should achieve the limits of detection (LOD) lower than the current regulatory levels of 0.05–2 mg/l or ppm [1]. Established field measurement technologies generally also fulfill the requirements of movability, low power consumption and long maintenance interval. Several technologies are used for the detection of dissolved metals in laboratory, such as atomic absorption spectroscopy (AAS) with different atomizers, inductively coupled plasma optical emission spectrometry (ICP–OES) or mass spectrometry (ICP–MS), X-ray fluorescence (XRF) spectrometry, anodic stripping voltammetry (ASV) and variety of biosensors [2,3]. The obstacles to their use in online measurement applications are typically the price, size and sample preparation procedure of the devices or the need for harmful reagents. Also, the pH-dependent operation, poor durability or insensitivity to light metals limits their suitability for water monitoring at mining sites.

Laser-induced breakdown spectroscopy (LIBS) [4] fulfills many of the desired requirements. However, numerous random processes disrupt the shot-to-shot repeatability of LIBS of water streams. The shock wave created liquid aerosol particles above the water surface scatter and absorb the plasma emitted light and the sequential laser pulse in the analysis of the surface. The liquid particles and splashes are also likely to contaminate the optical components. When plasma is created in the bulk liquid, quenching and pressure broadening occur inside the bubble produced by the expanding plasma, weakening and broadening the emission lines. In addition, the plasma shielding inhibits the trailing edge of the laser pulse to heat the focal volume [5] thus lowering the plasma temperature. The formed bubbles and cavitation bubble oscillations [5] may also interfere with the collection of plasma emitted light. To outweigh these effects, the use of the wavelengths of an excimer laser [6] or a double pulse configuration [7,8] has been demonstrated. A more suitable approach for a field device is the generation of aerosols from the sample solution that has been proposed for the fast sample preparation procedure for the LIBS analysis of liquid samples [9]. The

☆ Selected paper from the 7th Euro-Mediterranean Symposium on Laser Induced Breakdown Spectroscopy (EMSLIBS 2013), Bari, Italy, 16–20 September 2013.

* Corresponding author. Tel.: +358 503237520.
E-mail address: samu.jarvinen@tut.fi (S.T. Järvinen).

http://dx.doi.org/10.1016/j.sab.2014.06.007
0584-8547/

measurement is conducted by analyzing the aerosol-rich air [9,10] or by focusing the pulse on a single aerosol particle [11,12]. Typically, plasma created in the center of a nebulized droplet cloud interacts with greater sample mass compared with the single-particle measurements, and a significant portion of the supplied energy is consumed to vaporize and dissociate the water from the droplets. Excitation pulse energies above 100 mJ are generally used for compensating the resulting overall plasma cooling and for decreasing the effects of the sample chemical composition on the plasma parameters. The factors interfering the LIBS signal can be mitigated with lower fluence in the single-particle measurement scheme. In addition, the analyte mass can be maintained nearly constant inside the plasma from pulse to pulse if monodisperse particles and a stable sample injection system is used and if the particles are small enough to undergo a complete vaporization and atomization. The challenge in the single-particle measurement is to introduce the micrometer-scale particles in a reproducible manner to the LIBS plasma. Even slight variations in the particle location will affect the time the analyte atoms equilibrate with the overall plasma by diffusion [13] and thus the LIBS signal.

Cahoon and Almirall [14] reported better LIBS detection limits for dissolved Sr, Mg, Ba, and Al from a nebulizer generated aerosol than from a single droplet. However, in their study, the repeatability of the droplet vaporization was dependent only on the stable 250 Hz continuous-mode operation of the similar piezoelectric single-droplet generator as used in the present study. As there can be a small variation in the droplet trajectory and velocity after the generator as well as jitter in the generation frequency, the sensitivity and precision of the single-droplet measurement is deteriorated by the fluctuating position of the droplet. A similar approach with the addition of triggering the droplet generator by the laser flashlamp was applied in the paper by Groh et al. [15]. They reported a fluctuation in the single-shot signal from dissolved Ca and Au due to the droplet being far from the center of the air-plasma and used a simultaneous hydrogen β line monitoring to confirm the presence of droplets in the plasma. Using a droplet generator in a continuous mode, also Janzen et al. [16] reported a significant signal decline when the droplet lies a few micrometers away from the optimal position. To overcome the fluctuation, they applied a diode laser based droplet detection system to trigger the exciting laser when the lateral displacement of the droplet was within a few micrometers.

In the papers by Cahoon and Almirall, Groh et al. and Janzen et al. the analyzed droplet diameters varied in the range of 40–100 μm and pulse energies between 60 mJ and 315 mJ. By further decreasing the amount of water that causes perturbations in the plasma parameters, the shot-to-shot repeatability of the LIBS signal could be improved [17]. An advisable method would be to decrease the size of an initially large droplet by evaporating the water and then to analyze the concentrated residual using relatively low LIBS excitation pulse energy. Such system requires a control or trapping of the droplet after injection by the single-droplet generator. Precise control of about 80 μm droplets by optical tweezers [18,19] requires a high power CW laser whereas the electrodynamic balance (EDB) technology [20,21] where a charged particle is levitated very precisely in one position by an electric field, offers more robust and low-cost solution. Previously, a LIBS analysis of an electrostatically levitated aerosol cloud was demonstrated by Dutouquet et al. by using an RF discharge cell [22].

We propose a preconcentration method for the LIBS analysis of water solutions that converts a drop of the sample solution into a single dry aerosol particle within a few seconds. The hollow particle that consists of trace metals in a NaCl matrix is trapped to the focal point of the exciting laser using the EDB technology. The constant mass and location of the sample material enable fixed excitation conditions for LIBS measurement and thus decrease the amount of averaged pulses that are required for a low detection limit. Moreover, the laser beam can be focused on a stationary 7 μm particle using a high numerical aperture lens to obtain high fluence with moderate pulse energy. The sample preparation system doesn't involve expensive components and has no moving parts. The stable NaCl-matrix can be utilized in the signal processing procedure for wavelength calibration. In this study, the aqueous solutions of nickel, lead and zinc, the essential heavy metals in Finnish mine waters, were analyzed using the EDB–LIBS technique. The novel measurement principle was found to have potential for a compact and sensitive online monitoring method of industrial waters.

2. Experimental

The measurement chamber is a vertically positioned hexagonal cylinder made of aluminum. The hexagonal cylinder has a side length of 50 mm and it has a one inch threaded through hole on every vertical face. The EDB electrodes, shown schematically in the leftmost picture of Fig. 1, consist of upper and lower pairs of round coaxial cylinders made of brass. The inner diameters of the cylinders are 8 mm and 2 mm and their respective thicknesses are 2 mm and 1 mm. The geometry and dimensions of the electrodes are the same as used by Heinisch et al. in reference [23]. The electrodes have been attached to top and bottom plates of the measurement chamber so that the cylindrical electrodes are aligned along the central axis of the measurement chamber and the vertical distance between the upper and the lower inner electrodes is 8 mm.

The outer electrodes are grounded and in contact with the measurement chamber walls whereas a high AC potential is applied to the inner electrodes which are insulated from the rest of the chamber by teflon. Between the upper and the lower electrodes, the resulting electric field is nonzero everywhere else but at the center of the trap [23] which equals the center point of the measurement chamber. The differential equation of motion of a charged particle brought in the vicinity of the EDB trap is presented, for example, in reference [21] with a graphical representation of the EDB parameters that result in a stable system. In the stable region, the AC field frequency and amplitude are selected suitably with relation to the size and mass of the particle, the geometry of the electrodes, and the ambient conditions of the measurement chamber. Consequently, the particle begins to oscillate vertically between the electrode pairs at the frequency of the AC field and experiences a time-average force towards the center of the trap. Moreover, with large particles, a weak 0–2 V DC voltage must be applied between the upper and the lower inner electrodes to cancel out the effect of gravitation. When a charged droplet of water is launched towards the EDB trap in typical indoor conditions with relative humidity of 20–80%, it starts to evaporate immediately. The decrease in the droplet mass makes the system unstable, and the oscillations will not attenuate but intensify violently until the droplet escapes the trap. The decrease in the droplet mass caused by the evaporation can be compensated with an increase in the AC field frequency or decrease in the AC field amplitude, and the system can be returned to the stable region. The levitation procedure is therefore automated using a LabVIEW program, a DAQ card (USB-6363, NI Corp.) and two high voltage amplifiers (2210, TReK Inc.) that are used to increase the AC frequency from its initial value of 80–150 Hz to the final value of 1.1–1.3 kHz as the droplet dries. The peak-to-peak value of the AC voltage between inner and outer electrodes is about 1.9 kV. Sodium chloride was dissolved in the water before pouring it to the sample container of the EDB–LIBS setup to prevent the complete extinction of the sample material due to the evaporation. After the water has evaporated, the salt forms a hollow spherical particle where the trace metals for analysis are present as additives [12,24]. The size of the dry salt particle depends on the size of the initial droplet and the salt concentration, and it can be adjusted in the range of 1–20 μm. With the applied NaCl concentration of 0.6 g/l, the evaporation increases the mass concentration of the trace metals by a factor of about 1600. The particle settling takes about 10 s from the droplet generation after which all the water has evaporated and the control program has stopped tuning the AC frequency. After stabilization to the center point of the chamber, the position of the particle can be adjusted some tens of micrometers in the vertical direction by the

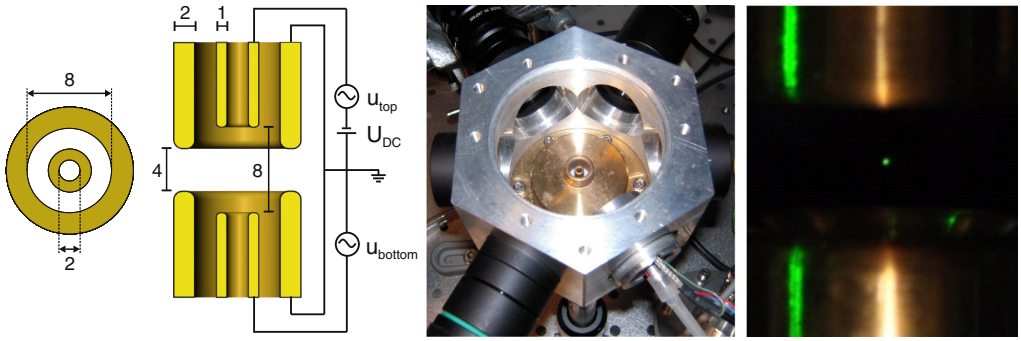

Fig. 1. Left: top and section views of EDB electrodes showing dimensions and connection diagram. Middle: designed EDB–LIBS measurement chamber photographed oblique without top plate. Right: trapped particle levitating between EDB electrodes. The photo is taken through a chamber window.

DC voltage. However, shifting the particle away from the point where the AC field is zero induces vibrations to the position of the particle.

Single droplets are produced one at a time with a piezoelectric demand mode ink-jet device and the generation of droplets is controlled by the LabVIEW program. The sample solution is injected to the droplet generator from its container via a plastic hose. The hose has a solid matter removing filter to prevent the droplet generator from clogging. The droplet generator is mounted in a custom made socket which can be fastened to one of the chamber through holes whereupon the generator points perpendicularly towards the central axis of the chamber and to the center of the trap. For successful trapping, the droplet momentum provided by the piezo element, must be adjusted accurately. The diameter of the droplet generator orifice, and the shape and amplitude of the voltage pulse supplied to the piezo element determine the exact size and initial velocity of the formed single droplet. In this study, a droplet generator having a 40 μm orifice (MJ-AB-01-40-6MX, MicroFab Technologies Inc.) and a bipolar waveform [25] having the amplitude of about 30 V were used. The formed droplets and dry salt particles had diameters of 74 μm and 7 μm, respectively. In the droplet generator mounting socket, the droplets were given a positive charge of about 5×10^6 unit charges using a steel washer having a −1.9 kV potential placed in front of the droplet generator output nozzle. As the droplet diameter decreases, the repulsion of the charges in the droplet will outweigh the surface tension leading to several exceedings of the Rayleigh limit. The resulting Rayleigh jets where the droplet shoots the extra charges away are clearly visible as the rapid deformations of the droplet during the last 1 s of the drying. The loss of mass in this process is negligible according to the papers by Duft et al. [26] and Smith et al. [27].

The LIBS measurement was excited with 14 mJ and 355 nm laser pulse from a Nd:YAG laser (NT 342/1/UVE, Ekspla Ltd.). An aspheric lens with a 30 mm focal length (84339, Edmund Optics Ltd.) was used to focus the 6 mm beam to the center of the trap where the beam waist diameter and peak irradiance were about 10 μm and 4 TW/cm^2. The particle is illuminated with the other laser beam from a 10 mW and 532 nm CW laser module (CW532-010 F, Roithner Lasertechnik GmbH). Fig. 2 represents the beam paths and the detector configuration of the EDB–LIBS setup. The scattering signal from the particle is detected by a CMOS camera and it is used for observing the size, the position, and the state of motion of the particle. The optics in front of the CMOS camera consists of a camera lens (MVL50M23, Thorlabs Inc.) and a 532 nm laser line bandpass filter. The plasma emission is collected using a 25 mm diameter and 50 mm focal length UV–VIS coated achromatic doublet lens (65976, Edmund Optics Ltd.). Another doublet having a 100 mm focal length (65979, Edmund Optics Ltd.) is used for focusing the light into a Czerny–Turner spectrometer (250is, Bruker Corp.). The dispersed light is recorded using an ICCD camera (4 Quik E, Stanford Computer Optics Inc.).

The TIFF image files from the ICCD camera software are fed to a signal processing program that converts the images to 566 × 733 pixel matrices, subtracts the dark background and sums up all the active rows of the pixel matrix. To improve the precision and the detection limit, LIBS spectra from several consecutive particles can be collected and averaged. Due to the good signal repeatability discussed in the next section, all the recorded spectra are included in the average spectrum. The spectra presented in this study, are either single-shot signals or the signal averages of 30 consecutive excitation pulses. For 30 pulses, the data acquisition and signal processing takes in total about 5.5 min. The custom signal processing program also performs the wavelength calibration which is based on the known emission wavelengths of sodium and trace metal atoms obtained from the NIST Atomic Spectra Database [28]. The measurement chamber was flushed with compressed air between the measurements to prevent contamination. The gas inlet and outlet ports are located on the top and bottom plates at the central axis of the chamber. During the measurement, the air flow is blocked to prevent any external forces affecting the trapped particle.

3. Results and discussion

The EDB–LIBS measurement scheme was demonstrated by analyzing solutions containing nickel, lead and zinc. Each three solution had a trace metal concentration of 5 ppm. Fig. 3 shows the spectra of the

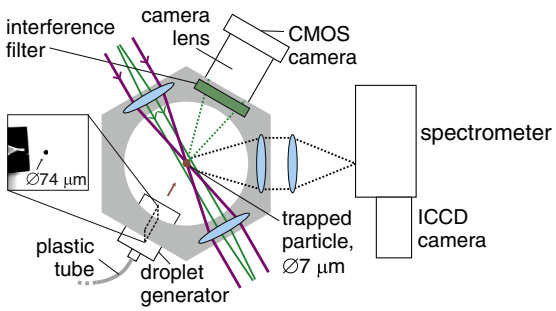

Fig. 2. Schematic of EDB–LIBS setup. Solid lines represent the 355 nm excitation beam and the illuminating 532 nm CW laser. Dashed lines show the collection angles of plasma emission and the scattering of the green laser. A photograph of an ejected droplet and the droplet generator orifice is shown in the inset.

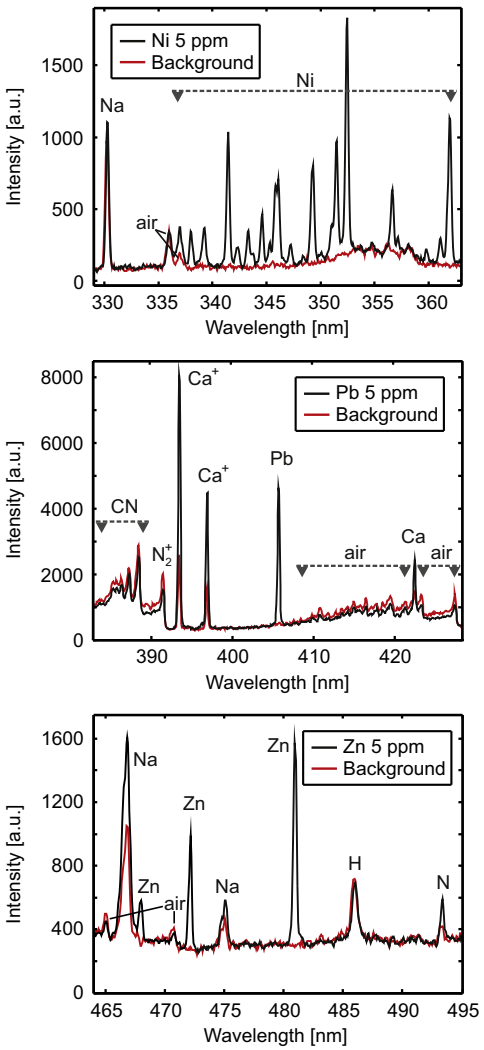

Fig. 3. Trace metal spectra. The averaged spectra of Ni, Pb and Zn superimposed over their respective background spectrum. The concentration of metals in each sample was 5 ppm corresponding to the analyte mass of 1 pg in each particle.

trace metals plotted on top of the corresponding background spectrum consisting of signals from a pure sodium chloride particle and the ambient air. All the spectra are an average of 30 consecutive laser pulses, thus only 6.3 nl has been consumed to obtain each spectrum. The small offset at the baseline levels of the trace metal and background spectra has been removed by the signal processing program. The intensifier gate was opened when the signal from the ambient air was almost extinct. The gate width was selected by visually inspecting the signal from the trace metals in question. Thus, the LIBS spectrum recording delay time with respect to the incident laser pulse was wavelength region specific whereas the exposure time was trace metal specific. No multicomponent samples were measured in this study. In the nickel measurements, the delay was set to 7 μs; it was 2.5 μs for lead and 3 μs for zinc. Temporal gate widths were 16 μs for nickel and 9 μs for lead and zinc. For lead, the probed peak was at the 406 nm wavelength and it consists of emission lines that correspond to transitions 6p7s $^3P_1^o \rightarrow 6p^2\ ^3P_2$ and 6p6d $^3D_1^o \rightarrow 6p^2\ ^1D_2$ [29]. In case of zinc, the corresponding wavelength and transition are 481 nm and 4s5s $^3S_1 \rightarrow 4s4p\ ^3P_2^o$ [30]. Nickel has several strong spectral lines between 337 nm and 362 nm of which the peak at 352 nm originating from the transition $3d^94p\ ^3P_2^o \rightarrow 3d^94s\ ^3D_3$ [31] had the highest SNR. The source of calcium was the impurities in the used sodium chloride chemical. The observed CN $B^2\Sigma^+ \rightarrow X^2\Sigma^+$ band system in the lead measurements was visible even without a particle in the measurement chamber and thus it most probably originates from the formation of CN radicals from the indoor air carbon and nitrogen [32].

The initial droplet size distribution was inspected by photographing the droplet directly after the droplet generator orifice using a CMOS camera (DCC1645C, Thorlabs Inc.) and about 5 μs flash from a xenon flashlamp (L7684, Hamamatsu K.K.). The average droplet diameter of 107 photographed droplets was 73.6 μm with a standard deviation of 0.8 μm. One of the photographs showing the initial droplet in front of the generator orifice is presented in the inset of Fig. 2. Inside the measurement chamber, the fluctuation in the position of the trapped dry particle was measured by imaging the particle using a CMOS camera with an exposure of 370 μs. The center coordinate of the particle in the images was determined by means of a 2D Gaussian fit. The standard deviations of the particle centroid in the vertical and horizontal directions were found to be less than 1.5 μm. Moreover, all particles were trapped in the very same position due to the equal size and charge of the initial droplets and the geometry of the electrodes. Because one droplet is a representative sample of the water volume under analysis and the plasma formation conditions can be kept static, the interpulse repeatability of the signal during the measurement was found to be very good. Single-shot spectra of 15 consecutive pulses from the nickel measurements are shown in Fig. 4. The relative standard deviation (RSD) of single-shot nickel signals, calculated using the 352 nm peak and 30 laser pulses, was 14% and it was possible to determine the metal concentration even using a single-shot spectrum. The mean of the estimated single-shot detection limits of nickel in the sample solution was about 470 ppb with 14% RSD. The small fluctuation in the signal was mainly due to the slight variations in the dry particle size and position. Only a weak correlation between the signal level and the fluctuating laser pulse energy was observed indicating the laser pulse energy was substantially over the complete vaporization threshold of the dry particle. The time-averaged plasma excitation temperature during the detection time window of each 30 single-shots was estimated using

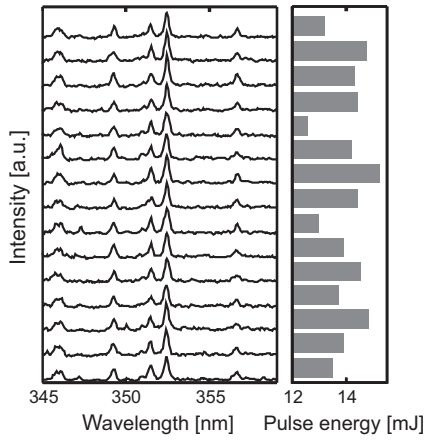

Fig. 4. Signal repeatability. 15 consecutive single-shot spectra from 15 consecutive laser pulses show the stability of the signal from 5 ppm nickel solution. The RSD of the 352 nm peak single-shot signals was 14%. Spectra are in chronological order and the bar diagram on the right represents the pulse energy of each laser pulse.

the Boltzmann plot method and the suitable emission lines of nickel between 338 nm and 362 nm. The excitation temperature was found to be 5400 K on average with a standard deviation of 730 K.

Earlier, we have shown that the trace metal analysis from monodisperse sodium chloride particles yields a linear calibration curve [12]. Because the standard error of the mean of 30 signals is only 2.6%, we can estimate the limits of detection of the EDB–LIBS technique with a good certainty using simply the averaged signal obtained from the 5 ppm solution. The calculated $3\sigma_b$ detection limits [33] for nickel and lead were 60 ppb in the original solution and 50 ppb for zinc. At the detection limit, each dry particle contains 12.5 fg of nickel and lead and 10.5 fg of zinc. The achieved detection limits were found to be the lowest values that have been obtained for dissolved nickel, lead and zinc using a LIBS-based water analysis system having pulse energy less than 20 mJ. In the calculations, the standard deviation of the background at the spectral bandwidth of the metal emission lines was obtained from the background spectrum. Before calculating the LOD, a baseline removal has been performed to the trace metal peak and the corresponding background at the peak bandwidth. In the baseline removal, the background level curve is formed by making a spline fit to the measured background spectrum. The obtained curve is then subtracted from the trace metal and background spectra. Compared with our previous approach, the limits of detection obtained using the EDB–LIBS method were clearly lower despite the significantly smaller solid angle for plasma emission collection; only 2.8% of the angle used in reference [12]. The EDB–LIBS technique also consumes less energy due to the absence of the oven for water evaporation.

In the present study, the added sodium chloride is primarily used for controlling the diameter of the dry particle to be trapped and atomized. Utilizing the added salt also for calibrating the signal intensity could further stabilize the signal [12] on conditions that the amount of salt is kept constant and the emission peaks of the internal standard element are not affected by changes in the sample composition. Sodium has been shown to cause matrix effects at the early stage of plasma due to the much lower boiling point than the trace metals [34]. As sodium chloride could be replaced by any soluble salt, matrix effects could potentially be avoided by choosing a salt of a transition metal having similar thermodynamic properties than the analyte elements. On the other hand, due to the precise position of the particle, the direct laser beam–particle interaction can be equally significant as the plasma–particle interaction in the plasma formation. Then, adding a salt, for example potassium iodide, having an absorption and a multiphoton absorption cross sections at 355 nm [35,36] greater than those of sodium chloride, could enhance the coupling between the laser pulse and the plasma.

4. Conclusions

A sensitive LIBS-based approach to the real-time elemental analysis of water samples was presented. In the presented methodology, a charged droplet of the sample solution containing added sodium chloride is trapped using an electric field. The LIBS analysis is performed from the consequential dry particle that levitates very precisely at the focal point of the light collecting optics. The method utilizes a solid matrix, a high preconcentration and a repeatable interpulse signal in the LIBS analysis of water and it is applicable to the detection of at least all the heavy metals of paramount environmental importance. In this study, we analyzed the aqueous solutions of nickel, lead and zinc. The estimated limits of detection, 60 ppb for nickel and lead and 50 ppb for zinc, were remarkably good, despite the low laser pulse energy of 14 mJ used in this work. The EDB–LIBS technique enables the engineering of a robust instrumentation for field applications that provides fast trace metal detection down to 50 ppb level using a low cost and compact excitation source. This study opens up new possibilities for online monitoring of water in harsh environments with lower costs associated with manufacture and maintenance.

Acknowledgments

This research is financially supported by Tekes—the Finnish Funding Agency for Innovation (grant number 40035/12), Metso Automation Oy, Outotec Oyj, Talvivaara Mining Company Plc and Ima Engineering Ltd Oy. Authors also acknowledge Professor Jonathan P. Reid and his research group in the University of Bristol, UK for the assistance in the EDB technology. S.T.J. acknowledges the support from the Graduate School of Modern Optics and Photonics in Finland. S.S. acknowledges the support from the doctoral school of TUT.

References

[1] Helsinki Comission (HELCOM), Baltic Marine Environment Protection Commission, Recommendation 23/11: Requirements for Discharging of Waste Water From the Chemical Industry, URL http://helcom.fi/Recommendations/Rec%2023-11.pdf (last accessed: 6-Oct-2013).
[2] I. Karube, K. Nakanishi, Immobilized cells used for detection and analysis, Curr. Opin. Biotechnol. 5 (1994) 54–59.
[3] S. Haron, A.K. Ray, Optical biodetection of cadmium and lead ions in water, Med. Eng. Phys. 28 (2006) 978–981.
[4] R.S. Adrain, J. Watson, Laser microspectral analysis: a review of principles and applications, J. Phys. D. Appl. Phys. 17 (1984) 1915–1940.
[5] P.K. Kennedy, D.X. Hammer, B.A. Rockwell, Laser-induced breakdown in aqueous media, Prog. Quantum Electron. 21 (1997) 155–248.
[6] K.M. Lo, N.H. Cheung, ArF laser-induced plasma spectroscopy for part-per-billion analysis of metal ions in aqueous solutions, Appl. Spectrosc. 56 (2002) 682–688.
[7] A. De Giacomo, M. Dell'Aglio, F. Colao, R. Fantoni, Double pulse laser produced plasma on metallic target in seawater: basic aspects and analytical approach, Spectrochim. Acta Part B 59 (2004) 1431–1438.
[8] S. Nakamura, Y. Ito, K. Sone, H. Hiraga, K.-i. Kaneko, Determination of an iron suspension in water by laser-induced breakdown spectroscopy with two sequential laser pulses, Anal. Chem. 68 (1996) 2981–2986.
[9] M. Essien, L.J. Radziemski, J. Sneddon, Detection of cadmium, lead and zinc in aerosols by laser-induced breakdown spectrometry, J. Anal. At. Spectrom. 3 (1988) 985–988.
[10] A. Kumar, F.Y. Yueh, T. Miller, J.P. Singh, Detection of trace elements in liquids by laser-induced breakdown spectroscopy with a Meinhard nebulizer, Appl. Opt. 42 (2003) 6040–6046.
[11] H.A. Archontaki, S.R. Crouch, Evaluation of an isolated droplet sample introduction system for laser-induced breakdown spectroscopy, Appl. Spectrosc. 42 (1988) 741–746.
[12] S.T. Järvinen, J. Saarela, J. Toivonen, Detection of zinc and lead in water using evaporative preconcentration and single-particle laser-induced breakdown spectroscopy, Spectrochim. Acta Part B 86 (2013) 55–59.
[13] P.K. Diwakar, S. Groh, K. Niemax, D.W. Hahn, Study of analyte dissociation and diffusion in laser-induced plasmas: implications for laser-induced breakdown spectroscopy, J. Anal. At. Spectrom. 25 (2010) 1921–1930.
[14] E.M. Cahoon, J.R. Almirall, Quantitative analysis of liquids from aerosols and microdrops using laser induced breakdown spectroscopy, Anal. Chem. 84 (2012) 2239–2244.
[15] S. Groh, P.K. Diwakar, C.C. Garcia, A. Murtazin, D.W. Hahn, K. Niemax, 100% efficient sub-nanoliter sample introduction in laser-induced breakdown spectroscopy and inductively coupled plasma spectrometry: implications for ultralow sample volumes, Anal. Chem. 82 (2010) 2568–2573.
[16] C. Janzen, R. Fleige, R. Noll, H. Schwenke, W. Lahmann, J. Knoth, P. Beaven, E. Jantzen, A. Oest, P. Koke, Analysis of small droplets with a new detector for liquid chromatography based on laser-induced breakdown spectroscopy, Spectrochim. Acta Part B 60 (2005) 993–1001.
[17] S. Groh, C.C. Garcia, A. Murtazin, V. Horvatic, K. Niemax, Local effects of atomizing analyte droplets on the plasma parameters of the inductively coupled plasma, Spectrochim. Acta Part B 64 (2009) 247–254.
[18] A. Ashkin, Acceleration and trapping of particles by radiation pressure, Phys. Rev. Lett. 24 (1970) 156–159.
[19] A. Ashkin, J.M. Dziedzic, J.E. Bjorkholm, S. Chu, Observation of a single-beam gradient force optical trap for dielectric particles, Opt. Lett. 11 (1986) 288–290.
[20] W. Li, E.J. Davis, Measurement of the thermophoretic force by electrodynamic levitation: microspheres in air, J. Aerosol Sci. 26 (1995) 1063–1083.
[21] E.J. Davis, Electrodynamic levitation of particles, in: P.A. Baron, K. Willeke (Eds.), Aerosol measurement—principles, techniques, and applications, 2nd ed., Electrodynamic Levitation of ParticlesJohn Wiley & Sons, 2001, pp. 603–625, (chap.).
[22] C. Dutouquet, G. Wattieaux, L. Meyer, E. Frejafon, L. Boufendi, Determination of the elemental composition of micrometric and submicrometric particles levitating in a low pressure radio-frequency plasma discharge using laser-induced breakdown spectroscopy, Spectrochim. Acta Part B 83–84 (2013) 14–20.
[23] C. Heinisch, J.B. Wills, J.P. Reid, T. Tschudi, C. Tropea, Temperature measurement of single evaporating water droplets in a nitrogen flow using spontaneous Raman scattering, Phys. Chem. Chem. Phys. 11 (2009) 9720–9728.
[24] M. Putkiranta, A. Manninen, A. Rostedt, J. Saarela, T. Sorvajrvi, M. Marjamki, R. Hernberg, J. Keskinen, Fluorescence properties of biochemicals in dry NaCl composite aerosol particles and in solutions, Appl. Phys. B Lasers Opt. 99 (2010) 841–851.

[25] MicroFab Technologies Inc., Drive waveform effects on ink-jet device performance, Technote 99-03, 1999.
[26] D. Duft, T. Achtzehn, R. Muller, B.A. Huber, T. Leisner, Coulomb fission: Rayleigh jets from levitated microdroplets, Nature 421 (2003) 128-128.
[27] J.N. Smith, R.C. Flagan, J.L. Beauchamp, Droplet evaporation and discharge dynamics in electrospray ionization, J. Phys. Chem. A 106 (2002) 9957–9967.
[28] Y. Ralchenko, A. Kramida, J. Reader, NIST ASD Team, NIST Atomic Spectra Database (Version 5.1), 2013. (last accessed: 22-Nov-2013).
[29] D.R. Wood, K.L. Andrew, Arc spectrum of lead, J. Opt. Soc. Am. 58 (1968) 818–828.
[30] D. Gullberg, U. Litzén, Accurately measured wavelengths of Zn I and Zn II lines of astrophysical interest, Phys. Scr. 61 (2000) 652–656.
[31] M.C.E. Huber, R.J. Sandeman, Oscillator strengths of ultraviolet NI I lines from hook-method and absorption measurements in a furnace, Astron. Astrophys. 86 (1980) 95–104.
[32] S. Abdelli-Messaci, T. Kerdja, A. Bendib, S. Malek, CN emission spectroscopy study of carbon plasma in nitrogen environment, Spectrochim. Acta Part B 60 (2005) 955–959.
[33] Analytical chemistry division (IUPAC), nomenclature, symbols, units and their usage in spectrochemical analysis-II. Data interpretation, Spectrochim. Acta Part B 33 (1978) 241–245.
[34] P. Diwakar, P. Jackson, D. Hahn, The effect of multi-component aerosol particles on quantitative laser-induced breakdown spectroscopy: consideration of localized matrix effects, Spectrochim. Acta Part B 62 (2007) 1466–1474.
[35] P. Davidovits, D.C. Brodhead, Ultraviolet absorption cross sections for the alkali halide vapors, J. Chem. Phys. 46 (1967) 2968–2973.
[36] I.M. Catalano, A. Cingolani, A. Minafra, Multiphoton transitions in ionic crystals, Phys. Rev. B 5 (1972) 1629–1632.

Paper 3

Samu T. Järvinen and Juha Toivonen

Analysis of single mass-regulated particles in precisely controlled trap using laser-induced breakdown spectroscopy.

Optics Express **24**(2), 1314 – 1323 (2016).

doi: 10.1364/OE.24.001314

Analysis of single mass-regulated particles in precisely controlled trap using laser-induced breakdown spectroscopy

Samu T. Järvinen* **and Juha Toivonen**

Tampere University of Technology (TUT), Department of Physics, Optics Laboratory, P.O. Box 692, FI-33101 Tampere, Finland

*samu.jarvinen@tut.fi

Abstract: We report the influence of water content, droplet displacement and laser fluence on the laser-induced breakdown spectroscopy (LIBS) signal of precisely controlled single droplets. For the first time in single particle LIBS scheme, the degree of evaporation of an additive-free droplet was followed and the position of the residual particle was adjusted at micrometer resolution using electrodynamic trapping. The results show signal intensification throughout the 6 s period of the complete evaporation of the droplet into a dry residual particle. The analyte line emission remained stable when the particle was moved within the focal spot area and almost tenfold compared with situation where the particle lies 15 μm outside the laser beam path. Combination of low, about 6 mJ, excitation laser pulse energy and short, about 1 μs detection delay time was found to be the optimal in the detection of most metals. The presented findings will pave the way for more sensitive and reproducible single particle elemental analysis exploited in the real-time monitoring of water, atmospheric aerosols or industrial emissions.

OCIS codes: (300.6365) Spectroscopy, laser induced breakdown; (350.4990) Particles; (010.7340) Water; (280.1545) Chemical analysis; (350.5400) Plasmas.

References and links

1. D. W. Hahn, W. L. Flower, and K. R. Hencken, "Discrete particle detection and metal emissions monitoring using laser-induced breakdown spectroscopy," Appl. Spectrosc. **51**(12), 1836–1844 (1997).
2. D. Beddows and H. Telle, "Prospects of real-time single-particle biological aerosol analysis: A comparison between laser-induced breakdown spectroscopy and aerosol time-of-flight mass spectrometry," Spectrochim. Acta, Part B **60**(7-8), 1040–1059 (2005).
3. F. J. Fortes, A. Fernández-Bravo, and J. J. Laserna, "Chemical characterization of single micro- and nanoparticles by optical catapulting-optical trapping-laser-induced breakdown spectroscopy," Spectrochim. Acta, Part B **100**, 78–85 (2014).
4. V. Lazic and S. Jovićević, "Laser induced breakdown spectroscopy inside liquids: Processes and analytical aspects," Spectrochim. Acta, Part B **101**, 288 – 311 (2014).
5. A. D. Giacomo, A. D. Bonis, M. Dell'Aglio, O. D. Pascale, R. Gaudiuso, S. Orlando, A. Santagata, G. S. Senesi, F. Taccogna, and R. Teghil, "Laser ablation of graphite in water in a range of pressure from 1 to 146 atm using single and double pulse techniques for the production of carbon nanostructures," J. Phys. Chem. C **115**, 5123–5130 (2011).
6. C. Janzen, R. Fleige, R. Noll, H. Schwenke, W. Lahmann, J. Knoth, P. Beaven, E. Jantzen, A. Oest, and P. Koke, "Analysis of small droplets with a new detector for liquid chromatography based on laser-induced breakdown spectroscopy," Spectrochim. Acta, Part B **60**(7-8), 993–1001 (2005).

#253087 Received 2 Nov 2015; revised 22 Dec 2015; accepted 3 Jan 2016; published 15 Jan 2016

25 Jan 2016 | Vol. 24, No. 2 | DOI:10.1364/OE.24.001314 | OPTICS EXPRESS 1314

7. S. Groh, P. K. Diwakar, C. C. Garcia, A. Murtazin, D. W. Hahn, and K. Niemax, "100% efficient sub-nanoliter sample introduction in laser-induced breakdown spectroscopy and inductively coupled plasma spectrometry: Implications for ultralow sample volumes," Anal. Chem. **82**(6), 2568–2573 (2010).
8. E. M. Cahoon and J. R. Almirall, "Quantitative analysis of liquids from aerosols and microdrops using laser induced breakdown spectroscopy," Anal. Chem. **84**(5), 2239–2244 (2012).
9. S. T. Järvinen, S. Saari, J. Keskinen, and J. Toivonen, "Detection of Ni, Pb and Zn in water using electrodynamic single-particle levitation and laser-induced breakdown spectroscopy," Spectrochim. Acta, Part B **99**, 9–14 (2014).
10. S. T. Järvinen, J. Saarela, and J. Toivonen, "Detection of zinc and lead in water using evaporative preconcentration and single-particle laser-induced breakdown spectroscopy," Spectrochim. Acta, Part B **86**, 55–59 (2013).
11. H. A. Archontaki and S. R. Crouch, "Evaluation of an isolated droplet sample introduction system for laser-induced breakdown spectroscopy," Appl. Spectrosc. **42**(5), 741–746 (1988).
12. E. S. Simpson, G. A. Lithgow, and S. G. Buckley, "Three-dimensional distribution of signal from single monodisperse aerosol particles in a laser induced plasma: Initial measurements," Spectrochim. Acta, Part B **62**(12), 1460–1465 (2007).
13. G. Lithgow and S. Buckley, "Influence of particle location within plasma and focal volume on precision of single-particle laser-induced breakdown spectroscopy measurements," Spectrochim. Acta, Part B **60**(7-8), 1060–1069 (2005).
14. P. K. Diwakar, S. Groh, K. Niemax, and D. W. Hahn, "Study of analyte dissociation and diffusion in laser-induced plasmas: implications for laser-induced breakdown spectroscopy," J. Anal. At. Spectrom. **25**(12), 1921–1930 (2010).
15. V. Hohreiter and D. W. Hahn, "Plasma-particle interactions in a laser-induced plasma: Implications for laser-induced breakdown spectroscopy," Anal. Chem. **78**(5), 1509–1514 (2006).
16. M. Asgill and D. Hahn, "Particle size limits for quantitative aerosol analysis using laser-induced breakdown spectroscopy: Temporal considerations," Spectrochim. Acta, Part B **64**(10), 1153–1158 (2009).
17. E. J. Davis, "Electrodynamic levitation of particles," in *Aerosol Measurement - Principles, Techniques, and Applications*, P. A. Baron and K. Willeke, eds. (John Wiley & Sons, 2001).
18. R. Warren, "Laser induced breakdown spectroscopy on suspended particulate matter in an electrodynamic balance: Interaction processes and analytical considerations," Ph.D. thesis, University of Florida (2013).
19. C. Dutouquet, G. Wattieaux, L. Meyer, E. Frejafon, and L. Boufendi, "Determination of the elemental composition of micrometric and submicrometric particles levitating in a low pressure radio-frequency plasma discharge using laser-induced breakdown spectroscopy," Spectrochim. Acta Part B **83-84**, 14–20 (2013).
20. P. Diwakar, P. Jackson, and D. Hahn, "The effect of multi-component aerosol particles on quantitative laser-induced breakdown spectroscopy: Consideration of localized matrix effects," Spectrochim. Acta Part B **62**(12), 1466–1474 (2007).
21. W. C. Hinds, *Aerosol Technology* (John Wiley & Sons, 1999). Chap. 13.7.
22. M. Chen, T. Yuan, Z. Hou, Z. Wang, and Y. Wang, "Effects of moisture content on coal analysis using laser-induced breakdown spectroscopy," Spectrochim. Acta, Part B **112**, 23–33 (2015).
23. D. R. Wood and K. L. Andrew, "Arc spectrum of lead," J. Opt. Soc. Am. **58**(6), 818–828 (1968).
24. D. Gullberg and U. Litzn, "Accurately measured wavelengths of Zn I and Zn II lines of astrophysical interest," Phys. Scr. **61**(6), 652–656 (2000).

1. Introduction

Measurement of elements in single aerosol particles, especially in small droplets, could provide new insight into several processes in the fields of research and industry. Applications can be found, for example, in cloud formation research, in analysis of very low sample volumes in bioanalytics, in monitoring of emissions [1], and in the characterization of microbes [2] and nanoparticles [3]. Laser-induced breakdown spectroscopy (LIBS) is a technique for a fast elemental analysis of the solids, liquids and gases and mixtures of these such as aerosols and can thus be utilized in single particle measurements. One of the major possibilities of single particle LIBS measurements is to perform a sensitive online analysis of liquids with nanoliter-range sample consumption as several processes suppress the signal in the direct LIBS analysis of liquid samples [4, 5]. The technique could be utilized in process and waste water control in metal production and power industry facilities, and in water treatment plants. LIBS analysis of water solutions by single droplet sampling has been previously presented in the papers by Janzen et al. [6], Groh et al. [7], Cahoon and Almirall [8] and Järvinen et al. [9, 10]. In [9] and [10], we presented a single particle LIBS methodology where the individual droplet is dried after generation and the residual particle containing the concentrated trace elements and additive salt is

#253087 Received 2 Nov 2015; revised 22 Dec 2015; accepted 3 Jan 2016; published 15 Jan 2016

introduced to the LIBS plasma.

Many referred applications require a measurement of a femtogram-level trace element mass per each particle. In the analysis of water by single droplet sampling, 1 ppb concentration limit of detection corresponds detection of only 0.5 fg in a 100 μm droplet. Such sensitivity is believed to be attainable for a real-time LIBS system if the measurement conditions are optimized and the pulse-to-pulse signal fluctuations minimized. Based on previous studies [3, 6, 11], the LIBS signal from a single droplet or a single dry particle is affected by the particle location and size at the moment of plasma initiation, and the applied laser fluence. However, the exact dependency and importance of these factors are not studied for precisely controlled particles and for low laser pulse energies of 1-20 mJ. The term 'particle' is used throughout this article to describe either a liquid droplet, a completely dry aerosol particle formed from the droplet by drying or a droplet which is at the stage of fast drying and between these two extremes.

The location of the aerosol particle with respect to the focal point of the laser affects the time the analyte atoms diffuse and equilibrate to the plasma and the location of the mass transfer origin [12–14]. Thus, analyte emission has temporal and spatial variation, yet plasma emission is typically collected only from a certain slice of the plasma volume to a spectrograph using a fixed detection time window. Using similar particles, a lower detection limit was found when the particle was precisely trapped [9] instead of moving along a 100 μm wide air flow [10]. The water content in the particle alters the size and composition of the single particle and affects the diffusion rate and plasma temperature via the energy that is required for the vaporizing and molecular dissociation of the particle [15]. Insufficient fluence with relation to particle size causes an incomplete vaporization of the particle and the elemental composition of the plasma may differ from the original particle composition. It also reduces the linearity of the analyte calibration curve [16]. On the other hand, unlike in the analysis of nebulized droplet clouds or any bulk sample, increasing the fluence significantly above the complete vaporization threshold does not add analyte mass in the plasma but only increases the temperature of different species and speeds up the expansion of the plasma.

In this study, LIBS signal from single particles was investigated when the water content and the exact position of the particles were varied. Single water droplets containing the known concentrations of Pb, Al, and Mn were trapped and levitated in the LIBS focal volume using electrodynamic balance (EDB) [17] trap and the vertical position of the particles was adjusted by an electrostatic force. The combination of LIBS and EDB has been previously presented in [18] and [9]. Moreover, Dutouquet et al. [19] demonstrated the LIBS analysis of a particle cloud levitating in a RF discharge cell. To our knowledge, this is the first time the LIBS analysis was done for single particles that were scanned across the focal spot of the laser beam with a resolution of a few micrometers. The amount of water in the aerosol particle was controlled by varying the drying time between the droplet generation and plasma initiation for monitoring the LIBS signal dependency on the level of analyte preconcentration. Scattering from the particle was used for determining the location and size of the particle and for the automatic operation of the setup. Also, LIBS signal-to-noise ratio versus excitation laser fluence was measured at different ICCD gate delay times to estimate the optimal pulse energy and gating. The results can be applied to LIBS analysis of any precisely controlled micrometer sized aerosol particles regardless of trapping technique or aerosol origin. They provide means to improve the single particle LIBS analysis with regard to sensitivity and reproducibility.

2. Experimental

Figure 1 represents the experimental EDB-LIBS setup schematically. The EDB-LIBS principle and the used EDB electrode structure and the electric potentials are described in more detail

#253087 Received 2 Nov 2015; revised 22 Dec 2015; accepted 3 Jan 2016; published 15 Jan 2016

25 Jan 2016 | Vol. 24, No. 2 | DOI:10.1364/OE.24.001314 | OPTICS EXPRESS 1316

in [9]. A piezoelectric droplet generator (MJ-AB-01-40-6MX, MicroFab Technologies Inc.) followed by a washer having -500 V potential are used to inject a charged single droplet between pairs of EDB electrodes. The droplet generator produces monodisperse droplets of about 74 μm diameter. The cylindrical electrodes are aligned along the center axis of a hexagonal measurement chamber. By controlling the electrode potentials the droplet can be trapped in the electric field and levitated with 1.5 μm precision at the focus of LIBS excitation laser beam. While levitating, the droplet dries into a dry residual particle in 3-10 s depending on the relative humidity (RH) of the surrounding air. The analyte elements in the droplet are preconcentrated due to the evaporation of the liquid matrix. The size of the residual particle depends on the total impurity concentration of the sample solution, which was conveyed to the droplet generator. Thus, each excitation laser pulse will sample almost equal trace element mass which is located in a well defined and repeated position.

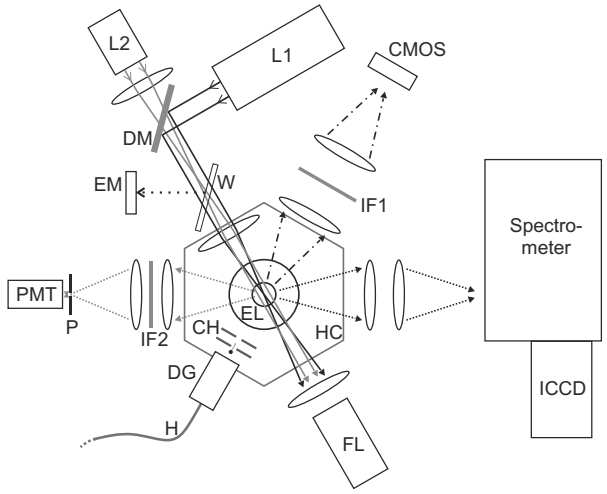

Fig. 1. The EDB-LIBS configuration. L1=pulsed Nd:YAG, L2=532 nm CW laser, DM=dichroic mirror, W=window, EM=energy meter, HC=hexagonal chamber, EL=cylindrical electrodes, DG=droplet generator, CH=droplet charger, IF1&2=interference filters, P=pinhole, FL=flashlamp, H=liquid sample hose.

After ejection from the generator orifice, the droplet oscillates vertically between the electrodes due to gravitational restoring force. The mass of the droplet is reduced by evaporation and the particle automatically settles at the focal point after complete drying. However, to measure LIBS signal versus the preconcentration level, the particle had to be driven to the LIBS focal point and the oscillation amplitude had to be suppressed before significant drying takes place. The gravitation affecting the droplet can be compensated by upward pointing electric force which is realized by applying a DC potential between upper and lower EDB electrodes. Thus, during the drying process, the DC potential was reduced continuously according to experimentally determined exponential function to settle the movement of the drying droplet already after 1 s levitation. Scattering from the droplet is used to determine if the droplet is sufficiently settled to the trapping point as discussed further in the text.

The droplet trapping requires control over the AC field frequency during the droplet drying. The levitation can be performed for different sample solutions with fixed device parameters if

#253087 Received 2 Nov 2015; revised 22 Dec 2015; accepted 3 Jan 2016; published 15 Jan 2016

the total impurity concentration in the droplets stays constant, and if the RH inside the chamber doesn't change significantly. The former condition was previously realized by adding soluble salt, such as NaCl, to the sample solution an amount that is much greater than the analyte concentration [9]. However, the added salt interferes with the detection of certain analyte emission lines and have been shown to cause matrix effects [20]. In this study, the EDB-LIBS analysis was done for the first time without using additive chemicals in the droplet. As illustrated in Fig. 1, the particle is illuminated using a 20 mW 532 nm CW laser module, and two aspheric lenses and a pinhole collect scattered green light from a small volume around the center point of the chamber. A PMT (H11706-01, Hamamatsu K.K.) detects the scattered light which provides feedback for the AC frequency adjustment algorithm. The PMT signal is also used for determining when the particle has settled and ready to be analyzed. As the particle slows down at the LIBS focal point, a 100 ms running average signal from the PMT first rises steeply, then decreases due to reduction in the droplet size, and then reaches a plateau level. After attaining the plateau, that is above certain threshold level, particle's movement is considered stopped and the system is ready to trig the LIBS excitation pulse. The trigger signal is sent to the pulse laser right after the predetermined drying time from the droplet ejection has elapsed. The trigger signal activates the function of the laser Q-switch and a pulse is emitted at the next operating cycle of the 10 Hz laser. The scattering based trigger system also enables the measurements of high purity liquid droplets that are analyzed before the complete drying.

1-15 mJ laser pulse having a temporal FWHM of 7.8 ns and FWHM diameter of 6 mm from an actively Q-switched Nd:YAG (NT 342/1/UVE, Ekspla Ltd.) emitting at 355 nm is focused on the trapped particle by a 30 mm focal length aspheric lens (84339, Edmund Optics Ltd.). The diameter of the focal spot was measured to be 19 μm. The plasma emitted light is collected at 120° angle from the direction of the incoming laser pulse using a 50 mm focal length and 25 mm diameter achromatic doublet lens (65976, Edmund Optics Ltd.). The light is focused into a spectrometer with another doublet lens having a focal length of 100 mm (65979, Edmund Optics Ltd.). An ICCD camera (DH340T-18U-E3, Andor Technology Plc.) is coupled to the Czerny-Turner spectrometer (250is, Bruker Corp.) having a 1200 grooves/mm grating. The slit of the spectrometer was set at 27 μm which is two times the ICCD pixel width and the theoretical maximum resolution of the system is 0.16 nm. The pixels in the 2048×512 CCD cell are vertically binned to speed up the signal processing program. Unless separately emphasized in the Results and discussion section, the ICCD gate delay and width times were 1 μs and 20 μs, respectively.

After the laser pulse and the following data acquisition, the whole procedure is repeated starting with a generation of a new droplet. Depending on the desired degree of drying and the RH, the period of single-shot measurements is 2 s at the shortest. Hence, the maximum sampling rate is 30 particles/min or 6.4 nl/min. The RH can be lowered by flushing the chamber with compressed dry air or nitrogen. The droplet generation, trapping and laser pulse triggering are automated using a DAQ card (USB-6363, NI Corp.) and LabVIEW software. The same software controls also the xenon flashlamp (L7684, Hamamatsu K.K.) and the CMOS camera (DCC1645C, Thorlabs Inc.) seen in Fig. 1. They are used for taking 5 μs exposure still images and videos of the levitating particle. The water samples measured in this study, were prepared by dissolving $PbCl_2$ and the hydrous compounds of $Al(NO_3)_3$ and $MnCl_2$ in deionized water and diluting the solutions in volumetric flasks. The water samples were found to contain trace amounts of calcium due to impurities in the used chemicals and deionized water.

#253087 Received 2 Nov 2015; revised 22 Dec 2015; accepted 3 Jan 2016; published 15 Jan 2016

25 Jan 2016 | Vol. 24, No. 2 | DOI:10.1364/OE.24.001314 | OPTICS EXPRESS 1318

3. Results and discussion

3.1. Effect of droplet evaporation stage

Figure 2 presents an example spectrum showing the response to Mn, Al and Pb. The LIBS signal dependency on water content in the particle was measured by varying the time between the droplet generation and the LIBS excitation laser pulse as described in the Experimental section. The excitation pulse energy was maintained at 4 mJ and the signal was collected from Al 396.2 nm and Mn 403.1 nm emission lines. The concentration of both trace metals was

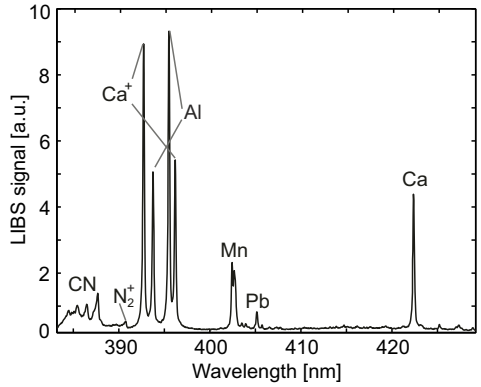

Fig. 2. EDB-LIBS spectrum from water sample containing 1 ppm of Mn and Al and 0.6 ppm of Pb using 4 mJ excitation laser pulse energy. The spectrum is an average of 20 single-shot spectra. The CN and N_2^+ bands originate from the ambient air.

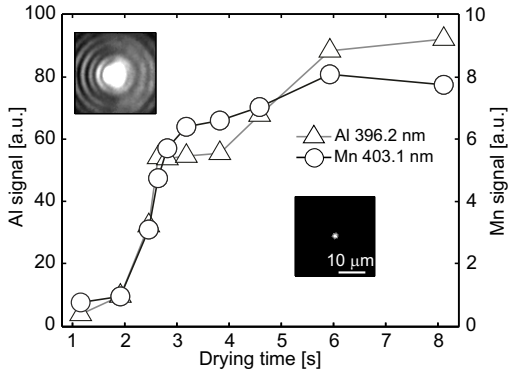

Fig. 3. LIBS signal from Al and Mn as function of drying time. The insets show 30μm$\times30\mu$m CMOS camera images of the particle at 1 s and 6 s after the droplet launch.

1 ppm corresponding 0.2 pg of Al and Mn in each droplet. The RH of the air inside the chamber was 25%. The results presented in Fig. 3 show a rise in the signal until drying time of about 6 s. After the rise, the signal settles at a saturation level which is assumed to correspond a

#253087 Received 2 Nov 2015; revised 22 Dec 2015; accepted 3 Jan 2016; published 15 Jan 2016

situation where all the water has evaporated from the droplet. The time of complete drying, 6 s, agrees well with the theoretical drying time for 74 μm water droplet in RH=25% air [21]. The signal remains constant at the saturation level even after significantly longer trapping times than presented in Fig. 3. The main reasons for the signal reduction at short drying times are the incomplete vaporization of the large droplet and the consumption of energy for phase transition. They result in lower temperature plasma having a lower analyte species density compared with the analysis of a completely dried particle. At longer drying times, the decreasing moisture content in the particle increases the signal until complete drying. The relation between sample moisture and LIBS signal was reported in a recent study by Chen et al. [22]. Large droplets are more difficult to settle accurately at the focal point due to their mass and initial velocity. It was not possible to settle the droplet faster in the focal volume than about 1 s which determined the shortest investigated drying time.

3.2. Effect of micrometer displacements in the single particle position

The effect of micrometer-scale displacements between the analyzed particle and the focal point of the excitation laser beam on the LIBS signal from Pb 405.8 nm emission line was investigated using the ability to control the particle location in the EDB chamber. The dependency is expected to be independent of the selected transition. The water sample contained 20 ppm of Pb which corresponds 4 pg per droplet, and all the analyzed droplets were dried completely into a dry residual particles. The LIBS excitation pulse energy was kept at 5 mJ which produced plasma in the chamber even without a particle in the trap. The vertical displacement of the particle was determined from the still images using the flashlamp and the CMOS camera. The inset in Fig. 4 presents the vertical displacement of the centroid of a 5.5 μm particle from the excitation beam focus for each DC voltage values between the upper and lower electrodes. The ordinate in the upper graph of Fig. 4 is an average LIBS signal of 20 single-shot spectra. At each measurement point, the plasma emission was guided to the spectrometer with constant

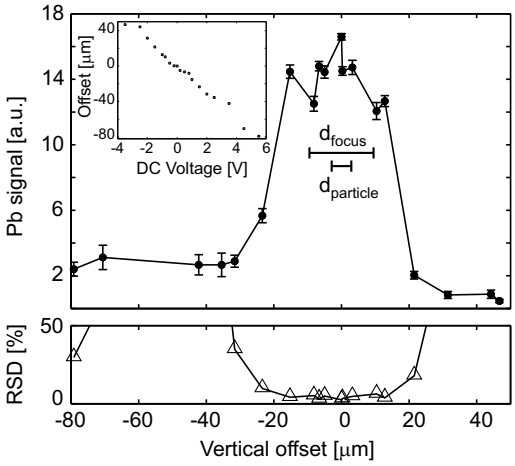

Fig. 4. LIBS signal from Pb and signal RSD as function of particle position. The error bars in the upper graph show the standard deviation of the mean signal whereas the signal fluctuation between successive points is due to a systematic error. Particle displacement versus bias voltage between upper and lower electrodes is shown in the inset.

#253087 Received 2 Nov 2015; revised 22 Dec 2015; accepted 3 Jan 2016; published 15 Jan 2016

light collecting efficiency. The signal remains stable while the particle lies in the interval which has a width of approximately 1.5 times the focal spot diameter. After the offset of ± 15 μm, there is a sharp signal decrease setting the collected analyte emission at a level of less than one seventh of the emission collected at the focus. These high-signal and low-signal levels are assumed to correspond the region where the laser pulse can directly interact with the particle and the region where plasma forms first in air and then surrounds the particle by expansion. In the latter, the analyte emission may be localized to a certain part of the plasma cloud [15]. The high signal was observed also when the particle was only partly located in the focal area. When the particle is well located at the focal spot, the fluctuation of the single-shot signals is about 15%. The lower graph shows the relative standard deviation (RSD) of the averaged signal. It is obtained by dividing the standard deviation of the mean by the average signal of 20 single-shots. The RSD is less than 4% when the particle is located at the focus. Applying a DC voltage different from the value that exactly cancels out the effect of gravitational force causes the particle to vibrate slightly in the vertical direction. Thus, moving away from the focus increases the deviation in the successive particle positions which also contributes to the rise in signal RSD.

3.3. Pulse energy in single particle measurements

Effect of LIBS excitation laser fluence was studied by varying the pulse energy between 1.5 mJ and 15 mJ. Atomic lines are visible with pulse energies greater than 1.5 mJ which is labeled as the threshold for the plasma generation E_{th} in Fig. 5(a). At this fluence, more than 50% of the excitation pulses do not vaporize the 3 μm residual particle but merely break it into small fractions that are still visible in the CMOS camera screen. The fractions levitate between the electrodes until they are removed by flushing air through the chamber. When the pulse energy is adequate to vaporize the particle in the trap, no fractions are observed and flushing is not required. Figure 5(a) shows the LIBS signal-to-noise ratio (SNR) of Pb 405.8 nm emission line as a function of excitation pulse energy using 700 ns, 1 μs and 5 μs ICCD gate delay times. In the measurement of SNR, the signal is the background subtracted peak height and noise is defined as three times the standard deviation of the background. The emergence of the background is considered the primary reason for decreasing SNR at higher pulse energy values. Less important factors are the larger diameter of the emitting vapor, the higher degree of ionization, and the temperature dependency of the electronic partition function $Z(T)$ of Pb atom. The emitting vapor is more confined using a combination of short delay and low pulse energy as shown in images 1-4 in Fig. 5(b). Thus, more analyte atoms are within the narrow field-of-view of the spectrometer which is considered the reason for higher SNR maximum at short gate delays. Using a delay time less than 1 μs can nevertheless be impractical due to the high sensitiveness of the SNR to the changes of pulse energy. Short delay also requires pulse energy to be near E_{th} and may cause signal fluctuation through the incomplete vaporization of the particle. The error bars in Fig. 5(a) present the standard deviation of the single-shot SNR values. Similar dependence as seen in Fig. 5(a) was found for other atomic transitions having the upper state energy less or comparable to 4.4 eV which is the upper state energy of the probed Pb 6p7s $^3P_1^o \rightarrow$ 6p^2 $^3P_2$ transition [23]. The measured transitions include Al 396.2 nm, Mn 403.1 nm, and Ca 422.7 nm lines. The requirement of higher plasma temperature and thus higher pulse energy is expected when probing transitions involving significantly higher upper energy states. For example, the SNR of the Zn 481.1 nm emission line having the upper state energy of 6.7 eV [24] was found to increase 145% when the pulse energy was raised from 6 mJ to 10 mJ.

The LIBS signal response to Pb mass was found to be linear in the concentration interval of 4–40 ppm Pb in the sample solution or equivalently 0.8–8 pg of Pb in each particle. The applied

#253087 Received 2 Nov 2015; revised 22 Dec 2015; accepted 3 Jan 2016; published 15 Jan 2016

25 Jan 2016 | Vol. 24, No. 2 | DOI:10.1364/OE.24.001314 | OPTICS EXPRESS 1321

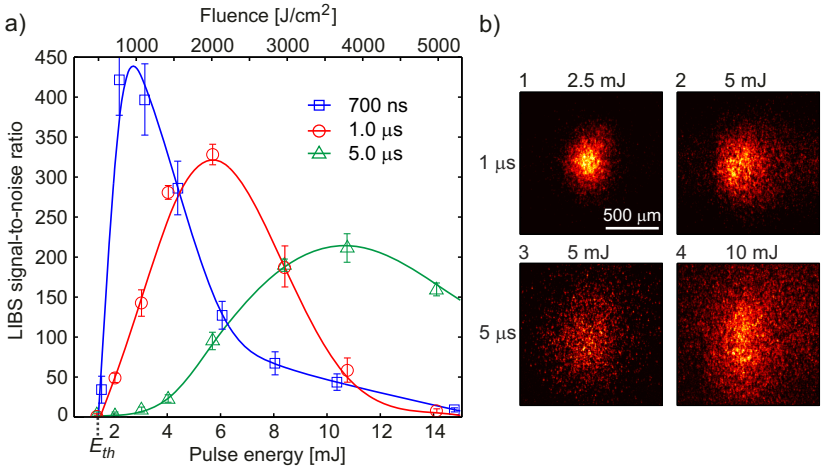

Fig. 5. a) LIBS SNR of 20 ppm Pb as function of excitation laser pulse energy using 700 ns, 1 μs and 5 μs gate delays. The spline fit curves are guides for the eye and have no physical interpretation. b) Pb 405.8 nm emission from plasma using different pulse energies and 1 μs (1 and 2) and 5 μs (3 and 4) gate delays. Imaged through a bandpass interference filter using 100 ns ICCD gate width.

pulse energy was 6 mJ which was found to be optimal in the detection of Pb in 3 μm particles. If the trapped particle is notably larger, for example, due to a high water impurity concentration, the signal saturates due to the incomplete vaporization of the particle mass. Higher pulse energy is then required for the linear dependency. The change in the pulse energy will also affect the value of the optimal gate delay according to Fig. 5(a). 40 ppm was the highest Pb concentration measured in this study due to the poor solubility of the $PbCl_2$ salt.

4. Conclusions

The LIBS signal dependency on the water content and the exact position of single particles was quantified. The measurements were carried out using an additive-free EDB-LIBS technique which enables the control of the particle position and the liquid aerosol particle size while holding other conditions fixed. The key benefit in the single particle analysis of liquids is the preconcentration of the trace elements as even a very small amount of water in the particle was found to depress the LIBS signal. The signal from both investigated elements saturated after 6 s period of droplet evaporation. When the particle was scanned across the laser beam path, the region of the high signal was observed where the particle could directly interact with the LIBS excitation pulse. Increasing the excitation pulse energy significantly above the plasma formation threshold energy is not advisable in a single particle LIBS scheme where the mass to be vaporized is limited. In the detection of several trace metals in micrometer sized particles, pulse energy around 6 mJ with gate delay of 1 μs was considered optimal in terms of SNR and pulse-to-pulse repeatability. However, the optimal pulse energy value also depends on the plasma imaging area and laser focusing optics. Based on the obtained results, simultaneous variation in the particle location and size and excitation pulse energy can fluctuate the single particle LIBS signal of successive pulses even orders of magnitude. On the other hand, for many

#253087
Received 2 Nov 2015; revised 22 Dec 2015; accepted 3 Jan 2016; published 15 Jan 2016

25 Jan 2016 | Vol. 24, No. 2 | DOI:10.1364/OE.24.001314 | OPTICS EXPRESS 1322

analytical purposes, the information from a single-shot spectrum is sufficiently accurate if the three factors are optimized and stabilized. The current findings pave the way for enhanced LIBS analysis for monitoring liquid and fine particle emissions, for industrial process and quality control and for atmospheric and biochemical research.

Acknowledgment

S.T.J. acknowledges the support from the Graduate school of TUT.

#253087 Received 2 Nov 2015; revised 22 Dec 2015; accepted 3 Jan 2016; published 15 Jan 2016

Paper 4

S. Saari, S. Järvinen, T. Reponen, J. Mensah-Attipoe, P. Pasanen, J. Toivonen and J. Keskinen

Identification of single microbial particles using electro-dynamic balance assisted laser-induced breakdown and fluorescence spectroscopy.

Aerosol Science and Technology **50**(2), 126 – 132 (2016).

doi: 10.1080/02786826.2015.1134764

Aerosol Science and Technology

ISSN: 0278-6826 (Print) 1521-7388 (Online) Journal homepage: http://www.tandfonline.com/loi/uast20

P4

Identification of single microbial particles using electro-dynamic balance assisted laser-induced breakdown and fluorescence spectroscopy

S. Saari, S. Järvinen, T. Reponen, J. Mensah-Attipoe, P. Pasanen, J. Toivonen & J. Keskinen

To cite this article: S. Saari, S. Järvinen, T. Reponen, J. Mensah-Attipoe, P. Pasanen, J. Toivonen & J. Keskinen (2016) Identification of single microbial particles using electro-dynamic balance assisted laser-induced breakdown and fluorescence spectroscopy, Aerosol Science and Technology, 50:2, 126-132, DOI: 10.1080/02786826.2015.1134764

To link to this article: http://dx.doi.org/10.1080/02786826.2015.1134764

AEROSOL SCIENCE AND TECHNOLOGY
2016, VOL. 50, NO. 2, 126–132
http://dx.doi.org/10.1080/02786826.2015.1134764

Identification of single microbial particles using electro-dynamic balance assisted laser-induced breakdown and fluorescence spectroscopy

S. Saari[a*], S. Järvinen[a*], T. Reponen[b,c], J. Mensah-Attipoe[b], P. Pasanen[b], J. Toivonen[a], and J. Keskinen[a]

[a]Department of Physics, Tampere University of Technology, Tampere, Finland; [b]Department of Environmental Science, University of Eastern Finland, Kuopio, Finland; [c]Department of Environmental Health, University of Cincinnati, Cincinnati, Ohio, USA

ABSTRACT

Online characterization of fungal and bacterial spores is important in various applications due to their health and climatic relevance. The aim of this study was to demonstrate the capability of the combination of electro-dynamic balance assisted laser-induced breakdown spectroscopy (LIBS) and laser-induced fluorescence (LIF) techniques for the online detection of single fungal spores (*Aspergillus versicolor* and *Penicillium brevicompactum*) and bacteria (*Bacillus aureus*). The method enabled sensitive and repeatable LIBS analysis of common elemental components (Ca, Na, and K) from single microbial particles for the first time. Significant differences in the concentrations of these elements were observed between the species, e.g., bacterial spores had over three orders of magnitude higher Ca concentration (2×10^{-12} g/particle) compared to fungal spores ($3–5 \times 10^{-16}$ g/particle). The LIF analysis has previously been used to distinguish bioaerosols from other aerosols due to their fluorescence ability. This study showed that combination of LIF and LIBS analysis is a promising tool for identification of different bioaerosol particle types.

ARTICLE HISTORY
Received 2 October 2015
Accepted 7 December 2015

EDITOR
Paul J. Ziemann

Introduction

Airborne microbial particles, such as fungal spores and bacteria, can cause a wide range of health effects with major public health impact, including infectious diseases, acute toxic effects, and allergies (Douwes et al. 2003). Moisture in water-damaged buildings enables microbes to grow, which may cause adverse health effects when microbes are released into the indoor air. Outdoor microbes can spread diseases and are health risk especially in urban environments where population is typically dense (Douwes et al. 2003). Drinking water should be free of pathogenic microbes, so it is important to control the microbial contents in drinking water before delivery to the customers (WHO 2004). Atmospheric fungal spores and bacteria are involved in the hydrological cycle on the Earth as they can act as cloud condensation nuclei and ice nuclei (Després et al. 2012). Clouds have an important role in the Earth's radiation balance, so microbial aerosols may be important in the global climate change (IPCC 2013).

As described above, online measurement of microbial concentrations is useful for several applications. Traditional methods for determining the concentration of airborne microbes, such as Andersen impactor and filter sampling, require a separate step for analysis before concentration can be determined. Furthermore, these methods have relatively low time resolution (Reponen et al. 2011). Laser-induced fluorescence (LIF) is a modern technique for real-time bioaerosol detection (Hill et al. 1995; Kaye et al. 2005; Pöhlker et al. 2012). It is an effective method for detecting biological molecules such as tryptophan, NAD(P)H, and flavins that are typically present in microbial cells (Lakowicz 2009). LIF enables the differentiation of bioaerosols from other airborne particles through their fluorescence ability (Pöhlker et al. 2012; Hill et al. 2013). Saari et al. (2013) demonstrated that bacterial and fungal spores may be distinguished from each other through their dissimilar fluorescence spectra. However, fluorescence analysis may include uncertainties due to interference by fluorescent non-biological particles in the atmosphere.

Laser-induced breakdown spectroscopy (LIBS) is a technique for a rapid elemental analysis of solid, liquid, and gaseous samples. It can be used for measuring elemental components in aerosol plumes or in a single

CONTACT S. Saari sampo.saari@tut.fi Department of Physics, Tampere University of Technology, P.O. Box 692, Tampere FI-33101, Finland.
Color versions of one or more of the figures in the article can be found online at www.tandfonline.com/uast.
*S. Saari and S. Järvinen contributed equally to this work.
Supplemental data for this article can be accessed on the publisher's website.

aerosol particle (Hybl et al. 2003, 2006; Järvinen et al. 2014). Dutouquet et al. (2013) demonstrated LIBS analysis on the particles injected in the radio-frequency plasma discharge and trapped in levitation. They reported that the use of such particle trap could improve particle sampling, making organic particle analysis possible and even obtaining a better signal-to-noise ratio. Fortes et al. (2014) reported spectral identification of individual micro- and nano-sized particles by the sequential intervention of optical catapulting, optical trapping, and LIBS having 30% relative standard deviation of LIBS signal for the inspection of Ni microspheres. LIBS also has been explored as a potential method detecting fungal spores and bacteria based on the concentrations of Na, Ca, and K (Hybl et al. 2003, 2006). One of the challenges in the single particle LIBS analysis is the control of particle location and hit rate (Hybl et al. 2006; Park et al. 2009; Tjärnhage et al. 2013), but this can be overcome by the use of the electro-dynamic balance (EDB) chamber (Järvinen et al. 2014).

In this study, we generated single, electrically charged, fungal spores and bacteria particles and levitated them in an EDB trap. The EDB enables accurate and repeatable particle trapping position (Heinisch et al. 2009; Järvinen et al. 2014) and both LIF and LIBS spectra can be measured from the same particle. We used LIBS to quantify the amount of Na, Ca, and K in single fungal spores and bacteria particles. The combination of EDB, LIF, and LIBS techniques enabled us to separate the different bioaerosol types from each other using an online measurement concept.

Materials and methods

Experimental setup

The EDB chamber and the measurement setup are the same as presented in our previous study (Järvinen et al. 2014) with a few minor modifications. Figure 1 represents the experimental setup of the EDB chamber coupled with LIF and LIBS analysis. A piezoelectric single droplet generator with a 40 μm orifice (MJ-AB-01-40-6MX, MicroFab Technologies Inc., Plano, TX, USA) equipped with a high voltage (−1.9 kV) charging plate was used to introduce a single charged droplet (about 5 $\times$ 10^6 positive unit charges per droplet) into the EDB chamber. A bipolar waveform (MicroFab Technologies Inc. 1999; Plano, TX, USA) having the amplitude of about 30 V was used in the generator that formed droplets with diameters of 74 μm. The EDB electrodes were used to trap and to keep the particle stable in the center of the chamber. Geometry of the EDB electrodes was similar to one reported by Heinisch et al. (2009). AC

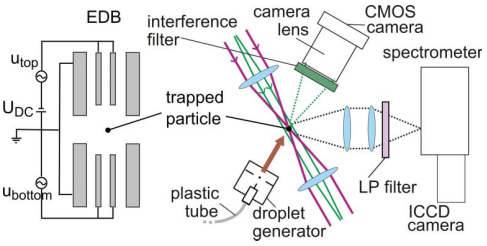

Figure 1. Left: Schematic electro-dynamic balance (EDB) configuration for particle trapping. Right: Optical setup for laser-induced fluorescence (LIF) and laser-induced breakdown spectroscopy (LIBS) and droplet generation. Violet and green (solid) lines represent the 355 nm LIF/LIBS excitation beam and the illuminating 532 nm diode laser. Dashed lines show the collection angles of plasma and fluorescence emission and the scattering of the green laser. A long-pass (LP) filter was used only in LIF measurements.

voltage with 950 V amplitude was used in the inner electrodes to generate the EDB. A small, 0–5 V, DC component between the electrodes was used to compensate the effect of gravitation. The decrease in the droplet mass caused by the evaporation can be compensated with an increase in the AC field frequency or decrease in the AC field amplitude, and thus, the droplet can be returned to the stable region. The AC frequency about 80–150 Hz was used to trap the droplet and the frequency was increased to the final value of 1.6–1.9 kHz as the droplet dried. The particle was illuminated with CW laser beam from a 10 mW and 532 nm laser module (CW532-010 F, Roithner Lasertechnik GmbH, Vienna, Austria). The stationary particle was then observed on the CMOS camera screen and the size of the dry residual particle or single spore could be determined from the camera image. Dry particle size distribution from the droplet generator was also measured separately using an aerodynamic particle sizer (APS; TSI Model 3021, TSI Inc, Shoreview, MN, USA). Before the APS, the droplets were dried using a heated tubular oven at the temperature of 100°C.

First, the LIF spectrum was recorded from a particle, and after that, the destructive LIBS analysis was performed to the same particle. The fluorescence was excited with 355 nm and 7.8 ns pulse from an Nd:YAG laser (NT 342/1/UVE, Ekspla Ltd., Vilnus, Lithuania). An UV–VIS coated achromatic doublet lens (65976, Edmund Optics Ltd., Barrington, NJ, USA) having a numerical aperture of 0.24 was used to collect the fluorescence. The collected light was focused into a Czerny–Turner spectrometer (250is, Bruker Corp., Billerica, MA, USA) with a 100 mm focal length achromatic doublet (65979, Edmund Optics Ltd.). A 355 nm long-pass filter (LP02-355RE-25, Semrock Inc.) before the spectrometer

was used to block the scattering of the excitation beam. The fluorescence spectrum was recorded with a 10 nm resolution using a 2048 × 512 pixel ICCD camera (DH340T-18U-E3, Andor Technology Ltd., Belfast, UK). The operational wavelength range of the spectrometer–ICCD camera combination is 320 nm–820 nm. In the LIF measurements, the ICCD gate delay with relation to the laser pulse was zero and the intensifier gate was kept open 80 ns after the LIF excitation laser pulse.

The LIBS analysis was excited after the LIF measurement using the same pulsed Nd:YAG laser. Laser pulse energy was 450 nJ in the LIF and 9 mJ in the LIBS analysis, and the selection between the two pulse energy levels was done by a switchable attenuator. An aspheric lens having a 30 mm focal length (84339, Edmund Optics Ltd.) focused the LIBS excitation beam to the center of the trap where the beam waist diameter was 19 μm. The plasma emission was guided into the spectrometer using the same components as in LIF. In the LIBS measurements, the optical resolution of the spectral imaging system was 0.2 nm and the ICCD gate delay and width were 1'μs and 20'μs, respectively. The LIF and LIBS measurements were repeated 20 times for each type of test particles. About 1 min delay between the LIF and LIBS measurements was determined by the manual adjustment of the ICCD camera settings.

Test aerosols

Spores from two fungal species (*Aspergillus versicolor* from Culture collection of the Institute for Health and Welfare, Finland: HT31, and *Penicillium brevicompactum* from American Type Cell Collection: ATCC 58606) and one bacterial species (*Bacillus aureus/licheniformis*, from State Scientific Center of The Russian Federation Institute for Biomedical Problems) were used as test biological particles. The fungal strains are common in indoor air worldwide (Hyvärinen et al. 2002; Reponen et al. 2012).

The fungi were first grown on agar plates. Malt extract agar (ME) (LabM, Lancashire, UK) was used for *A. versicolor*, whereas dichloran glycerol 18% agar (DG18) (Merck, Darmstadt, Germany) was used for *P. brevicompactum*. Inoculated agar plates were incubated at room temperature (21 ± 2°C) for two weeks. Fungal spores were harvested from agar plates by applying glass beads (Ø = 425–600'μm; Sigma-Aldrich Co., Saint Louis, MO, USA) to agar plates containing individual fungal cultures and shaking them gently back and forth to get spores attached to the beads. Thereafter, the beads were transferred to a tube containing 10 ml of de-ionized (DI) pure water. The spores were suspended from the beads by shaking the tube and decanting the spore suspension. The concentration of the spore suspension was adjusted to 10^7 spores/ml using a hemacytometer (Fuchs-Rosenthal: Hirschmann Laborgeräte, Eberstadt, Germany) resulting in roughly a single spore in a droplet generated by the single droplet generator. Typical particle size distribution of the generated fungal spores (*A. versicolor*) measured by aerodynamic particle sizer (APS Model 3321, TSI) after drying is shown in Figure S1 in the online supplementary information (SI). The measured mean particle size (2.8'μm) is characteristic for single *A. versicolor* spores (Reponen et al. 2001). This confirms that single fungal spores were analyzed with the EDB.

B. aureus was first inoculated on typticase soy agar (TSA) (Sigma-Aldrich Co., St. Louis, MO) for 24 ± 2 h at 37°C. Thereafter the colonies were harvested with an inoculation loop (V = 0.4 ml, Ø = 0.9'μm) into physiological solution (phosphate buffer-0.05% Tween 20) and then inoculated on potato agar (PA) (Thermo Scientific Oxoid, Basingstoke, UK) and incubated for 48 ± 2 h at 37°C. Incubation was continued under natural light at room temperature (21 ± 1°C) for five days. After the seven days of incubation, *B. aureus* suspension was prepared by applying 5 ml of sterile DI water to the sporulating bacterial culture and gently scraping the culture with an inoculation loop (V = 0.4 ml, Ø = 0.9'μm) to release the spores into suspension. The resultant suspension was decanted into 50 ml tubes and mixed well. The well-mixed suspension was filtered through a filter (Black ribbon, grade 589/1, Ø = 90 mm) to remove all debris of growth media and possible agglomerates of bacterial colonies. The concentration of the suspension was about 10^8 spores/ml. The volume of generated droplet was 2 × 10^{-7} ml, in which case the number of bacterial spores per droplet was estimated to be 20.

Calibration of Na, Ca, and K

To calibrate LIBS signals to mass concentrations in the system, pure NaCl, $CaNO_3$, and KCl (purchased from VWR International Oy, Helsinki, Finland) were dissolved in purified DI water with varying concentrations as discussed below, and particles with certain mass concentrations were fed into the EDB chamber. Na, Ca, and K have strong emission lines within the bandwidth of the spectrometer used in this work. They have been reported acting as dominant compounds in LIBS spectra of bacterial and fungal spores (Hybl et al. 2003, 2006; Singh and Rai 2011) and the detection of Na, Ca, and K is not interfered by the elements present in the ambient air. In this study, we measured actual mass concentrations of these elements in single spores. Pure DI water was used as a reference particle material to estimate background levels of LIBS signals.

The calibration particles were produced from sample solution containing 0.05–100 ppm of Na, 0.1–100 ppm of Ca, and 0.05–100 ppm of K. The smallest measured concentrations correspond to the analyzed mass of 11 fg, 21 fg, and 11 fg in each particle for Na, Ca, and K, respectively. The detection limit of the signal was restricted by electrical noise and laser pulse energy fluctuations as well as by impurities in (DI) water. The calibration curves for Na, Ca, and K are shown in Figure S2 in the SI. The extrapolated theoretical detection limit values were estimated from the intersection of the calibration curve and noise level at triple the standard deviation of the background signal. The theoretical detection limits based on the noise in the measurement system were clearly well below ppb level for all the studied elements. However, practical detection limits in this study were limited by impurities in used DI water. These detection limits were estimated by taking the intersection point between the dashed DI water curve and the extrapolated calibration curve in Figure S2 (see the SI), leading to 30 ppb, 1.5 ppb, and 0.4 ppb detection limits for Na, Ca, and K, respectively.

Na, Ca, and K mass concentrations in single microbial particles were calculated based on the LIBS signals and calibration described above. We also used analysis of variance method (one-way ANOVA followed by Student's *t*-test) to calculate statistical significant differences ($p < 0.01$) of concentrations between the species.

Results and discussion

LIBS spectra of fungal spores and bacteria

LIBS analysis was performed for single fungal spores and bacterial spore aggregates. Typical single shot LIBS spectra from bacterial spores (*B. aureus*, B.a.), fungal spores (*A. versicolor*, A.v., and *P. brevicompactum*, P.b.), and DI water particles are shown in Figure 2. Characteristic Na lines (589.0 nm and 589.6 nm) were strong from all the microbial particles as well as from the particles aerosolized from DI water. Bacterial particles showed also high peaks at characteristic Ca and K wavelengths (393.4 nm and 396.8 nm for Ca, and 766.5 nm and 769.9 nm for K), whereas A.v. and P.b. fungal spores exhibited clearly weaker signals at these wavelengths. Mass concentrations of Na, Ca, and K in the microbial particles and detection limits are discussed below.

Farooq et al. (2014) reported LIBS spectroscopy of bacteria samples on glass substrate and found a number of elements (Ca, Mg, Na, K, P, S, Cl, Fe, Al, Mn, Cu, C, H, and CN-band). However, the highest peaks were observed for Ca and Na as shown also in this study. Glass substrate may include impurities that can evaporate in

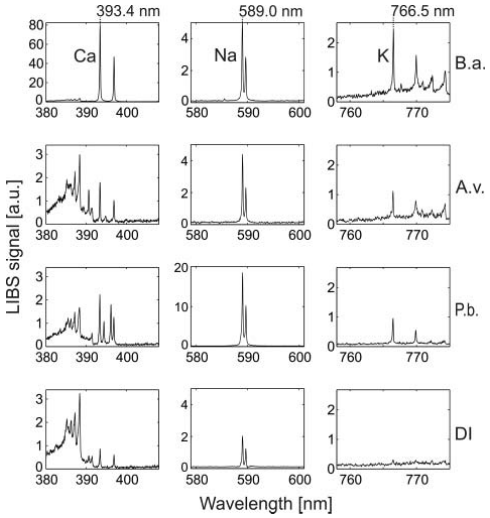

Figure 2. Typical single shot LIBS spectra of bacterial (*Bacillus aureus*, B.a.) and fungal spores (*Aspergillus versicolor*, A.v., and *Penicillium brevicompactum*, P.b.) as well as background signals from de-ionized water (DI). Characteristic peaks of Ca, Na, and K are 393.4 nm, 589.0 nm, and 766.5 nm, respectively.

LIBS analysis and thus have effect on the LIBS spectrum. This problem was avoided here as the plasma was formed only from particle and from ambient air. In the previous studies by Hybl et al. (2003, 2006), LIBS spectroscopy has been examined as a potential method for detecting airborne single biological agents. Ca, Na, Mg, and K were typical elements in the LIBS spectra for airborne bacterial and fungal spores, which is in line with our results. Hybl et al. (2006) also showed that Na and K signals decreased in single- and double-washed bacterial samples.

Na, Ca, and K concentrations in microbial particles

The geometric means of 20 repeats and standard deviations of the elemental concentrations (g/particle) are shown in Figure 3. The limit of detection based on the background from DI water is also shown in the figure. B. a. bacterial spores had over three orders of magnitude higher Ca concentration (2×10^{-12} g/particle) compared to the fungal spores ($3–5 \times 10^{-16}$ g/particle) that had concentrations close to DI water (3×10^{-16} g/particle). It is well known that during sporulation bacterial spores concentrate calcium dipicolinate (Gould and Hurst 1969), but this study confirmed the previous observations that Ca is not abundant component in fungal spores. Statistically significant differences in Ca

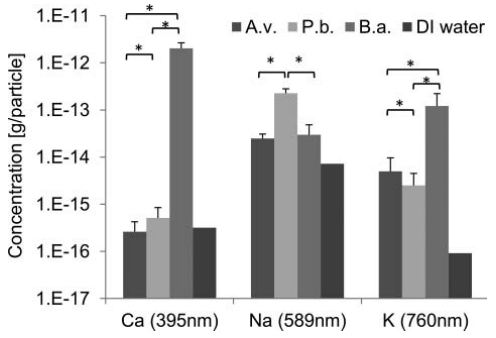

Figure 3. Geometric mean concentrations (g/particle) of elemental components for fungal (*Aspergillus versicolor*, A.v., and *Penicillium brevicompactum*, P.b.) and bacterial (*Bacillus aureus*, B.a.) spores. De-ionized (DI) water represents the limit of detection based on the background from DI water. Error bars represent geometric standard deviations of 20 repeats. Asterisks (*) represent statistically significant difference ($p < 0.01$) between species.

concentrations were observed between bacterial and fungal spores as well as between fungal species.

The highest Na concentration (2.3×10^{-13} g/particle) was in the P.b. fungal spores, whereas the Na content of A.v. fungal spores and B.a. bacterial spores was 2.5×10^{-14} g/particle and 3.0×10^{14} g/particle, respectively. The higher Na content in the P.b. particles may be due to different surface structure of the spores (see Figure S3 in the SI). Statistically significant differences in Na concentrations were observed between A.v. and P.b. spores as well as between B.a. and P.b. Bacterial spores had over one order of magnitude higher K concentration (1.2×10^{-13} g/particle) compared to fungal spores ($3–5 \times 10^{-15}$ g/particle). Na and K concentrations were well above the DI water background levels for all species.

The EDB-assisted method has earlier been shown to have good repeatability for LIBS analysis of heavy metals in water (Järvinen et al. 2014). In the current study, good repeatability of LIBS analysis was also shown for microbial suspensions, which is shown in Figure 3 wherein the standard deviations between the repeats were relatively small. Due to the precise positioning of the trapped particle, the LIBS excitation laser pulse can be focused tightly to obtain high irradiance on the microbe surface. Relatively low laser pulse energy (9 mJ) was therefore used to generate the plasma and vaporize the microbial particle. For comparison, e.g., Hahn and Lunden (2000) used 400 mJ and Hybl et al. (2006) 50 mJ pulse energy for aerosol particle analysis by LIBS. Lasers with low pulse energy are typically more compact and applicable in field use.

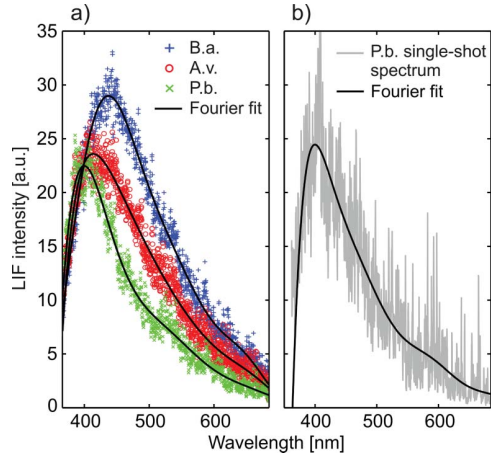

Figure 4. (a) Average fluorescence spectra of 20 repeats for fungal (*Aspergillus versicolor*, A.v., and *Penicillium brevicompactum*, P.b.) and bacterial spores (*Bacillus aureus*, B.a.). (b) A typical single-shot fluorescence spectrum recorded from single fungal P.b. spore.

Recent LIBS study by Dixon and Hahn (2005) reported that Ca was detectable in washed, single *Bacillus globigii* spores, but other elements such as Na and K were not detectable at the single-spore level. In this study, we demonstrated EDB-assisted LIBS analysis of single fungal spores having typical 2.8'μm particle diameter (see Figure S1 in the SI) and bacterial spore aggregates having circa 20 spores per particle. Strong LIBS peak to background ratio (P/B-ratio) values of Na (3–31) and K (27–55) were detected from single fungal spores. The results indicate that the method enables very sensitive LIBS analysis at single-spore level and the major limitation factor was impurities of used DI water.

LIF spectra of microbial particles

Both the LIF and LIBS spectra were measured from the same particle in our measurement system. The average LIF spectra of 20 repeats recorded from fungal (A.v. and P.b.) and bacterial spores (B.a.) are shown in Figure 4. The fluorescence peak of bacteria was located at 440 nm and fluorescence maximum of fungal spores located around 400 nm. Clear difference can be seen between the fluorescence spectra of fungal and bacterial spores.

Fluorescence spectra or fluorescence band (single or multiple) intensity measurement can be utilized to discriminate bioaerosols from other aerosols (Pöhlker et al. 2012; Pan 2015). Fluorescence-based online bioaerosol instruments, such as BioScout, WIBS, and UV-APS, have been used in various environments, but it is really

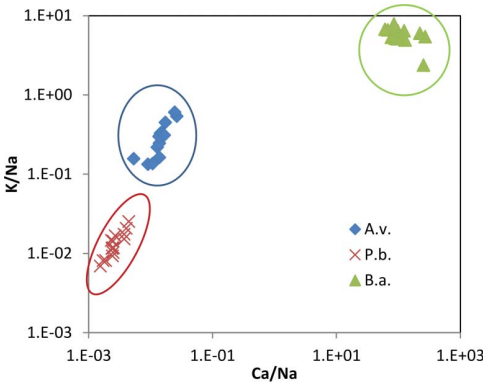

Figure 5. Normalized Ca/Na and K/Na signals from single shot LIBS spectra for fungal (*Aspergillus versicolor*, A.v., and *Penicillium brevicompactum*, P.b.) and bacterial (*Bacillus aureus*, B.a.) spores.

challenging to classify different types of bioaerosols with these instruments (Gabey et al. 2010; Huffman et al. 2010; Saari et al. 2014). It should be noted that fluorescence analysis alone may include uncertainties due to fluorescent non-biological artifacts in ambient air leading to false counts of bioaerosols (Pöhlker et al. 2012; Saari et al. 2013).

Identification of microbial particles

Normalized Ca/Na and K/Na signals from single shot LIBS spectra for fungal (A.v. and P.b.) and bacterial spores (B.a.) are presented in Figure 5. The results show that fungal spores are distinct from bacterial spores and even fungal species, A.v. and P.b., are readily distinguishable. The figure demonstrates that different bioaerosol species can be classified when normalized K/Na LIBS signal values are plotted in the function of normalized Ca/Na LIBS signal values.

Previously it has been reported that real-time LIF analysis enables classification of bioaerosols from other aerosols in atmosphere (Gabey et al. 2010; Huffman et al. 2010; Pan 2015). Our results show that combined LIF and LIBS analysis is promising tool for online classification of atmospheric bioaerosols. The present EDB-assisted combined LIF and LIBS analysis method enabled high sensitivity, repeatability, and classification of different types of bioaerosols generated from water suspension. The major limitation factor in the method was impurities of used DI water in droplet generation. Sensitivity of the method may be improved a lot when aerosol particles are trapped and analyzed directly from ambient air. Besides Ca, Na, and K, other elements can be included in the data analysis to improve the identification accuracy if the corresponding spectral lines are clearly resolved in a single-shot spectrum and their intensity does not significantly fluctuate between the spores of the same species. The next step is to enhance the method further for real-time identification of different types of ambient aerosols such as soot, mineral dust, sea salt, fungal spores, bacteria, and pollen. The research on these aerosols is important in atmosphere due to their health and climatic relevance.

Conclusions

We successfully applied the EDB, LIF, and LIBS techniques in order to characterize single fungal spores and bacteria online. The EDB-assisted system enabled relatively low laser pulse energy to break down the microbe particles and highly sensitive and repeatable LIBS analysis of common elemental components (Ca, Na and K) in microbes. Statistically significant differences in the elemental concentrations were observed between the species. Combination of LIF and LIBS is a potential technique for online identification of different types of atmospheric aerosols or microbes in drinking water.

Funding

The work is financially supported by Doctoral School of TUT and TEKES FiDiPro-project named BITEFA (decision number 40371/11) and Academy of Finland project named ICINA (decision number 272041).

References

Després, V., Huffman, A., Burrows, S., Hoose, C., Safatov, A., Buryak, G., Fröhlich-Nowoisky, J., Elbert, W., Andreae, M., Pöschl, U., and Jaenicke, R. (2012). Primary Biological Aerosol Particles in the Atmosphere: A Review. *Tellus, Series B: Chem. Phys. Meteorol.*, 64(1):DOI: 10.3402/tellusb.v64i0.15598.

Dixon, P. B., and Hahn, D. W. (2005). Feasibility of Detection and Identification of Individual Bioaerosols Using Laser-Induced Breakdown Spectroscopy. *Anal. Chem.*, 77:631–638.

Douwes, J., Thorne, P., Pearce, N., and Heederik, D. (2003). Bioaerosol Health Effects and Exposure Assessment: Progress and Prospects. *Ann. Occup. Hyg.*, 47:187–200.

Dutouquet, C., Wattieaux, G., Meyer, L., Frejafon, E., and Boufendi, L. (2013). Determination of the Elemental Composition of Micrometric and Submicrometric Particles Levitating in a Low Pressure Radio-Frequency Plasma Discharge Using Laser-Induced Breakdown Spectroscopy. *Spectrochimica Acta B.*, 83:14–20.

Farooq, W. A., Atif, M., Tawfik, W., Alsalhi, M. S., Alahmed, Z. A., Sarfraz, M., and Singh, J. P. (2014). Study of Bacterial Samples Using Laser Induced Breakdown Spectroscopy. *Plasma Sci. Technol.*, 16(12):1141.

Fortes, F. J., Fernández-Bravo, A., and Laserna, J. J. (2014). Chemical Characterization of Single Micro-and Nano-Particles by Optical Catapulting—Optical Trapping—Laser-Induced Breakdown Spectroscopy. *Spectrochimica Acta B.*, 100:78–85.

Gabey, A. M., Gallagher, M. W., Whitehead, J., Dorsey, J. R., Kaye, P. H., and Stanley, W. R. (2010). Measurements and Comparison of Primary Biological Aerosol Above and Below a Tropical Forest Canopy Using a Dual Channel Fluorescence Spectrometer. *Atmos. Chem. Phys.*, 10(10): 4453–4466.

Gould, G., and Hurst, A. (1969). *The Bacterial Spore*. Academic Press, London, p. 247.

Hahn, D. W., and Lunden, M. M. (2000). Detection and Analysis of Aerosol Particles by Laser-Induced Breakdown Spectroscopy. *Aerosol Sci. Technol.*, 33(1–2):30–48.

Heinisch, C., Wills, J. B., Reid, J. P., Tschudi, T., and Tropea, C. (2009). Temperature Measurement of Single Evaporating Water Droplets in a Nitrogen Flow Using Spontaneous Raman Scattering. *Phys. Chem. Chem. Phys.*, 11:9720–9728.

Hill, S., Pan, Y.-L., Williamson, C., Santarpia, J., and Hill, H. (2013). Fluorescence of Bioaerosols: Mathematical Model Including Primary Fluorescing and Absorbing Molecules in Bacteria. *Opt. Express.*, 21:22285–22313.

Hill, S. C., Pinnick, R. G., Nachman, P., Chen, G., Chang, R. K., Mayo, M. W., and Fernandez, G. L. (1995). Aerosol-Fluorescence Spectrum Analyzer: Real-Time Measurement of Emission Spectra of Airborne Biological Particles. *App. Optics.*, 34(30):7149–7155.

Huffman, J. A., Treutlein, B., and Pöschl, U. (2010). Fluorescent Biological Aerosol Particle Concentrations and Size Distributions Measured with an Ultraviolet Aerodynamic Particle Sizer (UV-APS) in Central Europe. *Atmos. Chem. Phys.*, 10(7):3215–3233.

Hybl, J. D., Lithgow, G. A., and Buckley, S. G. (2003). Laser-Induced Breakdown Spectroscopy Detection and Classification of Biological Aerosols. *App. Spectrosc.*, 57(10):1207–1215.

Hybl, J. D., Tysk, S. M., Berry, S. R., and Jordan, M. P. (2006). Laser-Induced Fluorescence-Cued, Laser-induced Breakdown Spectroscopy Biological-Agent Detection. *App. Optics.*, 45(34):8806–8814.

Hyvärinen, A., Meklin, T., Vepsäläinen, A., and Nevalainen, A. (2002). Fungi and Actinobacteria in Moisture-Damaged Building Materials—Concentrations and Diversity. *Int. Biodeterior. Biodegradation.*, 49:27–37.

Intergovernmental Panel on Climate Change. (2013). *Climate Change 2013: The Physical Science Basis*. IPCC, Geneva. www.ipcc.ch.

Järvinen, S. T., Saari, S., Keskinen, J., and Toivonen, J. (2014). Detection of Ni, Pb and Zn in Water Using Electrodynamic Single-Particle Levitation and Laser-Induced Breakdown Spectroscopy. *Spectrochimica Acta B*, 99:9–14.

Kaye, P., Stanley, W. R., Hirst, E., Foot, E. V., Baxter, K. L., and Barrington, S. J. (2005). Single Particle Multichannel Bio-Aerosol Fluorescence Sensor. *Opt. Express*, 13(10):3583–3593.

Lakowicz, J. R. (2009). *Principles of Fluorescence Spectroscopy*. Springer, New York, pp. 205–231.

MicroFab Technologies Inc. (1999). *Drive Waveform Effects on Ink-Jet Device Performance*. Technote 99-03. Author, Plano, TX.

Pan, Y. L. (2015). Detection and Characterization of Biological and Other Organic-Carbon Aerosol Particles in Atmosphere Using Fluorescence. *J. Quantit. Spectr. Radiat. Transfer.*, 150:12–35.

Park, K., Cho, G., and Kwak, J. H. (2009). Development of an Aerosol Focusing-Laser Induced Breakdown Spectroscopy (Aerosol Focusing-LIBS) for Determination of Fine and Ultrafine Metal Aerosols. *Aerosol Sci. Technol.*, 43(5):375–386.

Pöhlker, C., Huffman, J. A., and Pöschl, U. (2012). Autofluorescence of Atmospheric Bioaerosols–Fluorescent Biomolecules and Potential Interferences. *Atmos. Meas. Tech.*, 5 (1):37–71.

Reponen, T., Grinshpun, S. A., Conwell, K. L., Wiest, J., and Anderson, M. (2001). Aerodynamic Versus Physical Size of Spores: Measurement and Implication for Respiratory Deposition. *Grana*, 40(3):119–125.

Reponen, T., Lockey, J., Bernstein, D. I., Vesper, S. J., Levin, L., Khurana Hershey, G. K., Zheng, S., Ryan, P., Grinshpun, S. A., Villareal, M., and LeMasters, G. (2012). Infant Origins of Childhood Asthma Associated with Specific Molds. *J. Allergy Clin. Immunol.*, 130:639–644.

Reponen, T., Willeke, K., Grinshpun, S., and Nevalainen, A. (2011). Biological Particle Sampling, in *Aerosol Measurement: Principles, Techniques, and Applications*, 3rd ed., P. Kulkarni, P. A. Baron, and K. Willeke, eds., Wiley, Hoboken, NJ, pp. 549–570.

Saari, S., Putkiranta, M. J., and Keskinen, J. (2013). Fluorescence Spectroscopy of Atmospherically Relevant Bacterial and Fungal Spores and Potential Interferences. *Atm. Environ.*, 71:202–209.

Saari, S., Reponen, T., and Keskinen, J. (2014). Performance of Two Fluorescence-Based Real-Time Bioaerosol Detectors: BioScout vs. UVAPS. *Aerosol Sci. Technol.*, 48(4):371–378.

Singh, V. K., and Rai, A. K. (2011). Prospects for Laser-Induced Breakdown Spectroscopy for Biomedical Applications: A Review. *Lasers Med. Sci.*, 26(5):673–687.

Tjärnhage, T., Gradmark, P. Å., Larsson, A., Mohammed, A., Landström, L., Sagerfors, E., Jonsson, P., Kullander, F., and Andersson, M. (2013). Development of a Laser-Induced Breakdown Spectroscopy Instrument for Detection and Classification of Single-Particle Aerosols in Real-Time. *Opt. Commun.*, 296:106–108.

WHO. (2004). *Guidelines for Drinking-Water Quality: Recommendations* (Vol. 1). World Health Organization, Geneva.

Tampereen teknillinen yliopisto
PL 527
33101 Tampere

Tampere University of Technology
P.O.B. 527
FI-33101 Tampere, Finland

ISBN 978-952-15-3727-1
ISSN 1459-2045